Physics – Uspekhi **65** (3) 270 – 312 (2022)

INSTRUMENTS AND METHODS OF INVESTIGATION

PACS numbers: **07.60. – j**, 42.30.Wb, 43.35.Sx, 43.35.Ud, 78.20.nb, 78.20.N – , 78.20.Pa, 81.70.Cv, 82.80.Kq, 87.19.Pp

Photothermal and optoacoustic spectroscopy: state of the art and prospects

M A Proskurnin, V R Khabibullin, L O Usoltseva, E A Vyrko, I V Mikheev, D S Volkov

DOI: https://doi.org/10.3367/UFNe.2021.05.038976

Contents

Abstract. The main issues and areas of application of photothermal and optoacoustic spectroscopy are reviewed. Progress in innovative techniques in the most actively developing areas is presented, including microspectroscopy, multispectral techniques, the measurements of single particles and objects with a resolution better than the diffraction limit (nanoscopy) by both optical and probe-based methods. Possible applications of photothermal and optoacoustic spectroscopy for determining the properties of materials, studying photochemistry and fluorescence, chemical reactions, and analytical and applied chemistry, and solving biomedical problems is discussed. Some prospects for the development of these methods are presented.

Keywords: photothermal spectroscopy, optoacoustic spectroscopy, photoacoustic spectroscopy, photonics, nanophotonics, biophotonics, microspectroscopy, optoacoustic tomography, nanoscopy, thermal spectroscopy, remote analysis and monitoring techniques, nondestructive testing, materials science, functional materials, theranostics, photochemistry, fluorescence, analytical chemistry, thermodynamics

M A Proskurnin (*), **V R Khabibullin, L O Usoltseva, E A Vyrko, I V Mikheev, D S Volkov**
Lomonosov Moscow State University, Chemistry Department, Leninskie gory 1, str. 3, 119991 Moscow, Russian Federation
E-mail: (*) proskurnin@gmail.com

Received 26 August 2020, revised 18 February 2021
Uspekhi Fizicheskikh Nauk **192** (3) 294 – 340 (2022)
Translated by M Zh Shmatikov

1. Introduction

Methods referred to as photothermal and optoacoustic (photoacoustic) or, in general, photothermoacoustic spectro-

scopy are one of the important areas in the development of spectroscopy and thermal physics, as well as chemical analysis, control, and diagnostics of natural and human-made materials and living systems. Photothermal and optoacoustic methods are based on the measurement and analysis of the thermal relaxation of absorbed electromagnetic radiation and its impacts — optical and acoustic phenomena, respectively. These methods, which are classified as absorption spectroscopy techniques, feature a wide spectrum of capabilities.

(1) First of all, they feature high sensitivity, which makes it possible to detect single particles and molecules. Photothermal and optoacoustic methods enable determination of light absorption in liquid and solid samples at a level of down to $10^{-9}-10^{-6}$ units of absorbance and substance concentrations of down to 10^{-11} M, and analysis of volumes down to 1 fL.

(2) Photothermal and optoacoustic methods provide simultaneous determination of various parameters, primarily optical and thermophysical, of the object under study, and they also enable studying objects in a nondestructive way.

(3) Due to the constantly improving technical level, photothermal and optoacoustic spectroscopy feature a wide spectral range, from the far ultraviolet (UV) to the far infrared (IR) regions.

(4) Photothermal and optoacoustic methods are characterized by a spatial resolution that can be higher than the diffraction limit, which resulted in the development of microscopy, microspectroscopy, and nanoscopy methods.

(5) Photothermal and optoacoustic spectroscopy techniques can be used for a wide range of compounds for almost all complex objects. In recent years, the trend has been to apply these methods to such objects as complex heterogeneous condensed systems, for which application of alternative methods for determining optical and thermal parameters *in situ* and *in vivo* is either difficult or impossible.

Photothermal and optoacoustic spectroscopy is increasingly in demand in materials science, in solving biomedical and complex photonics problems, and in chemical and microscopic analysis of complex objects, and standards of studies are constantly being enhanced. This progress is accompanied by an increase in the number of applied and combined solutions. Recent developments include instruments and methods for applied materials science, clinical diagnostics and theranostics (simultaneous diagnostics and therapy under the same exposure conditions), and chemical microanalysis.

In recent years, quite a few monographs or separate chapters in monographs have been devoted to the considered methods [1–8], and a large number of reviews [9–35] have been published. This review differs from previous publications for several reasons. Attention was focused in those studies on the basics of phenomena and processes or the parameters of instruments and their types and a description of the main established areas of use and objects studied. More specialized reviews [9–11, 14, 15, 17, 36–38] are devoted to specific applications of individual methods: detection, monitoring, nondestructive testing, preclinical and clinical diagnostics, etc. or to certain objects of special interest.

The goal of this review is to generalize to some extent the capabilities of photothermal and optoacoustic spectroscopy described above. However, we do not consider here in detail the basics of the methods or their most widespread applications — all these topics are covered in reviews and monographs [1–3, 5, 9–16, 18–20, 36]. On the contrary, based on the breakthrough achievements made lately in optoacoustic tomography, multispectral imaging, nanoscopy, photothermal probe spectroscopy, and other areas and approaches, we consider the prospects for the development of photothermal and optoacoustic spectroscopy, including those in materials science, chemistry, and biomedicine.

Finally, many of the reviews published to date refer either to the underlying physics of photothermal and optoacoustic phenomena or often to specific solutions to biomedical and clinical problems. However, the chemical sciences, by their very nature, underlie multidisciplinary research in this area. One more focus of this review is physical and analytical chemistry, as sciences oriented to achieving key goals of the development of natural sciences and which employ research technology (methodology) and rely on state-of-the-art instrumental research capabilities.

2. Photothermal and optoacoustic spectroscopy: a brief description

Both photothermal and optoacoustic spectroscopy are based on the detection and analysis of thermally induced changes in a sample in the process of its interaction with electromagnetic radiation. These methods are based on nonradiative transitions of excited molecules caused by the *absorbed* part of the radiation that passes through the sample (*photothermal effects*) and their consequences, which are *thermooptical and optoacoustic* phenomena (Fig. 1). Photothermal and optoacoustic spectroscopy complement other, primarily highly sensitive, methods of molecular absorption spectroscopic analysis based on the *transmission* or *reflection* of electromagnetic radiation. Moreover, photothermal and optoacoustic methods are less affected by light scattering, since photothermal effects are only due to absorbed radiation.

In addition, photothermal and optoacoustic spectroscopy is also classified as thermophysical research methods, since the effects explored are related to heat distribution and, therefore, depend on the thermophysical parameters of the test sample. Thus, photothermal and optoacoustic methods are used to obtain information about thermal conductivity, thermal diffusivity, heat capacity, specific heat, thermal expansion coefficient, viscosity, etc. These methods also make it possible to obtain the excitation spectra of photothermal properties, the so-called *thermal spectra*, of the objects under study [39, 40].

This dual nature of photothermal and optoacoustic spectroscopy enables the simultaneous measurement of several signals, which depend on the optical and thermal properties of the object under examination in a different way. Moreover, photothermal methods are superior in sensitivity to both purely optical and purely thermal methods, since they are based on the interdependence of changes in optical and thermal properties, which together contribute to an increase in sensitivity [41].

Finally, the methods of photothermal and optoacoustic spectroscopy are applicable to both bulk-absorbing and surface-absorbing samples, as well as to layered and discretely absorbing materials. An important characteristic of many of these methods is the possibility of depth profiling by changing the chopper frequency (or pulse repetition rate) of the excitation radiation, which leads to different depths of thermal wave propagation in the object under study.

Since the source of excitation of photothermal and optoacoustic effects is often a laser whose beam can be focused

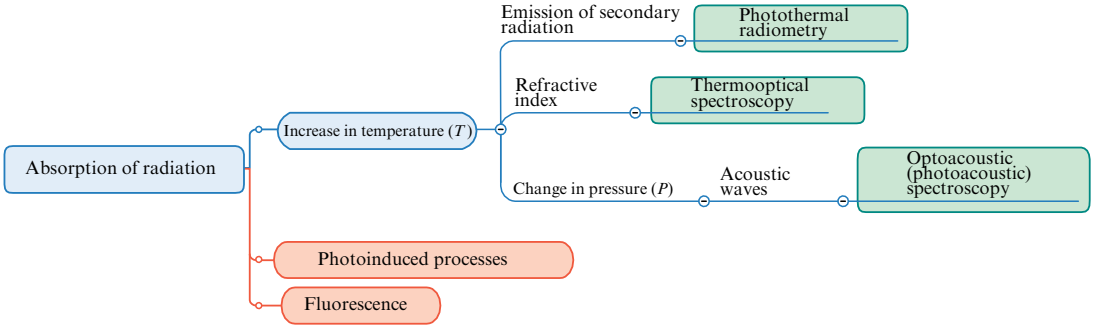

Figure 1. (Color online.) General layout of the formation of photothermal and optoacoustic processes and competing processes.

up to a wavelength-limited space (diffraction limit), most of the corresponding methods are implemented as microscopic, imaging, or microspectroscopic techniques (see Section 3).

Photothermal methods are classified according to the result of photothermal excitation during heating, which is due to energy absorption and subsequent thermal relaxation (see Fig. 1). This leads to the following processes in the entire sample or in its surface (subsurface) layers: (1) the photothermal generation of thermal waves; (2) the formation of an inhomogeneous spatial temperature field (profile), which manifests itself as a refractive index or density field (thermooptical effects and *thermooptical methods* of photothermal spectroscopy); (3) the emission of secondary radiation by the heated surface of the sample (*photothermal radiometry* methods).

The *optoacoustic effect* was discovered by J Bell in gases more than 100 years ago. The current stage in the development of optoacoustic spectroscopy (OAS) began with the emergence of laser excitation sources. Since the 1980s, OAS has been used for condensed media, since the physical foundations of the optoacoustic effect have been developed for such media [42, 43]. Many of the OAS methods are quite simple and are characterized by a wide linear range of signals, short measurement times, and small volumes of test samples [6]. Similar to transmission spectroscopy, there are two main types of OAS implementation. The first technique is single-wavelength or scanning spectrometry based on lasers or lamps operating in the near UV, visible, and near IR ranges. The second option is the use of OAS in IR interferometers. Very often, in describing OAS capabilities, only laser-induced variants are indicated; however, the capabilities of OAS-FTIR spectroscopy are no less significant [6, 37]. OAS is applicable to objects in any state of aggregation.

Photothermal spectroscopy (PTS) is based on other effects of the thermal relaxation of absorbed energy (see Fig. 1). The term 'photothermal spectroscopy' is the common name for a fairly large number of methods. Thermooptical PTS methods are usually classified according to the action (or shape) of a spatial profile resembling a certain optical element [1], i.e., a *thermooptical element* (thermal lens, thermal mirror, thermal diffraction grating, etc.). [1]

[1] The term *thermooptical* is used more frequently for methods of measurement and analysis, while *phototermal* is used for phenomena. Thus, a general term for the group of methods under consideration is 'thermooptical spectroscopy,' and the names of particular methods should include the word 'photothermal,' since they include the name of a phenomenon, for example, 'photothermal deflection spectroscopy.' For historical reasons, an exception is the term 'thermal lens', although, in this case, the term 'phototermal lens' would be more correct.

The use of thermooptical methods is based on the fact that the characteristic parameter of a thermooptical element (e.g., the thermal lens strength) is directly proportional to the light absorption parameters of the sample and, consequently, to the concentration and absorption coefficient of the compound under study. Similar to OAS, although to a lesser extent, the thermooptical signal is less dependent on light scattering than in the case of transmission spectroscopy. Photothermal methods are considered to be more sensitive than most OAS methods. The linearity of the PTS signal (usually spanning about three orders of magnitude) is comparable to that in conventional transmission measurements and is narrower than in optoacoustic measurements due to the nonlinear nature of the parameters of optical elements used as approximation models for linear signals, which depend on absorbance or concentration [1].

Thermal lens spectrometry (TLS) is the most common photothermal method for studying liquid media and is used more often than other PTS methods in applied and analytical chemistry [1, 4]. Thermal relaxation leads to an inhomogeneous spatial profile of the refractive index in the sample, acting as a lens (*thermal lens* effect). Its optical power is proportional to the absorption of the sample and, consequently, to the absorber concentration and absorptive capability.

For solid samples in the optical and infrared ranges, *photothermal deflection spectroscopy* (PDS) is the most common among thermooptical methods [1, 44–47]. Modulated or pulsed photothermal heating of a sample with a flat surface leads to thermal relaxation, which creates a temperature field and thermal waves not only in the sample itself but also in the so-called *contact medium* (air, purge gas, or contact liquid) above it. As a result, a refractive index gradient arises in this medium, which in turn leads to the deflection of the probe beam that propagates in the contact medium parallel to the sample surface (*mirage effect*) or at a certain angle to the sample (*photothermal mirror*) [48]. The magnitude of the effect is related to the absorptivity and thermal properties (heat capacity, thermal conductivity) of the surface and the ambient medium. In addition to high sensitivity, the advantage of PDS spectroscopy is that, in most cases, it is not necessary to prepare the surface of complex samples. Minimal sample preparation, which consists of a slight grinding, enhances the sensitivity and makes it possible to avoid spectral reflection effects [1, 44, 49, 50].

Photothermal radiometry (PTR) is used to study the absorption of surfaces and layered objects [1, 2]. Partial absorption of modulated or pulsed laser radiation leads to

thermal waves. A photothermally sample excited emits secondary IR radiation due to thermal relaxation, which is detected by an IR detector. The amount of energy emitted is proportional to the absorption coefficient of the sample. In PTR, the rate of signal development is much higher than in other photothermal methods, explained by the fact that the development of surface deformation and the temperature gradient in the environment requires significant time in comparison with the thermal relaxation time.

The advantages of PTR are remote sensing, simple design of the experimental setup, and high spatial and time resolution ($10^{-6}-10^{-5}$ s, down to $10^{-8}-10^{-7}$ s for pulsed methods) [2, 14, 51–54]. The lateral spatial resolution of the PTR is determined by the focusing of the excitation radiation and does not differ from that in other optoacoustic and photothermal methods. Similar to OAS and PDS spectroscopy, the thermal diffusion length of a material characterizes the limiting depth of penetration of a thermal wave down to which PTR is effective. The time resolution of the method is determined by the response of the secondary radiation recorded by a thermal or infrared detector and is limited by its response time. In general, the PTR parameters enable using this method to obtain absorption spectra of intermediate products and to monitor fast processes [55–58].

Photothermal and optoacoustic methods are also divided into two main categories: *contactless*, which use a remote detection system, and *contact*, when the sample is in direct contact with the detection system [48].

In addition to stationary signals that correspond to the establishment of thermal equilibrium, the transient parameters of the formation and dissipation of induced thermal fields and waves are of importance for the phenomena under consideration, due to which *time-resolved measurements* are fundamentally important. In the first approximation, the signal amplitude in photothermal spectroscopy is proportional to the light absorption, and the rate of signal variation is determined by the thermophysical properties of the object under study and its dynamic characteristics, primarily thermal diffusivity and thermal effusivity.

As in other areas of spectroscopy, photothermal and optoacoustic methods can be classified according to the method applied to study the thermal response as a function in the time domain or in the frequency domain [59]. In many measurement options, evanescent thermal waves are also employed, which are used to calculate the light absorption and/or thermophysical parameters of an object. This variant of measurements in the frequency domain is referred to as the spatial domain of PTS (spatial-domain photothermics) [60, 61]. In general, due to the difference in characteristic times, the main information depends on the process examination times. As a result, photothermal methods can be classified according to the characteristic times of the main probe process.

The first group includes methods based on fast (microsecond or smaller time scales) photothermal phenomena, such as PTR, the method of time-resolved photothermally induced thermal diffraction grating [62–64], the method of impulsive stimulated thermal scattering (ISTS) [65–67], and other *heterodyne* methods (see Section 3.4.2). Typically, the detectors used in these methods are coherent and operate in the time domain. These methods are applied to study charge transfer dynamics [68, 69], thermoelastic properties [65], and ultrafast heat transfer in the interior of nanoparticles (NPs) [70–72].

The second group of methods includes TLS and PDS, which correspond to the establishment of a stationary state or transient measurements on scales ranging from several milliseconds to several seconds. The time resolution of these methods is limited from below by the characteristic time of propagation of the sound wave outside the irradiated area [58]. Detection in such methods most often corresponds to the frequency domain. These relatively slow photothermal methods are used to study established equilibria, estimate the thermal macroparameters of liquids, obtain spectra, and study heat transfer between dispersed medium phases and, thus, the thermophysical parameters of an object as a whole [73, 74].

Since all the methods based on the absorption of electromagnetic radiation by complex objects involve spectral interferences, an important role in photothermal and optoacoustic spectroscopy is played by *differential* methods, which make it possible to reduce the effect of interfering signals. The implementation of these methods depends on whether they operate in the frequency or time domain. In amplitude-based and slow methods, such as TLS, the differential measurement option is based on background signal compensation. In this variant, a cell with a reference sample is placed before the waist of the excitation laser. A thermal lens is formed in the cell, the signal of which is proportional to the sum of light absorption of all components responsible for the background signal. The signal in the second (main) cell located at the same distance, but after the excitation beam waist, is determined by the light absorption of both the target component and the background. As a result, the focusing action of the thermal lens in the first cell compensates for the broadening of the probe beam, which occurs due to the absorption of the components responsible for the background signal in the second cell [75–81]; then, the resulting signal only depends on the absorption of the analyzed component in the second cell. The considered differential variant is rarely used directly in TLS, but it has primarily acquired significance in correlation photothermal spectroscopy (see Section 3.4.3), where the local signal in the sample under study, caused by photothermally excited NPs, is measured relative to the signal of the reference volume, which contains no particles.

3. Photothermal and optoacoustic microscopy and microspectroscopy

With the progress in technologies, the instrumental and methodological potential of photothermal and optoacoustic spectroscopy is constantly growing, and the employment of these methods is becoming more and more associated with the study of objects for which other methods intended to determine both optical and thermophysical parameters encounter difficulties. At present, the development of photothermal and optoacoustic spectroscopy methods is aimed at studying and analyzing heterogeneous condensed media with a complex composition [1, 5]. The importance of PTS and OAS as the methods of research and analysis in materials science, chemistry, and biomedicine is growing, which is reflected both in the increase in the total number of publications (the number of articles per year has almost tripled over the past five to seven years) and in the increasingly wide application of these methods in biophotonics, microspectroscopy, imaging, the spectral analysis of surfaces, and micro- and nanofluidics [1, 4, 29, 31, 82–89].

In this section, we briefly summarize the achievements and directions of development, which pertain to either relatively new methods of photothermal and optoacoustic spectroscopy or the most rapidly developing areas. Unfortunately, it is not possible to describe all areas with a sufficiently high degree of detail in even the most extensive review or a monograph. Therefore, we focused in Sections 3.1–3.5 on the areas mainly related to microscopy: photothermal and optoacoustic microspectroscopy, multispectral methods, and measurements of single particles and objects with a spatial resolution above the diffraction limit (nanoscopy), including both optical and probe methods.

3.1 Photothermal microscopy

Photothermal microscopy, or microspectroscopy, which is used to image samples of nonfluorescent substances down to the size of individual clusters, nanoparticles (NPs), or molecules without the use of labels, exhibits the highest sensitivity among all methods based on optical absorption [90–93]. Microspectroscopic photothermal methods make it possible to obtain high-resolution images of living tissues [90, 92], cells [94, 95], single NPs, and their aggregates [45, 93]. Confocal photothermal microscopy (PTM) versions [91, 96–98] (see Section 3.1.1) feature ultrahigh resolution due to the combined use of optical and thermal images, the resolution of which is determined by the characteristic rates of nonradiative heat transfer and the time resolution of measurements [91, 96, 99]. Thus, PTS provides imaging of both thermal and optical properties of a sample with submicrometer resolution [1, 100–103].

3.1.1 Thermal lens microscopy and confocal thermal lens microscopy. In thermal lens microscopy (TLM), as well as in its macro version, thermal lens spectrometry, the signal is the spatial distribution of the amplitude and phase of the probe beam [12, 104]. The signal formation method in and the theoretical basis of TLS and TLM are largely similar [25, 94, 96, 105–109]. Lately, the target objects for TLM are biological fluids, proteins, cells, and NPs used in therapy and theranostics. For example, blood components were studied using TLM [83], and various components were determined *ex vivo* in a single cell at low concentrations [110]. A quantitative analysis of DNA hybridization *in situ* due to the difference in light absorption of single- and double-stranded DNA on Au NPs in volumes of the order of several femtoliters in a microfluidic chip has been demonstrated (see below in this section and in Section 8). For concentrations of 50–500 nM, detection limits of 30 nM have been achieved. The smallest detectable amount of DNA was 3 zmol (3×10^{-21} mol) at a measurement time of 5 min; the relative standard deviation of the measurements was 2–3% [111]. TLM makes it possible to study the features of reactions at the level of nanogram amounts of reactants and can be combined with microflow analysis methods (microflow injection analy-

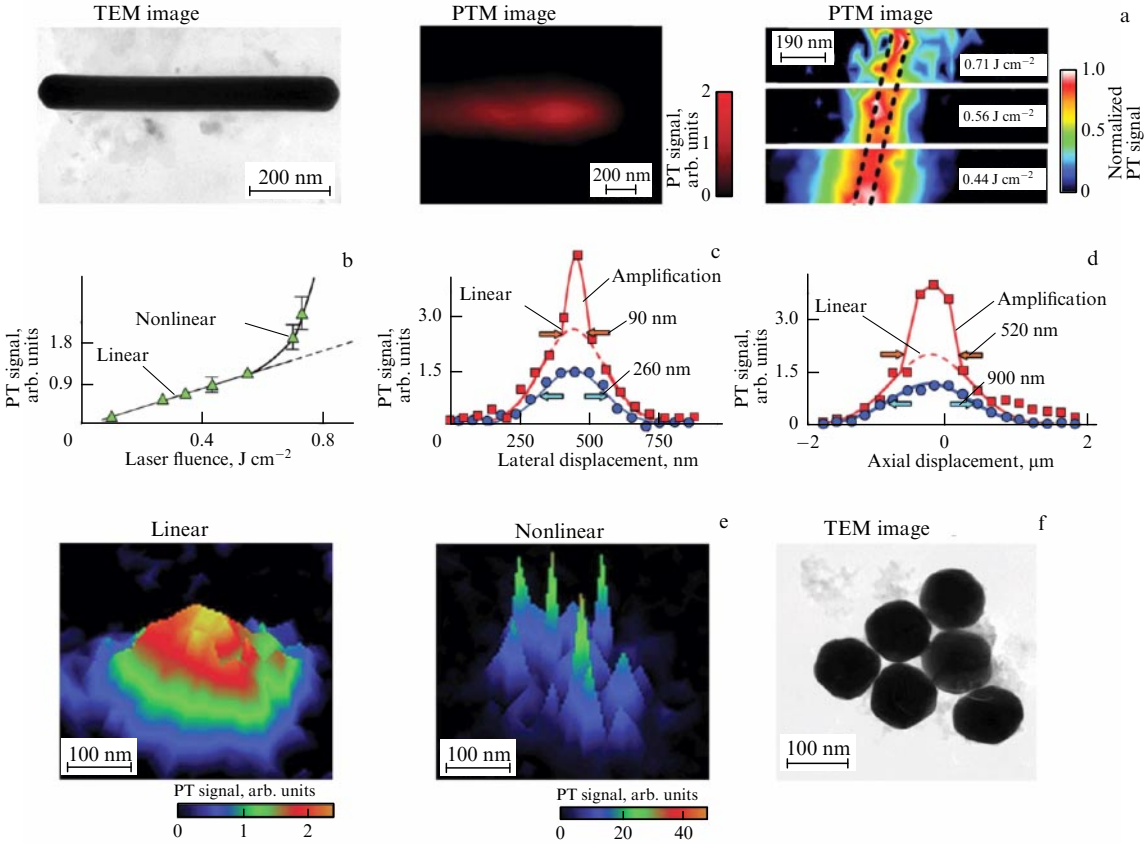

Figure 2. (Color online.) Photothermal (PT) microscopy signal from ultra-high-resolution imaging (PTM) of gold nanostructures. (a) Transmission electron microscopy (TEM) image (left), parts of linear (center) and nonlinear (right) PTM images of a gold nanowire 75 nm in diameter under different conditions. (b) Amplitudes of the photothermal signal from the nanowire at different laser fluences. Lateral (c) and axial (d) PTM resolution in linear and nonlinear modes. Dashed line is the Gaussian function calculated using the linear part of the signal. (e) Linear (left) and nonlinear (right) PTM images of a cluster of spherical gold nanoparticles 90 nm in size. (f) TEM image of a typical cluster of gold nanoparticles. (Figure from [99], reproduced with permission, © 2013 John Wiley and Sons.)

sis, microfluidic electrophoresis, and microchromatography) and, in general, with integrated microanalysis systems (microfluidic systems) [12, 104, 112, 113]. The main advantage of TLM over fluorescent methods is the absence of the need to derivatize most of the studied substances into fluorophores.

Similar to confocal variants of most other optical methods, the maximum signal in confocal photothermal microscopy corresponds to an object in the probe beam waist [97, 98]. However, in photothermal microscopy, the probe beam interacts not with the object itself, as is the case in fluorescence microscopy or Raman microscopy [114], but with a photothermally excited refractive index field around the absorbing object, i.e., with a nanosized thermal lens (*nanolens*) [93, 115]. The most important feature of confocal photothermal microscopy is a nonlinear effect, i.e., a significant (by a factor of 10–50) signal amplification for high radiation fluences due to nanobubbles formed around photothermally excited nanoobjects [99, 116, 117]. The nonlinear optical response is explained by the significant difference between the refractive indices of the bubble and the environment [118, 119]. The lifetime of a photothermal nanobubble depends on heating and power fluence and, for pulsed excitation with a duration of about 10 ns, ranges from 100–200 ns to 300–1000 ns for larger bubbles (1–3 μm in diameter) [117]. An important feature of this nonlinear photothermal effect is that the light absorption or concentration calibration remains linear for a certain energy range after the onset of nonlinearity (up to fluences that are 3–5 times the threshold for the onset of nonlinearity) [99] (Fig. 2).

3.1.2 IR microspectroscopy based on a photothermal mirror. US-based Photothermal Spectroscopy Corp. (USA) announced the release of the mIRrage®, an IR microscope based on the principle of optical photothermal infrared microspectroscopy (O-PTIR), which fills the niche of instruments for thermooptical IR microscopy. Conceptually, the method is very close to photothermal deflection and photothermal mirror methods and is an implementation of their microscale version. A tunable laser beam with a wavelength in the mid-IR range is focused and directed to the surface under study. Sample components in the heated zone absorb IR radiation, which results in the formation of a photothermal element. This element is probed by a more strongly focused laser beam with a wavelength in the visible range, which is collinear to the excitation beam. Owing to tunability, the excitation source can be used for selective measurements and recording of the spectrum. In the case of a nonuniform distribution of IR absorbers, this method enables obtaining images of surfaces with a resolution that depends both on the sample microstructure and on the probe beam size. The manufacturer claims that the method ensures submicrometer spatial resolution.

The method has been used to analyze submicrometer particles of atmospheric aerosols [120] and to visualize the aggregation of amyloid proteins in studies related to Alzheimer's disease [121]. Malignant and nonmalignant lung cells have been studied to reveal the IR spectral differences between these cells placed on standard glass slides, and it was shown that O-PTIR can be used to obtain high-quality IR spectra of cells in both the lipid area (3000–2700 cm^{-1}) and part of the fingerprint area (between 950 and 1770 cm^{-1}) [122]. The opportunities provided by nondestructive O-PTIR analysis of works of art [123] and registration of IR spectra of living cells with submicrometer spatial resolution, in combination with Raman spectra, have been demonstrated, thus providing a complete set of characteristic vibrations of cell components [124].

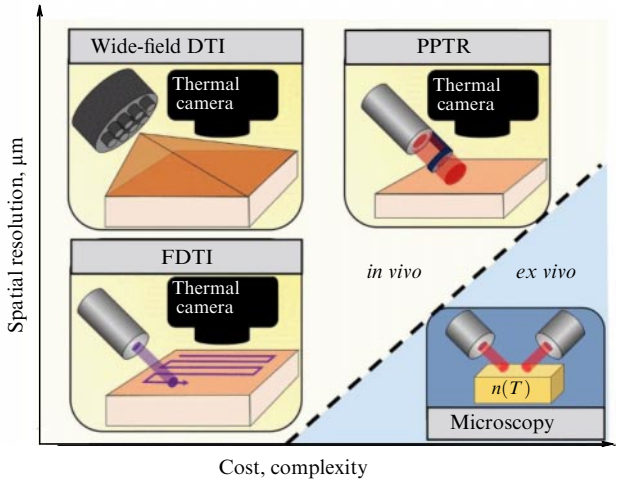

Figure 3. (Color online.) Resolution of dynamic thermal imaging (DTI) depending on the complexity and cost of the experiment for *in vivo* and *ex vivo* conditions [131]. PPTR is pulsed photothermal radiometry, FDTI is focal dynamic thermal imaging.

3.1.3 Thermal mapping. Because OAS and PTS typically feature micrometer or nanometer spatial resolution, they provide highly reproducible thermal mapping or thermal imaging of complex samples. OAS and PTS are used to detect micro- and nanosized defects in various materials, including optical coatings [125], in particular, in bulk heterogeneous materials [126]. The number of particles and their size have a critical effect on the formation of the thermooptical response of solid nanocomposite polymeric materials [127, 128]. In using photothermal radiometry, such measurements often enable determination of the temperature profiles of objects over depth, e.g., for damaged skin [129, 130]. The possibilities of contactless measurement of thermal parameters for diagnosing diseases are considered in [131]. Figure 3 shows a comparison diagram of the resolution of dynamic thermal imaging depending on the complexity and cost of equipment for *in vivo* and *ex vivo* diagnostics.

3.2 Optoacoustic microscopy and tomography

Currently, a significant increase in OAS research in biomedical microscopy, imaging, and tomography *in vivo* is being witnessed [29–33, 84, 132–140]. A discussion of all the material and the biological clinical part of these studies is far beyond the scope of this review, and we confine our consideration to only the key achievements in this area, which shape the general directions of its development.

The penetration depth in optical microscopy for *in vivo* studies in the visible range is limited to a few hundred micrometers. Since ultrasonic scattering in tissue is weaker than optical scattering, optoacoustic microscopy can provide high resolution images at depths greater than other microscopy methods [28, 29, 101, 114]. This advantage fundamentally expands the possibilities of visualization beyond the depth range accessible for optical microscopy, and thus extends the scope of optoacoustic microscopy to biological objects and preclinical and clinical diagnostics [141, 142].

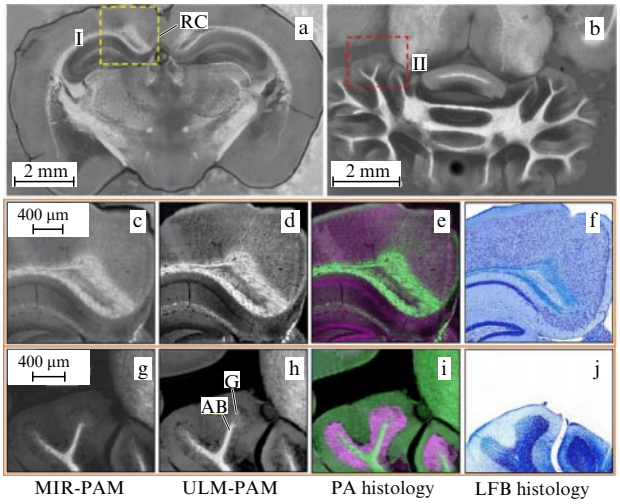

Figure 4. (Color online.) Visualization of mouse brain sections. Distribution of myelin (optoacoustic microscopy in the mid-IR region — Mid-Infra Red PhotoAcoustic Microscopy (MIR-PAM)) in sections 300 μm thick (a) of the brain and (b) of the cerebellum (restrosplenial cortex part of brain (RC)). Distribution of myelin in the brain, an enlarged image of area I, shown in Fig. a: (c) MIR-PAM, (d) ultraviolet localized optoacoustic microscopy (Ultraviolet-Localized MIR-PAM (ULM-PAM)), (e) optoacoustic (PA) histological image, (f) histological image after staining with Luxol Fast Blue (LFB). Distribution of myelin in the cerebellum, an enlarged view of area II, shown in Fig. b: (g) MIR-PAM, (h) ULM-PAM (AB is the arbor vitae, G is the granular layer of the cerebellar cortex), (i) optoacoustic histological image, (j) histological image after LFB staining. In optoacoustic histological images, green color corresponds to myelin and violet corresponds to nucleic acids. In histological images stained with LFB, myelin is shown in blue, and dark blue indicates nucleic acids [146].

3.2.1 Optoacoustic microscopy and mesoscopy. A key task in optoacoustic mesoscopy is the development of multispectral imaging and mapping (see Section 3.3.2) with a high-rate 2D and 3D video signal, which ensures fast spectral differentiation of individual light-absorbing fragments [143]. Approaches to the implementation of optoacoustic mesoscopy have been described, including optoacoustic imaging with acoustic resolution and broadband ultrasonic detection [141, 144].

Optoacoustic microscopy in the mid-IR region provides chemical and structural information about biological samples without staining them. Typically, long wavelengths severely limit lateral resolution due to optical diffraction; in addition, strong water absorption in biological samples results in a high background, low contrast, and low signal-to-noise ratio. To overcome these limitations, the studies use confocal optoacoustic detection of effects excited by a pulsed UV laser with a tunable wavelength (210–280 nm, pulse duration of 10 ns) based on the temperature dependence of the Grüneisen parameter, so-called *relaxation optoacoustic spectroscopy* [145]. For cells, the method provides background-suppressed IR images of lipids and proteins with a spatial resolution at least an order of magnitude higher than the diffraction limit in this spectral range (Fig. 4). The results of a histological study of thick brain sections without staining are presented in [146]. Donor-acceptor conjugated heterocyclic structures operating due to intramolecular charge transfer [147] and porphyrin-like polymer structures in the near infrared (NIR) range, which have an acceptable penetrating ability into tissues and a minimal ability of photobleaching [148], have been studied. The results of the use of functionalized Au, Pd, Bi, Ti, Fe_3O_4, and C NPs have been summarized, and preclinical application of optoacoustic microscopy for the identification of cancer cells using bimodal mapping (imaging) in cancer therapy has been reviewed [149].

The use of optoacoustic microscopy is not limited to biomedicine. In forensic science, approaches to detecting changes made to documents using a setup with a nanosecond pulsed laser, a microphone, and a sample holder have been studied. The signal amplitude depends on the type of writing instrument [150].

3.2.2 Optoacoustic tomography. Optoacoustic tomography (OAT) makes it possible to obtain multiscale multicontrast images of living biological structures, from organelles to individual organs [28, 151–156] (Figs 4–6). The method is based on the optical excitation of biological tissue by a light beam of a pulsed laser to create a thermal and acoustic nanosecond-long pulse [151, 157]. The absorption of the pulse causes an increase in the temperature of ΔT and, consequently, an initial increase in pressure $p_0 = \beta\Delta T/\kappa$ due to thermoelastic expansion, where β is the thermal expansion coefficient and κ is the isothermal compressibility. An increase in temperature of 1 mK results in an increase in pressure of approximately 0.8 kPa, which is above the noise level of a typical ultrasonic transducer. Ultrasonic waves are received by a spatial array of acoustic detectors to form three-dimensional images. In describing the propagation of an optoacoustic wave, a tissue sample is considered a biomechanical system that supports the propagation of mechanical perturbations from one point to another, while, in describing visualization, it is considered a hydrostatic thermodynamic system [158]. The method provides a high signal-to-noise ratio without thermal damage to the tissue. Various implementation options allow scaling the spatial resolution of the method with the required imaging depth in tissues, while maintaining a high depth-to-resolution ratio. As a rule, the spatial resolution is about 1/200 of the image depth, which can be as large as 7 cm. The method provides anatomical, functional, metabolic, molecular, and genetic contrasts of the vascular system, hemodynamics, oxygen metabolism, biomarkers, and gene expression [28, 31, 101, 132, 134, 136, 138, 151, 154, 155, 159–161].

Optoacoustic endoscopy is a minimally invasive tool for visualizing internal organs and tissues. Available solutions provide visualization of the vascular system along the esophagus and intestines using an *in vivo* 3.8 mm endoscope with a pulsed laser (wavelength 584 nm); three-dimensional imaging has been demonstrated [162]. The simultaneous use of optoacoustic and ultrasound imaging in an integrated endoscopic scheme (Nd:YLF pulsed laser, wavelength of 562 nm) has been reported [163]. Using this method, images of plaque in large arteries [164], uterine mucosa [165], and the brain during monitoring of its activity [166] have been obtained.

The *optoacoustic Doppler technique* is suitable for measurements in living tissues with a high spatial resolution down to a depth of several millimeters [8, 167], including functional diagnostics of the human brain [168]. This method enables determination of microvascular blood flow anomalies characteristic of certain diseases.

In general, OAT covers the whole range of approaches, from optogenetics to functional methods, photostimulation, optical dissection, multiscale imaging, microscopy, and struc-

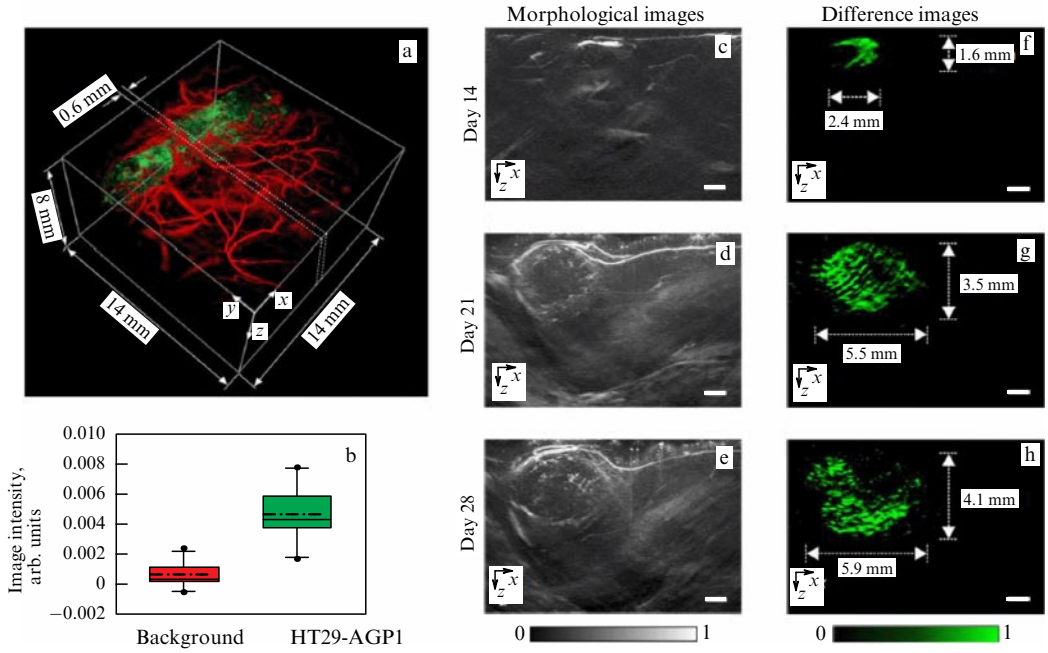

Figure 5. (Color online.) Longitudinal optoacoustic imaging of a subcutaneous tumor expressed with AGP1 (Alpha-1-Acidic Glycoprotein), (a) 3D image of the tumor (green) surrounded by vasculature in the skin and underlying muscle tissue (red) obtained on the 21st day after inoculation. The tumor area is manually segmented for visual clarity. The dotted lines indicate the tissue volume from which cross-sectional image datasets were obtained. (b) Intensities of different optoacoustic images for the background and tumor regions calculated from longitudinal images obtained from five experimental animals. Boxes show medians and 25th and 75th percentiles; error bars represent 10th and 90th percentiles; dashed-dotted line shows the mean value. Paired *t*-criterion for determining the statistical significance of differences in paired measurements yields $p = 0.008$, i.e., the signal for all measured image datasets is significantly higher than the background signal. (c–e) Peak intensity projections of *x*–*z* cross-sectional image sets obtained on day 14, day 21, and day 28 after inoculation. (f–h) Projections of the maximum intensity of *x*–*z* differential images of the distribution of AGP1-expressing tumor cells. Scale bars in panels c–h correspond to 1 mm; color scale shows normalized brightness of the differential image. Image acquisition time is 1.5 hours [175].

tural imaging (hemodynamic, multiphoton, time multiplexing, multiplane microscopy, optoacoustic imaging, near-IR spectroscopy, and the creation of miniature neuroimaging devices for monitoring brain activity) [28, 138, 154, 157, 158, 160, 169].

3.3 Multispectral methods

Despite significant development, PTS and OAS often imply the use of nontunable lasers to generate photothermal and optoacoustic effects. For example, single-wavelength measurements provide a high speed of measurements, and they are expedient when the main chromophore (e.g., hemoglobin or markers for biomedical images) and its absorption characteristics are known or when establishing the thermophysical parameters of media [30–32, 84]. Single-wave versions of OAS and PTS are also used to determine thermal parameters of homogeneous solid materials or to study processes in solutions if a stable and sufficiently powerful excitation without wavelength tuning is required, for which lasers are most often used. However, single-wave measurements have a very significant drawback for an increasing number of problems precisely because of the lack of spectral information about the sample. Variants of multispectral measurements, which use simultaneous or sequential excitation of photothermal and optoacoustic phenomena at various wavelengths (see Fig. 6), are becoming common practice [28, 135, 136, 160, 170–173]. The number of wavelengths in the methods under consideration, primarily in their microversions, is constantly increasing. This has already led to the emergence of multispectral OAS [88, 174], in particular, multispectral optoacoustic tomography [135, 138, 141, 175]. This trend is very similar to that in the development of multispectral methods in fluorescence microspectroscopy and Raman microspectroscopy, which eventually led to a principal breakthrough in the measurements capabilities and the development of hyperspectral methods [155, 176, 177].

In addition, today's progress in technologies has led to the active introduction into practice of less complex photothermal and optoacoustic measurements of optical parametric oscillators (OPOs), quantum-cascade lasers, and supercontinuum sources. The stability of nonlaser sources made it possible to develop instruments on their basis. In IR spectroscopy, both optoacoustic and photothermal measurements based on continuous heat sources have already been implemented. Owing to the advantages of PTS and OAS listed above, they are now as versatile as optical and IR absorption transmission spectroscopy, while maintaining the high sensitivity and precision of PTS and OAS, since stable high-quality laser sources and highly sensitive detectors are used for probe.

3.3.1 Nonlaser thermal-lens spectroscopy of continuous spectrum (white light). Continuous spectrum sources can be used to generate photothermal effects in the visible range. In this case, either a Gaussian distribution of radiation intensity is generated in the initial beam using a spatial filter or a cell is used, in which a temperature profile is established due to a significant difference between the thermal conductivity of its material and the liquid under study [178–181]. For example, the replacement of the excitation laser in a thermal lens spectrometer by a halogen lamp with interference filters provides a tunable and close to monochromatic source in a

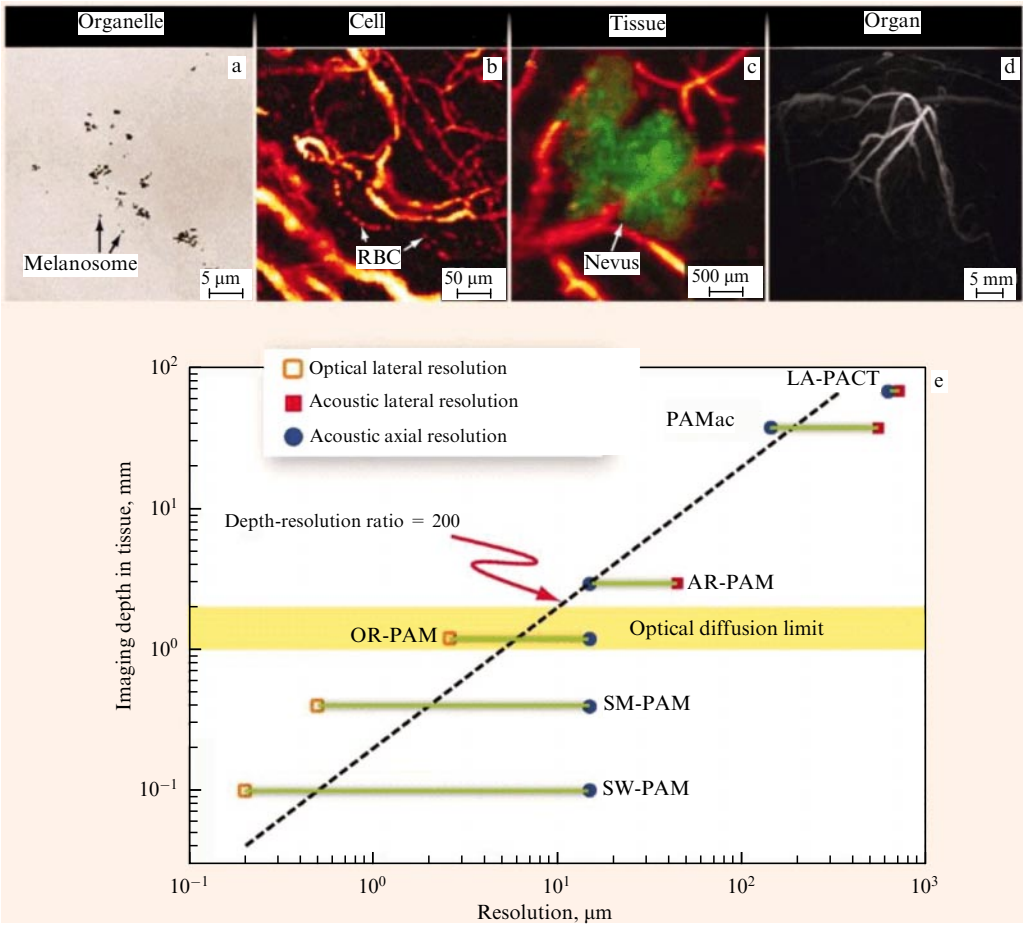

Figure 6. (Color online.) *In vivo* multimodal optoacoustic (OA) tomography of organelles, cells, tissues, and organs. (a) Sub-long-wavelength OA microscopy of melanosomes in a black mouse ear. (b) Single red blood cells (RBCs) in a stream in a mouse ear capillary. (c) Nevus on a human forearm. (d) Computer OA tomography of a human chest. (e) Depth of signal registration as a function of spatial resolution in OA tomography. SW-PAM (Sub-Wavelength PhotoAcoustic Microscopy) is sub-wavelength photoacoustic (PA) microscopy. SM-PAM (Sub-Micron PAM) is submicron PA-microscopy. OR-PAM (Optical-Resolution PAM) is a PA-microscope with optical resolution. AR-PAM (Acoustic-Resolution PAM) is PA microscopy with acoustic resolution. AR-PAMac (Acoustic-Resolution PhotoAcoustic Macroscopy) is PA microscopy with photoacoustic resolution. LA-PACT (Linear-Array PhotoAcoustic Computed Tomography) is computed PA tomography with a linear array. (Figure from [151], reproduced with permission, © 2012 American Association for the Advancement of Science.)

wavelength range of 430–710 nm. A cell for a sample with an optical path length of 1 mm combined with an interference filter form an optical cavity, which yields an additional amplification of the signal [180], thereby enhancing the measurement sensitivity to an absorbance level of 5×10^{-6}. Data are processed by a compact unit on an Arduino platform.

Thus, a simple and compact portable instrument has been developed, which is also suitable for field conditions. The limit of determination of Fe(II) using 1,10-phenanthroline at wavelength $\lambda = 510$ nm is 10 μg L^{-1}, and the average measurement precision is 4%. The versatile character of the instrument has been demonstrated by recording the photothermal spectra of Au NPs and iron(II) 1,10-phenanthrolinate. Study [182] presents a thermooptical microscope with the excitation of a thermooptical element by a white-light lamp, which makes it possible to obtain the light absorption spectrum, including from single particles, without the use of complex laser equipment.

Another way to implement wavelength-tunable thermal lens measurements with nonlaser sources is to use *cylindrical channel cells*. In this case, the excitation radiation passes along the channel of a photometric cell made of a material whose thermal conductivity is significantly higher than that of the measured solution. As a result of the large difference in thermal conductivity, a parabolic refractive index profile is formed in the channel due to the uniform outflow of heat from the irradiated sample through the channel walls [183–186]. The spatial distribution of the refractive index, which depends on the channel size, is a constant parameter of the cell. This signal generation option has a number of advantages. First of all, the signal is independent of source beam parameters, and the signal is only generated due to thermal diffusivity. In addition, the noise level is reduced due to the absence of convective heat transfer. Another unquestionable advantage is the cell volume down to several nanoliters, owing to which this method is attractive for studying small samples. To date, white-light TLS is not fully used, since the experimental methodology has not been completely developed.

3.3.2 Multispectral optoacoustic tomography. For single-wavelength OAS, despite its widespread use in biomedical microscopy and imaging [28, 29, 187–189], as well as in the thermal microscopy of materials [137], the lack of spectral information can be a fundamental problem. This was a driver

for the development in recent years of multispectral optoacoustic tomography, MSOT, based on these methods [133, 135, 190–192]. This technique combines all the capabilities of optoacoustic microspectroscopy and tomography described in Section 3.2 (obtaining images with a spatial resolution of 10–200 μm and high sensitivity) with those of spectral methods (using various chromophores and labels and recording spectra). This advantage makes it possible to obtain in a noninvasive way structural, functional, metabolic, and molecular information about physiological processes in organs and tissues *in vivo*, at both the molecular and cellular (subcellular) levels.

At the current stage, commercial MSOT platforms have been developed that use spherical array detectors, parallel-stream data collection, and rapidly tunable laser sources, which ensure the collection and visualization of spectral information from the entire volume of an object in real time [192]. The foundation for the creation of so-called *five-dimensional* (spatial three-dimensional plus multispectral plus real-time) optoacoustic imaging is already virtually completed, which implies unprecedentedly wide possibilities compared to those of existing biomedical imaging methods [193].

Biomedical applications of MSOT include functional neuroimaging, rapid tracking of the kinetics and biodistribution of agents, studies of the cardiovascular system, monitoring, therapy, and evaluation of drug efficacy and their targeted delivery, as well as molecular imaging [190, 194]. Portable optoacoustic devices provide a high level of accuracy in clinical diagnostics for a number of indications, such as breast and skin cancers, lymph node metastases, thyroid conditions, and inflammatory bowel diseases [159]. Several reviews are devoted to practical applications of MSOT [28, 136, 145, 152, 153, 160].

Companies such as TomoWave Laboratories, Inc. (USA) and iThera Medical GmbH (Germany) have been established, which offer commercial equipment for optoacoustic tomography and MSOT as independent methods of preclinical and clinical diagnostics and in combination with other methods, primarily with ultrasound diagnostics. We are witnessing a sharp increase in interest in MSOT technologies among major manufacturers of spectral and biomedical equipment.

3.4 Optical photothermal nanoscopy

Methods based on the measurement of luminescence and light scattering are poorly applicable to nanometer-sized particles, since the quantum yield of luminescence is often small, and the degree of light scattering by a particle decreases with decreasing particle size. For example, for most particles smaller than 100 nm, luminescence and light scattering are much weaker than light absorption [195]. Conventional methods of electron and scanning atomic force microscopy make it possible to detect NPs, including achieving an atomic-level resolution, but require complex sample preparation and have limitations, e.g., in studying biological objects [196].

Photothermal microscopy methods provide visualization and recording of high-resolution spectra with high sensitivity. However, there is also a limitation related to diffraction in these optical and infrared methods. The corresponding methods of microspectroscopy, thus, cannot be used to study individual objects of submicrometer size; therefore, efforts have been focused in the last 15 years on the development of photothermal methods capable of measuring single submicrometer particles [38].

3.4.1 Photothermal phase contrast. One of the first techniques to be developed was the *photothermal interference contrast method*. The interferometric detection scheme in its microscopic version requires the division of the probe beam into the main and reference beams [197, 198]. This differential contrast is used to detect the photothermal effect caused by single nanosized particles [197, 198]. The method was applied to study 5-nm Au NPs in the bulk of polymer films [197].

Thermal lens microscopy (see Section 1.1) cannot be used for detection in channels with a width and depth of 100 nm, whose dimensions are smaller than the visible light wavelength [111]. A method of thermal lens microscopy with differential interference contrast has been proposed [112]. The channel width problem is solved in this method by enhancing optical diffraction from the nanochannel after light absorption, heat release, heat diffusion, and refractive index change [199]. Heat diffusion into the microfluidic chip substrate also contributes to the signal, allowing the detection of nonfluorescent molecules. This method was used to observe unlabeled protein molecules in the 21 μm × 900-nm channel, with a detection limit of 600 molecules [200]. However, the sensitivity of the analysis is reduced for objects smaller than 900 nm due to thermal diffusion. Photothermal enzyme immunoassay in a 700-nm-wide channel made it possible to detect a countable number of protein molecules [201]. The detection of nonfluorescent sunset yellow dye in channels about 400 nm wide has been demonstrated. The detection limit of 5 μM corresponds to 500 molecules (0.84 zmol) in a volume of 230 aL. Reducing the channel size to 200 nm does not impair the detection characteristics [202].

3.4.2 Photothermal heterodyne spectroscopy and visualization. Somewhat later, a related method was developed, photothermal heterodyne spectroscopy (more correctly microspectroscopy), which is simpler from a technical point of view. In this case, the photothermal effect that occurs when the excitation beam is absorbed by a nanosized object results in the scattering of the probe beam, which is detected as a power fluctuation due to interference between the initial and scattered radiation [72, 203, 204]. This method provides a higher sensitivity than photothermal interference contrast; it is able to detect changes in the thermophysical characteristics of the medium near heated particles and even single large molecules [205]. The method has been used to study aggregates and single Au NPs 1.4 nm in size (about 70 Au atoms) [203], carbon nanotubes [206], semiconductor CdSe/ZnS NPs [207], and DNA molecules [205]. In all cases, single nanometer-sized particles were determined and studied. This method can also be used in the variant of multispectral measurements [208], including the recording of the absorption spectra of single nanosized particles [206] and for mapping [71, 72, 209].

IR photothermal heterodyne imaging is visualization and spectroscopy with ultrahigh resolution in the mid-IR range (2.5–10 μm) [72]. The achieved spatial resolution equal to 300 nm is 30 times higher than the diffraction limit in the IR range. Pioneering study [197] is devoted to the optical photothermal detection of labeled molecules under ambient conditions for fluorescent dyes due to their photobleaching. Optical detection of Au NPs up to 2.5 nm in size has been shown. The mechanism of signal contrast has been established and its capabilities were evaluated using the characteristic bands of polystyrene and poly(methyl methacrylate)

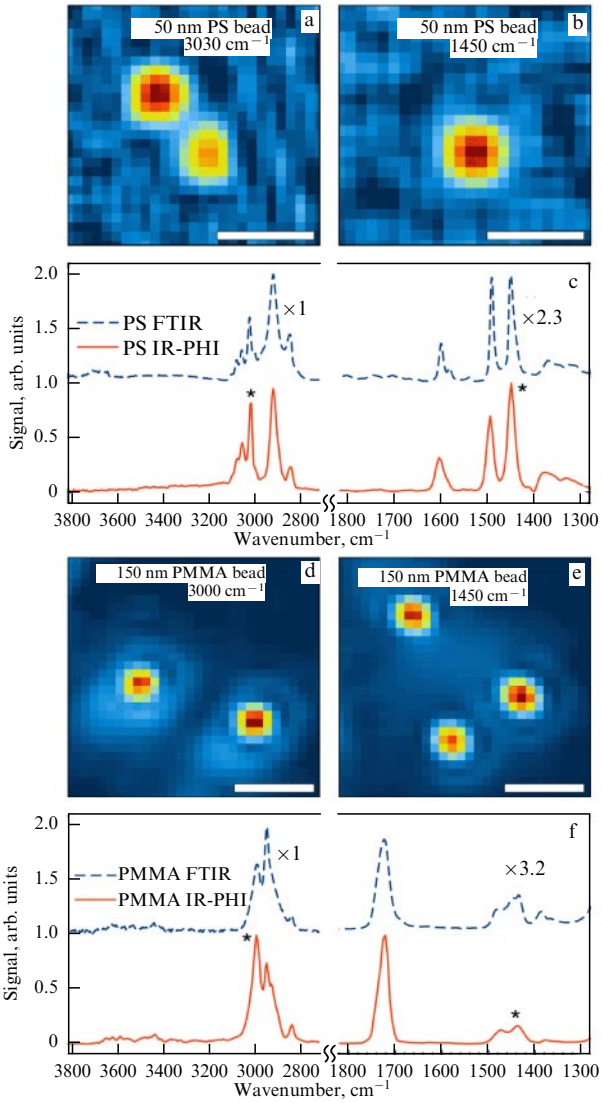

Figure 7. (Color online.) (a, b) IR photothermal (IR-PT) images of single polystyrene (PS) granules with a size of ≈ 50 nm at 3030 and 1450 cm^{-1} using heterodyne measurements. (c) Corresponding PT spectra in comparison with results of IR spectroscopy. (d, e) IR-PT images of single granules of poly(methyl methacrylate) (PMMA) with a size of ≈ 150 nm obtained at 3000 and 1450 cm^{-1}. (f) Corresponding IR-PT spectra compared with results of FT-IR spectroscopy. Scale bars in panels a, b, d, and e correspond to 1 μm. Asterisks in panels c and f label the excitation wavelengths used for IR-PT imaging. PS FTIR — PS, Fourier-transform IR-spectroscopy; PS IR-PHI — PS, IR-PT mapping; PMMA FTIR — PMMA, Fourier-transform IR-spectroscopy; PMMA IR-PHI — PMMA, IR-PT mapping. (Figure taken from [210], reproduced with permission, © 2020 AIP Publishing.)

[210] (Fig. 7). The quantitative relationships between the observed signals and the photothermal parameters of the samples have been determined. In particular, an analysis of a dimensional series of polystyrene granules has been carried out to quantitatively relate the photothermal signal from a contrast agent to the heat capacity of the sample, the thermooptical coefficient, and the light absorption and light scattering cross sections [211].

3.4.2 Photothermal correlation spectroscopy. Another measurement option based on the principles of photothermal heterodyne spectroscopy is *photothermal correlation spectroscopy*[2] [24, 212, 213], based on the construction of the autocorrelation function G for a time-resolved photothermal (in the first approximation, thermal lens) signal $S(t)$:

$$G(\tau) = \frac{\langle S(t)S(t+\tau)\rangle}{\langle S(t)\rangle^2}.$$

Provided that the characteristic times of the instrument (e.g., the time constant of a lock-in amplifier) are known, the function $G(\tau)$ can be used to obtain the characteristic times τ of heat release during photothermal excitation. Since photothermal processes for NP dispersions depend on the thermal and optical properties of NPs and their velocity, photothermal correlation spectroscopy is used to detect, monitor, and characterize such objects [93, 115, 214].

In fact, a single absorber particle acts as an analogue of a 'macro-thermal lens,' i.e., a *nanolens*, which can be detected using the scattering pattern of probe radiation from a *halo* (thermally induced field from a heated single particle) (Fig. 8). The combination of the nanolens concept and correlation spectroscopy is a microscopic analog of differential photothermal measurements (see Section 2) — *twin-focus photothermal correlation spectroscopy* [215], which is based on the detection of two spatially separated sample volumes that correspond to the beam configuration (as for photothermal Z-scanning) and the construction of two autocorrelation functions for each of the volumes separately. Similar to differential TLS methods with a large dynamic reserve, this method is used for sensitive and high-precisions measurements. It provides measurement of the slow motion of particles along a beam propagation axis or detection of any small spatial inhomogeneity with a spatial resolution better than the diffraction limit. This is due to the enhancement of differences between photothermal responses in two equal microvolumes, one of which is used as a reference sample [24, 115, 213–215].

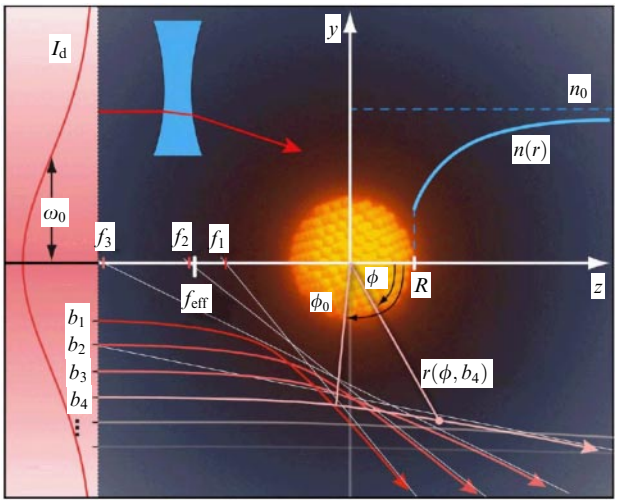

Figure 8. (Color online.) Nanolens formation principle. A heated nanoparticle creates refractive index profile $n(r)$, which forms a thermal lens. A treatment with ray-optics provides a focal length when probed by a confined Gaussian beam (see details in [214]). For typical material parameters, focal lengths f are much larger than size R of the particle, $f \gg R$ [214].

[2] Since this method is based on microscopic instruments, it is more correct to call it "photothermal correlation microspectroscopy."

3.5 Probe-based photothermal microspectroscopy (nanoscopy)

The methods described in Section 3.4 primarily refer to studies of solutions or single NPs located on a surface. However, studying the solid state is a problem of no less importance. Analysis of chemical compositions and physical and mechanical properties *in situ* is needed in materials science and for many environmental objects, in particular, soils and minerals. These problems can be resolved using *photothermal probe microscopy* (otherwise referred to as *photothermal resonance spectroscopy*), which, despite its name, significantly differs from both absorption spectroscopy (microspectroscopy) and photothermal spectroscopy methods described above, and is actually a version of probe microscopy. To obtain signals, probes are used that are employed in thermal microscopy methods (scanning atomic force microscopy (AFM), scanning thermal microscopy (SThM), or scanning near-field optical microscopy (SNOM)).

3.5.1 Photothermal IR microscopy. Photothermal probe microspectroscopy is based on the detection of short-duration and local dilatation of a sample under resonance heating with a lamp, an IR source, or — preferably — a (tunable) laser. The main sources of excitation are laser sources, such as CO_2-lasers [216, 217] or, lately, quantum-cascade lasers. To improve the quality of the spectra, synchrotron sources of IR radiation are used [218]. The absorption of the pulse by the sample leads to local heating and broadening of the sample (photothermal signal) and deflection or movement of a high-frequency cantilever [35, 219]. Cantilever deflection is used to measure the forces between the probe tip and the sample and thus for topography with nanoscale lateral resolution [35, 219, 220].

Since the resolution depends on the probe size and thermal properties of the sample, rather than on the IR radiation wavelength, these methods make it possible to obtain spectra with a spatial resolution of down to 20–30 nm or better, which significantly exceeds the capabilities of IR spectroscopy methods for condensed media. The resolution is also affected by the finite thermal conductivity of the probe, the finite dimensions of the contact area between the probe and the sample, the complex temperature distribution in heterogeneous media, and the change in the absorbed heat flux depending on time and wavelength.

Photothermally induced IR resonance or Atomic Force Microscope-InfraRed spectroscopy (AFM-IR) is one of the most widely used methods of photothermal probe spectroscopy [221, 222]. An AFM probe in the contact mode is used to measure the dynamics of thermal expansion due to the absorption of an infrared radiation pulse by the sample. The objects under study placed on a transparent prism are irradiated in the total internal reflection mode to minimize the direct interaction between the excitation beam and the AFM probe (Fig. 9).

Photothermal spectra, which depend on the light absorption coefficient, are similar to conventional IR spectra [223]. Therefore, they can be used with IR spectra libraries. Similar to OAS, the changes in the spectra of photothermal probe spectroscopy, in contrast to those in other versions of IR spectroscopy, are associated with thermal factors and the formation and propagation of thermal waves. The spectra can exhibit photothermal saturation (suppression of peaks in the spectrum) due to violation of the linear dependence between the signal magnitude and the absorption coefficient at high values of the latter [223]. In addition, differences in the shapes of band intensity are caused by the characteristics of

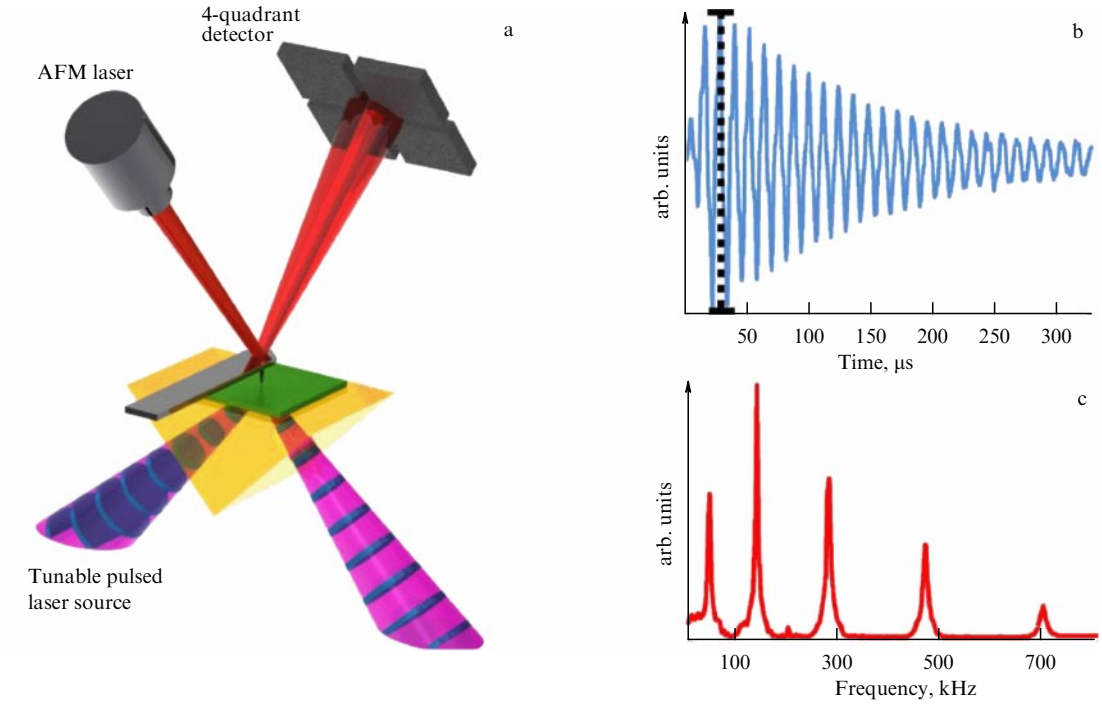

Figure 9. (Color online.) Measurements with an IR photothermal probe. (a) Sample exposed to IR laser pulses (depicted at the bottom left of the figure) expands rapidly deflecting the AFM cantilever, which is optically detected by a four-quadrant detector. (b) Maximum peak-to-peak deflection of the cantilever, which is proportional to the absorbed optical energy, is used to generate signals. Sample and the cantilever have time to return to the equilibrium state before excitation by the next pulse begins. (c) Fourier transformation of a ring down signal provides the amplitude of the different contact resonance modes excited by the sample expansion [221].

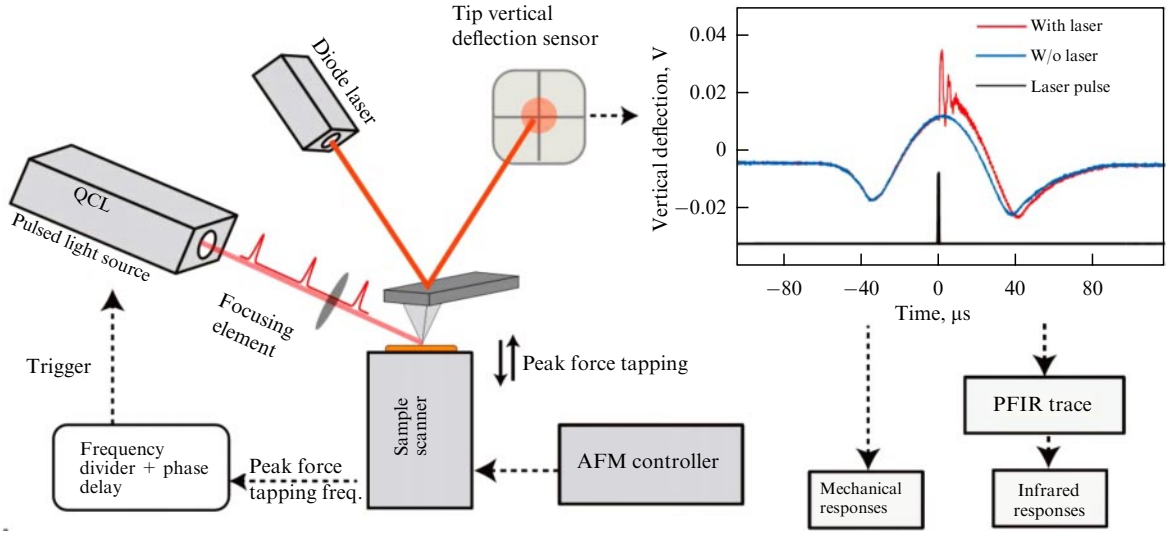

Figure 10. (Color online.) Schematic diagram of PFIR microscope operations. Inset in the upper-right corner of the figure shows gate-averaged traces of vertical deflections of the cantilever with (red curve) and without (blue curve) laser interaction. Pulse timing of the IR laser (black curve) is chosen to be within the contact regime of the peak force tapping cycle [229].

preparation of solid samples. Finally, the reason for the low quality of the spectra is the insufficient intensity of IR radiation in the sources of commercial instruments. A solution to this problem is to use powerful sources, which are laser sources, e.g., a CO_2-laser [216] or a tunable pulsed OPO [217]. In addition, replacing a globar with a more powerful source significantly reduces the measurement time.

In the case of probes for microthermal analysis, the photothermal spectra of the probe with a material sample fixed on it are recorded [216]. Such spectra are distinguished by a high level of noise, but the main characteristic bands, e.g., C–H stretching vibration bands, are clearly visible. The undoubted advantage is the ease of cleaning the probe by transferring the sample substance into solution. A resolution higher than that of the SThM probe is provided by a probe in which a tiny truncated pyramid, on the flat top of which is a 150×50-nm palladium element, performs as a sensor [218]. A disadvantage of suchlike probes is the low signal intensity compared to that of the SThM probe.

Another method that combines the capabilities of IR spectroscopy and an atomic force microscope is called *photothermal IR microscopy*. In this case, the SThM probe is not located on a conventional movable stand but is part of an atomic force microscope. A special design of a built-in AFM instrument has been developed, which can be placed directly in the cell compartment of most IR spectrometers [224]. The method makes it possible to obtain an AFM image of the sample surface along with its photothermal spectrum. The sensitivity of the method is higher than that of the photothermomechanical method, which uses conventional AFM probes as sensors. The range of objects is rather diverse, but studies of the spectra of polymeric materials are the most common practice [216]. In addition, more complex problems have been solved: identification of hidden polymer layers and determination of the dependence of the layer signal on the coating thickness [223]. Paper [223] reports on the study of actual objects: fungicides in the form of a finely dispersed powder and aqueous solutions of surfactants. The spectra of the latter were recorded by introducing a probe into microdroplets formed on glass after partial evaporation of water. Using the example of paracetamol, the possibility of determining pico- and femtogram amounts of a chemical compound was demonstrated [224]. The results of studying objects with complex geometry, such as human hair [224] and a copper wire coated with a polymer layer, are also presented. An analysis of the spectra of the polymer coating made it possible to identify material 3 μm thick and the impurities it contains.

An important area for the use of photothermal IR microspectroscopy is the development on its basis of a method for diagnosing cancer [225–227]. Such diagnostics are based on analyses of the vibrational spectra of cells. The presence of cells with pathologies is determined by spectrum distortion [225] (DNA spectra can be recorded separately). The photothermal IR microspectroscopy method makes it possible to observe the cell life cycle and the distribution of sample cells over cycle phases [225].

An enhancement of this technique is *time-resolved IR microspectroscopy, PFIR* (PeakForce IR) [228, 229]. In this method, pulses of a frequency-tunable IR quantum-cascade laser are directed onto an AFM probe and sample area in Bruker PeakForce Tapping™ operating in the imaging mode at low frequencies, 1 or 2 kHz (Fig. 10). This ensures controlled contact of the probe tip with the sample; the excitation pulses are synchronized with each peak force cycle of the cantilever contact resonance [229]. The absorption of IR radiation by the sample results in volumetric thermal expansion, which excites the contact resonance of the cantilever. The volume expansion is maintained for a certain time. The position sensor detects the time-resolved deflections of the cantilever both after and without the laser pulse. The difference between them is the PFIR signal due to the photothermal excitation of the sample. According to [229–231], a time-resolved PFIR curve contains three sections: (1) excitation of contact resonance, (2) shift of the baseline due to volume expansion during the photothermal effect, (3) change in the curve slope after the excitation pulse, associated with the rate of thermal dissipation due to local thermal conductivity or with possible changes in the sample after absorption. The amplitude of the contact resonance

oscillation is proportional to local IR absorption. Similar to other methods of photothermal probe spectroscopy, a Fourier transform is used to obtain a signal. PFIR provides a spatial resolution of < 10 nm [229].

Regarding measurement methodology, the main characteristics of photothermal probe spectroscopy are similar to those of IR microspectroscopy methods: sample preparation is minimal or absent, and the methods are nondestructive and suitable for spectroscopic measurements of complex heterogeneous samples. The methods of photothermal probe spectroscopy make it possible to study small amounts of substances. These methods are applicable to inhomogeneous solids less than 1 μm in size with simultaneous mapping of both inorganic and organic components with a spatial resolution of about several ten nanometers [232, 233]. In the analysis of minerals and soils, this provides an important advantage over, e.g., pyrolytic techniques for determining chemical composition, which require the sample to be heated to several hundred degrees Celsius. Similar to microspectroscopy techniques, photothermal probe spectroscopy methods provide images with a resolution higher than that of conventional FT-IR techniques (although not for all samples), and further increases in spatial resolution can be expected due to progress in this technology [234].

The capabilities of photothermal probe spectroscopy have led to the appearance of commercial Bruker desktop instruments, which are used in applied research [235, 236]; a detailed review of the application of photothermal probe spectroscopy in studies of interfaces and materials science has been published [237].

3.5.2 Cantilever thermal deflection spectroscopy. In the 1990s, another variant close to photothermal probe spectroscopy based on photothermal deflection, photothermal cantilever deflection spectroscopy (PCDS), was developed. The method was designed to provide high sensitivity and selectivity using portable sensors for highly sensitive determination of trace substances in the gas phase [238]. Miniature sensors such as microcantilevers feature high sensitivity but poor selectivity. On the other hand, many spectroscopic methods provide high selectivity but are not very sensitive. This problem can be removed by combining PDS and a microcantilever made of two materials. The method is based on the use of such a microcantilever as a sample carrier. Molecules of target substances are adsorbed on the cantilever due to physisorption. A beam of monochromatic IR radiation from a laser or a nonlaser IR source is absorbed, resulting in resonant excitation of molecules and nonradiative processes of its relaxation. This raises the cantilever temperature and leads to a change in its bending, which can be measured using an optical scheme similar to PDS [239]. The cantilever deflection depending on the wavelength of the excitation radiation corresponds to the IR absorption spectrum of the adsorbed molecules. The latter ensures high selectivity with absolute detection limits at a level of subnanograms, in particular, for explosives: pentaerythritol tetranitrate, cyclotrimethylenetrinitramine, and trinitrotoluene [240, 241]. Details of laser PTS and OAS hardware for remote measurements are discussed in review [242] and book [2].

PCDS has been used to selectively and sensitively detect complex hydrocarbons such as naphtha adsorbed on a cantilever. The spectra of polychlorodibenzofurans agree with the spectra obtained by conventional IR spectroscopy [243]. The method makes it possible to simultaneous extract information about the mechanical and chemical properties of films. For example, the nanomechanical IR spectra of a microcantilever coated with poly(methyl methacrylate) (PMMA) are in good agreement with the IR spectra of PMMA on a gold-coated silicon wafer. Photothermal measurements can be used to study the processes of photodegradation of materials caused by UV irradiation, which cannot be implemented using standard versions of IR spectroscopy [244].

One of the most recent developments in this area is aimed at imaging with submicrometer spatial resolution based on a commercially available inverted microscope [245]. The authors called the method *mid-infrared photothermal microscopy* (*MIPS*). This is an interesting implementation of multispectral photothermal probe microspectroscopy. The capabilities of the method for obtaining images of complex organic materials (drugs) and visualization of living cells have been demonstrated [246, 247].

4. Determination of the properties of materials

Determination of the properties of materials was always one of the main tasks in the development of photothermal and optoacoustic methods. Lately, the number of applications in this area has been continuously increasing, including the study of the properties and assessment of the physicochemical parameters of many types of new materials [248]. This section presents the most typical examples, such as the determination of thermophysical and optical and spectral characteristics for materials science.

4.1 Thermophysical parameters

The coefficients of thermal diffusivity and thermal conductivity are the main thermophysical parameters. Thermal conductivity is of importance in solving many engineering problems: heat transfer in electronic devices, nuclear reactors, aircraft and spacecraft, etc. [73, 249]. Stationary or equilibrium methods for determining the thermal conductivity coefficient are primarily implemented in facilities and equipment for solid samples with fixed geometric parameters. Nonstationary methods for determining thermal diffusivity are now widely used due to the speed of measurements (the thermal conductivity coefficient is calculated in an indirect way). However, to obtain reliable results by nonstationary methods, measurement conditions should be strictly observed, and in calculating the thermal conductivity coefficient based on thermal diffusivity, bias in determining the density and heat capacity using third-party methods must be taken into account. Photothermal methods, which are singled out among nonstationary methods, are related to both optical molecular and thermal spectroscopy and provide high accuracy, precision, and multisignal measurements.

4.1.1 Thermophysical parameters of liquids. Standard methods for measuring the thermal conductivity of liquids (the method of hot plates, the method of coaxial cylinders, the hot wire method, the 3ω-method, the hot-disk method, the temperature oscillation method, and the laser flash method) have been known for a long time. At present, the selection process is greatly influenced by the availability of a commercial solution, which greatly simplifies the obtainment of results. In addition, an advantage is the availability of relatively inexpensive equipment that allows conducting rapid measurements, e.g., the KD2 Pro instrument (Decagon Devices,

Inc., USA) based on the hot wire method, which provides an accuracy of measuring thermal conductivity of ±5% in the range from 0.2 to 2 W (m K)$^{-1}$. However, when complex objects such as colloidal systems are the subject of study, simplicity and versatility can be sources of incorrect data.

An assessment of photothermal methods for determining the thermal conductivity of liquids shows that they are promising for a comprehensive analysis of both homogeneous and heterogeneous media. Basically, their task is to determine the thermal diffusivity or thermal effusivity. The advantage for colloidal solutions is that the photothermal spectroscopy signal depends on the thermophysical properties of the object and its thermal heterogeneity.

The *photopyroelectric method*, which is a contact method, is based on the use of a pyroelectric detector. Modulated laser radiation causes heating of the sample due to light absorption. When temperature fluctuations reach the sensor–sample interface, an electric current is induced in the sensor, yielding information about the structure and the thermal and optical properties of the sample. Two detection configurations are available: frontal for measuring thermal effusivity and rear for thermal diffusivity. The method is used for liquid samples, since, in this case, the thermal contact between the sensor and the sample can be considered ideal. As a result, the accuracy of determining the thermal conductivity and thermal effusivity is 2 and 1%, respectively, and the precision is about 2% [26]. The method is inexpensive, and measurements require a small (0.2–0.3 mL) sample volume and little time (several minutes), which is of importance for dispersed systems [250]. The method is used to measure the thermal effusivity of colloidal solutions (Al_2O_3 and CuO NPs stabilized in various solvents), sometimes in combination with thermal lens spectrometry [251, 252].

Thermal-wave interferometry or a *thermal-wave resonator cavity* is a variation of the photopyroelectric method (rear configuration). The method uses pyroelectric detection of thermal waves propagating through the gap between a pyroelectric sensor and another material acting as a source of thermal waves (modulated laser radiation directed at a metal foil). Two operational modes are supported: one with a constant gap length and the other with a constant frequency. In both cases, resonance-like extrema of thermal waves are observed, the location of which can be used to determine the thermal diffusivity [253]. Usually, the dependence of the signal amplitude on the gap length is recorded, and a linear approximation is plotted in semi-logarithmic coordinates to find the thermal diffusivity from the slope of the curve. The analysis requires up to 15 mL of liquid, the precision is 1%, and the accuracy is 1–2% [254]. The method is used for colloidal solutions: Au NPs in water, ethanol, and ethylene glycol [255]; Ag NPs in water [256]; and TiO_2 dispersions in polyvinyl alcohol [257].

Optoacoustic detection makes it possible to determine the thermal diffusivity coefficient and thermal effusivity. Initially, this method was used for solid samples and gases [48] and, later, for liquids. Typically, an 'open optoacoustic cell' is used, in which the frontal configuration is intended for determining thermal effusivity [258] and the rear configuration, for thermal diffusivity [259]. When the modulated laser radiation is absorbed, the sample is heated, and the sound waves propagate, being recorded by a microphone. The methodology for measuring the thermal diffusivity of solid samples consists of recording a signal from the laser modulation frequency; in handling with liquid samples, the signal at a certain frequency is analyzed as a function of the thickness of the liquid layer. Usually, both the amplitude (its logarithm) and the phase shift of the optoacoustic signal with respect to the laser pulse are recorded. These dependences on the thickness of the liquid layer are described by two straight lines, the slopes of which are inversely proportional to the square root of the thermal diffusivity of the liquid. In handling liquids, a special glass seal is used, so there is no contact between the liquid and the sensor, which implies that there is no restriction on the type of liquid [259].

The method has been applied to heterogeneous liquids [260]. The thermal diffusivity coefficients are determined for aqueous colloidal solutions containing Au NPs [261] and Al_2O_3; the accuracy and precision of determining the thermal diffusivity are 1–2% and 2%, respectively [262]. A 'closed' optoacoustic cell was used to determine the thermal diffusivity and thermal effusivity of aqueous colloidal solutions of TiO_2 and Al_2O_3 [263]. The optoacoustic method with piezoelectric detection was used to study dispersions that contain carbonyl fluoride mesoparticles [264]. The thermal-wave interferometry method was used to measure the thermal diffusivity of samples, while the open optoacoustic cell method was applied to determine the thermal effusivity of aqueous colloidal solutions containing silver nanorods [265].

The *photothermal deflection* method for determining the thermal diffusivity of liquids is rarely used. A collinear configuration was used for aqueous solutions of magnetic NPs [266]; the thermal diffusivity was determined against water. A perpendicular configuration was used to determine the thermal diffusivity of paraffin oil; however, since the heat diffusion depth in liquids becomes small as the excitation laser frequency increases and only results in the deflection of part of the probe laser beam, the theoretical model needs to be modified [267]. This is one of the main drawbacks of the method [59], and so far the number of studies on its application for determining the thermal diffusivity of liquids is limited.

Separately, the methods of *thermal diffraction spectroscopy* (*dynamic thermal gratings*, transient thermal grating) [268, 269] should be singled out; they are based on the pulsed heating of a sample due to the formation of a spatially periodic structure of a thermally induced grating formed by the intersection of two beams of a pulsed laser and the closely related methods of a *traveling wave* [270] and *thermal reflection* (thermoreflectance) [59, 271]. Pulsed thermal expansion is accompanied in thermal diffraction spectroscopy by acoustic waves (usually an acoustic response occurs in the first 300 ns) and a dynamically changing refractive index pattern with a certain spatial period (diffraction grating). This leads to diffraction of the continuous probe beam. The method is complicated from the instrumental and analytical points of view, but it was used to determine the thermal diffusivity of liquids [272, 273], Ag NPs in water [66], Al_2O_3 NPs in n-decane and polyalphaolefin [274] and the speed of sound in these substances, as well as characterization of the anisotropy of materials [275]. The time scale of the method is several microseconds; a slower (several milliseconds) variant is the method of *stimulated Rayleigh scattering*. It is used to determine the thermal diffusivity of water (estimation accuracy is about 2%) and colloidal solutions: Al NPs in water and Al_2O_3 NPs in engine oil at various temperatures [276]. A comparison of the results with data obtained by the hot wire method for close values of concentration revealed significant disagreements [276]. The

thermooptical method shows a much smaller increase in the thermal conductivity of the nanofluid [3] than that of the base fluid.

Photothermal radiometry is rarely used to study liquids; examples of practical importance include water and sunflower oil. The possibility of working with small (~ 0.5 mL) volumes and the absence of convection are distinguished as advantages, since the temperature change during measurement can remain small (2 K). This is not true for the laser flash method, the instrument design of which is very similar. In approximating experimental data with a model (frequency dependence of the phase shift), the density and volumetric heat capacity of the object must be known to determine the thermal conductivity with a precision of 3–5% [277].

The most common and universal method for liquid media is *thermal lens spectrometry*. In recent years, the emphasis on its use for the characterization of materials has shifted towards more complex multicomponent systems and heterogeneous media [74, 251, 278–282]. For both homogeneous and heterogeneous media, the thermal diffusivity is obtained from the characteristic time (several milliseconds) of thermal lens development, which is determined as a fitting variable in approximating experimental data by the theoretical equation of the transient thermal lens signal for a homogeneous medium. For calculations, only the probe laser beam radius in the sample is needed, the measurement of which can introduce inaccuracy; therefore, measurements are sometimes used relative to a reference sample with a known thermal diffusivity, water [281], or toluene [282]. Occasionally, the thermal conductivity is obtained from a steady-state signal, but should this be the case the refractive index temperature derivative must be known for each sample [283].

Basically, the available data pertain to the determination of the thermal diffusivity of two-phase systems containing NPs of metals and their oxides. An increase in thermal diffusivity is usually observed with concentration [279, 281, 284] and size [74, 280] of nanoparticles; however, results with opposite patterns are known [278, 285]. Studies of variously shaped Ag NPs stabilized by micelles of cetyltrimethylammonium bromide have shown that rod-shaped NPs improve the thermal diffusivity most efficiently [286]. It should be noted that, for colloidal solutions with similar compositions, the increments in the thermal conductivity coefficient differ greatly, and the regularities of the dependences of the thermal properties on concentration and size do not agree. This situation is typical of dispersed systems, regardless of whether thermal or optical methods are used, and it can be associated with different physicochemical properties of two-phase liquids. Nevertheless, these disagreements may be the result of obtaining incorrect data due to the use of standard homogeneous models of the thermal lens signal, which probably need to be corrected, as has been done in [287].

In concluding this section, we emphasize the following limitations and disadvantages of photothermal methods for determining the thermophysical parameters of liquids: similar to all nonstationary methods, they enable determining thermal diffusivity (to calculate the thermal conductivity coefficient, third-party methods are needed to determine the density and specific heat of the object under study). Any photothermal spectrometer is characterized by a certain dynamic range in terms of the absorption coefficient; therefore, to make measurements for highly concentrated (strongly scattering) solutions, it is necessary to reduce either the optical path length or the excitation laser power. Both of these factors lead to a loss in measurement precision. Since most of the methods are time resolved, the processing of a large amount of data for dispersed systems requires considerable time and consideration of additional factors. In addition, many photothermal methods were originally created for testing solids, and, for liquid media, the setup configuration should be changed or special cells should be used. Finally, there is a limitation, which seems to be one of the most important: the theoretical basis of many photothermal methods is based on models for homogeneous media; thus, for heterogeneous liquids, rather significant development of more complex models of photothermal effects is required.

4.1.2 Thermophysical parameters of solids. Photothermal methods are one of the few contactless methods for studying the thermal and optical properties of solid materials (polymer nanocomposites, glasses, and crystals) [20, 288–291]. PTS is used for opaque samples with smooth and rough surfaces, and transparent substances, including films, and for studying interfaces [292]. Modern laboratory facilities and experimental setups provide 2D images of the surface and 3D images of near-surface layers (see Section 3), owing to which photothermal analysis is highly informative.

TLS, as a method with a simple hardware design, is used to measure the thermooptical parameters of materials for optical devices. For example, the thermal diffusivity and the temperature coefficient of the optical path length (ds/dT, which describes the thermal distortion of a laser beam as it passes through a sample [36]) in Er_2O_3- and Nd_2O_3-doped glasses were determined in [293–295]. The method makes it possible to carry out measurements at various temperatures [295]; the limitations are related to the sample thickness and light transmission (thin plates up to 0.3 cm with an absorbance up to 0.2 can be used) [296]. Study [297] examined fluoride crystals (CeF_3, KTb_3F_{10}, etc.) as potential optical insulators instead of conventional crystals using TLS in the parallel-beam mode with continuous irradiation. The thermooptical coefficient of crystals was measured in Ref. [298] by comparing the slopes of the probe beam phase shift versus the excitation radiation power. It is shown that the calculations of focus shift using TLS are in good agreement with the theory, differences being only observed in the high power region due to a change in the beam shape. It should be noted that the thermal lens effect arising in solid-state laser crystals upon reaching high power values requires a detailed understanding of the physics of these processes, and photothermal spectroscopy, in particular TLS, is currently the main tool for such studies [299, 300].

In the optical schemes, where components (lenses, crystals, mirrors, etc.) are exposed to a strong thermal effect of laser radiation, crystals with a low absolute value of the temperature coefficient of refractive index (dn/dT) should be selected. Owing to the possibility of studying thermooptical and optical parameters (absorbance) and the temperature coefficient of the optical path length of glasses, crystals, and films, TLS is an informative method for this purpose [301, 302].

The advantage of OAS, also over many methods of photothermal spectroscopy, is that it can be used to study

[3] A nanofluid (NF) is a colloidal solution that consists of a base liquid (a solvent) and nanoparticles dispersed in the liquid that improve the thermal conductivity of the entire system.

samples with a high absorption coefficient, layered or containing strongly scattering particles (composite materials, films, etc.) [303], which it is difficult or impossible to analyze by conventional transmission and reflection methods (e.g., spectrophotometry) [304]. Two conditions can be distinguished among the limitations of OAS, which must be met to obtain a significant optoacoustic signal: (1) the sample thickness is several tenths of a millimeter; (2) absorbed light power is ~ 1 W. Violation of these requirements can result in periodic deformations of the sample, which affect the signal [305]. The thermophysical parameters of the $CdTe_xS_{1-x}$ nanocrystalline composite have been calculated. It has been shown that the thermal diffusivity D and the thermal conductivity coefficient k for a nanocomposite are an order of magnitude greater than for a macrocomposite of the same composition [306]. Study [307] showed the possibility of using OAS to determine the thermal diffusivity and porosity of natural rocks.

OAS does not require pretreatment of samples [308], in contrast, e.g., to UV-visible spectroscopy, for which samples must be sufficiently thin, transparent, and uniform and have a smooth surface. OAS is applicable to study the optical, electronic, and thermal properties of opaque, rough, and highly reflective materials. OAS was used to study the optical properties of three-component doped $CdTe_xS_{1-x}$ quantum dots. The obtained optoacoustic absorption spectra agree with the data of UV-visible spectroscopy, and the particle sizes estimated using optoacoustic spectra are consistent with the data of transmission electron microscopy [306].

Thermooptical properties of solids are studied using PDS. To use theoretical models, it is necessary to compare the light penetration depth with the heat diffusion depth (optically opaque in the case of a large heat diffusion depth and transparent samples) and the sample thickness with the heat diffusion depth (thick, if the thickness exceeds the diffusion depth, and thin samples). For each case, it is possible to determine the thermal diffusivity from linear relationships between the measured value and the geometrical parameters of the optical scheme [309]. For example, the method was used to determine the thermal conductivity of the BGaAs ternary alloy [310] and the temperature dependence of the thermal diffusivity of lithium-ion cell electrodes [311]. Of interest is the use of PDS to study the heating and cooling of a sample by laser irradiation in creating and using optical elements [312]; if the probe beam is deflected towards the excitation beam, then cooling occurs; if vice versa, heating occurs.

The group of *thermal reflection* methods is based on the use of a powerful pulsed laser as a source of periodic heating and a probe laser to control the surface temperature by changed reflection. These methods, which differ in experimental configurations and analytical models, were developed to determine the thermal conductivity of both bulk samples and thin films and for thermal resistance at the interface [59].

Photothermal radiometry methods are also used to study thin films on a substrate, which are used in electronics, aerospace, and various industries. Here, of importance are not only the thermophysical properties of the film itself but also the processes that occur at the film–substrate interface. For example, PTR is used to estimate the thermal conductivity of GeTe-based thin films [313] with an accuracy greater than that of other methods. Two PTR versions, with continuous-beam modulation and pulsed, were used to determine the thermal conductivity of CrN films on silicon substrates, the thermal resistance at the film–substrate interface, and the specific heat of the films. The last is consistent with the heat capacity of a bulk material, since, in contrast to the thermal conductivity coefficient, the specific heat primarily depends on the chemical composition and nature of the material and, to a lesser extent, on its microstructure [314].

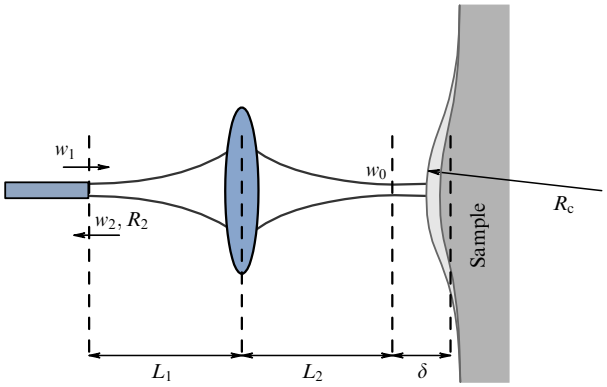

Figure 11. (Color online.) Optical setup [315]. Excitation and probe beams emerge from the optical fiber and are focused at distance δ from the sample surface. Excitation beam heats the surface, which, expanding, creates a curved profile with radius R_c. Probe beam is reflected back and partially collected by the same fiber; w_1 is the probe beam waist at the optical fiber end, w_0 is the probe beam waist in front of the sample, w_2 is the size of the returning probe beam in front of the fiber, where it has a phase shift, with radius R_2.

To study the distribution of thermophysical parameters of complex polymer composite materials, *photothermal reflection microscopy* is used [34, 315]. Used as the signal is the intensity of the probe laser beam reflected from the photothermally heated sample surface (Fig. 11). The method makes it possible to obtain thermal diffusivity maps with micrometer spatial resolution. Such mapping shows the distribution of pores and microbumps on the surface.

4.2 Diffusive mass transfer

The thermal lens signal for liquid samples can be poorly described by a theoretical model due to the thermally induced concentration gradient (diffusion mass transfer). This effect is well pronounced for multicomponent objects. TLS makes it possible to determine the mass diffusion coefficient D_m, which is related to dynamic viscosity [316]. The D_m value can be used to control the quality of materials such as fuels and foodstuffs. The Soret effect, which yields an additional signal, especially in the case of a minimal addition of the second solvent, can be 25% of the signal. The characteristic time of thermophoresis is 200–400 times higher than that of development of the thermal lens [1], which makes it possible to separate the signal into components.

Photothermal methods are also used to study the dynamics of nonequilibrium thermal processes. Thus, the nanosecond dynamics of vapor nanobubbles formed in a liquid around nanoparticles during plasmon heating was observed [317]. Vapor nanobubbles, which are nonlinear objects with nanosecond-scale dynamics, are very sensitive to external perturbation. For example, a nanobubble can be pressure sensitive and perform as a fast acousto-optic transducer. Study [318] has demonstrated the dynamics of

shrinkage of plasmon bubbles formed around Au NPs immersed in a liquid and irradiated by a resonant light source. Laser irradiation enables a bubble in NP solutions to be displaced by centimeter distances [319]. Cantilever-based force measurements show that the motion is due to millisecond-long bursts of force that are synchronized with the sound emission. The mechanism for taking into account the driving force, which is based on the thermophoretic instability of NPs, is similar to the Jeans instability that occurs in gravitational systems.

4.3 Absorption spectra, weakly absorbing media, nonlinear phenomena

Since most of the PTS and OAS methods are laser-based (power-based) nondestructive and contactless techniques, this determines an important feature of their application. Many applications require absorption band parameters to be measured simultaneously with high sensitivity and accuracy. To elucidate the mechanisms of a chemical reaction or bioprocess, it is especially important to determine the absorbing capability at low concentrations and in small volumes of real samples. However, in this case, the possibilities of conventional transmission measurements are limited [20, 320, 321], while indirect methods can lead to incorrect results.

Due to its specific features, photothermal spectroscopy and optoacoustic spectroscopy are in demand for recording light absorption spectra at a very low level, e.g., for pure water in the visible range [322] and near-IR range [323], stable particles [324, 325], crystals [326], and dispersed solutions [327–329]. The proportion of studies in which weakly absorbing media (e.g., ultrapure water) are studied using photothermal spectroscopy is very large [322, 330]. The minimum linear absorption coefficient of 2×10^{-5} cm^{-1} has been calculated for the wavelength range of 360–400 nm [322]. The overtone spectra of valence C–H stretching vibrations of formaldehyde, acetaldehyde, and n-butyraldehyde in the liquid phase were studied using standard absorption methods and thermal lens spectrometry. Based on these data, the vibrational frequencies and anharmonicity constants of the stretching vibrations of the methyl and aldehyde groups were determined [331].

Microscopic photothermal methods, such as TLM [19, 332, 333], are used for biomedical purposes [19, 99, 105, 113, 334], which require high accuracy of data on the absorption of chromophores and the entire object as a whole (see also Section 8).

Photothermal methods are apparently applicable for determining the optical properties of optical materials [5, 335, 336]. It is often necessary to verify the accuracy of measured values by comparing them with data obtained by conventional methods. PDS spectroscopy makes it possible to determine weak absorption in thin films [50, 337–340] and to reliably detect light absorption at a level of $10^{-4}-10^{-6}$ absorbance units, while the level of 10^{-2} absorbance units is only attainable using standard transmission methods, and, moreover, it is difficult in these methods to distinguish between the effects of light absorption and light scattering. Thermooptical methods are used in the study of optical materials containing nanosized particles. For example, a method related to thermal lens spectrometry, Z-scanning [341], has experimentally shown unique nonlinear optical characteristics of Cr-based nanocomposites [342] and an alloy of Zn and Cu [341]. Thermooptical methods make it possible to determine nanosized defects in optical coatings [125] and materials [126]. In particular, the development of defects in the bulk of an optical element containing a single Au NP was studied by thermooptical microscopy [126]. The development of a defect is associated with the initial melting of the particle. However, especially for complex objects, it is necessary to improve both the correctness and accuracy of photothermal measurements, and this problem has not yet been completely solved.

Lately, variants of photothermal measurements based on multiphoton absorption have been introduced into practice [343, 344]. Photothermal methods are based on highly sensitive measurements of temperature changes due to multiphoton absorption processes [345]. These studies, which explored nonfluorescent diphenylacetylene (DPA) and diphenylbutadiine (DPB) molecules, provided the estimated fraction of multiphoton absorption for wavelengths of 516, 472, 440, and 424 nm. Two-photon absorption cross sections strongly depend on the π-conjugation length; e.g., the two-photon absorption cross section at a wavelength of 472 nm for DPB is approximately 2.2 times larger than for DPA [346]. Nonlinear absorption in solvents was measured using the standard [347, 348] and modified Z-scan methods using femtosecond laser pulses with a repetition rate of several MHz [349]. The use of a dual-beam scheme for visualization of cells with high sensitivity was presented [350] (Fig. 12).

5. Photothermal and optoacoustic spectroscopy in studies of photochemistry and fluorescence

This section contains descriptions of applications and objects where, along with the thermal quantum yield (i.e., the photothermal effect per se), there are alternative channels for dissipation of the absorbed energy (see Fig. 1). If the absorption band parameters are known with high accuracy, the conditions of photothermal measurements, especially in the case of laser-induced variants, can be used in more complex experiments for processes that compete with photothermal ones, which are, most often, photochemical transformations. In addition, Sections 5.3–5.5, in view of a certain similarity of methodology, present a combination of photothermal and fluorescence spectroscopy as mutually complementing methods.

5.1 Monitoring photochemical and photo-induced reactions. Determination of quantum yields

If there are processes that compete with the thermal relaxation of samples excited by excitation radiation, then the strength of the photothermal effect decreases due to a decrease in the thermal quantum yield, which can be used to study such processes and evaluate their yields. The yields of photochemical reactions for fast processes were measured using transient thermal lens spectrometry [351–354]. A model has been developed that describes photobleaching at various temperatures of eosin Y, which is used as a cytoplasmic dye and photosensitizing agent for the generation of singlet molecular oxygen. This model was used to quantify the rates of molecular diffusion, photobleaching, and the quantum yield of eosin Y fluorescence [355]. Study [356] examined the photochemical chlorination of chloroform dissolved in carbon tetrachloride using thermal diffraction spectroscopy.

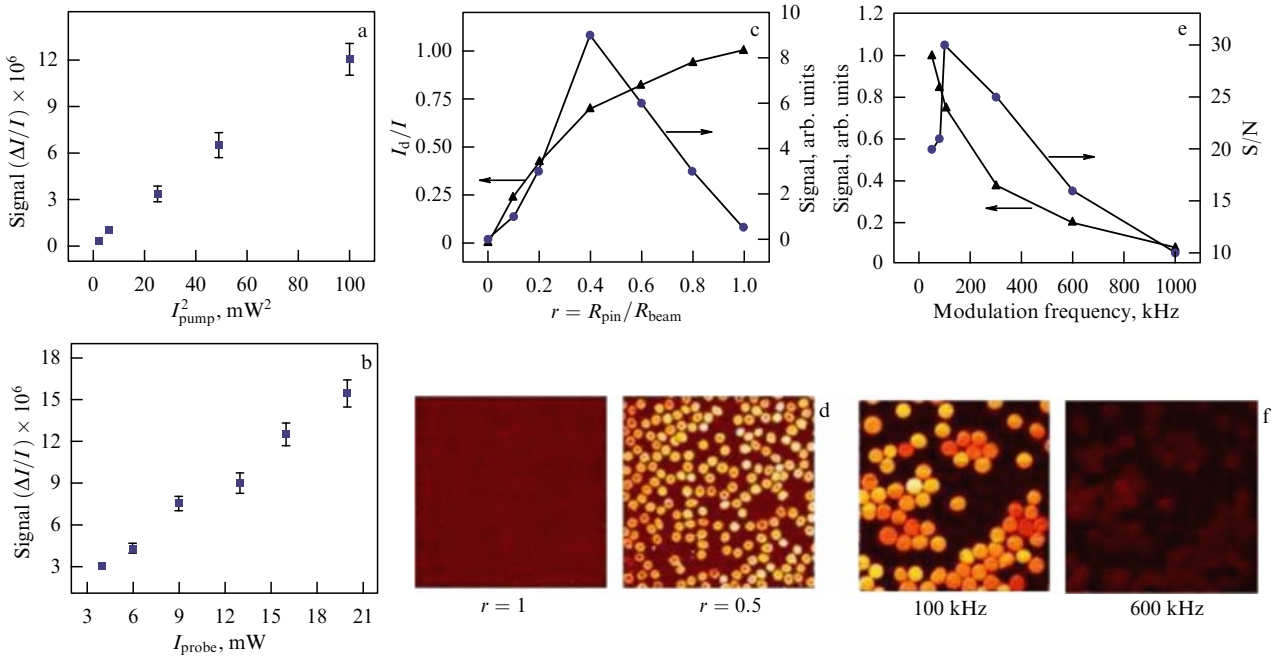

Figure 12. (Color online.) Two-photon thermal lens spectrometry (TLS). Characterization and optimization of image parameters. (a) Dependence of photothermal (PT) yield on power I_{pump} of the excitation laser in a hemoglobin solution (100 μM). (b) Dependence of the PT signal on power I_{probe} of the probe laser. (c) Dependence of the PT signal and detected intensity of the probe on ratio r of aperture radius R_{pin} to probe beam radius R_{beam}. (d) PT image of single erythrocytes with $r = 1$ and $r = 0.5$. (e) PT signal and signal-to-noise ratio (S/N) as a function of modulation frequency in the range from 50 kHz to 1 MHz. (f) PT image of single erythrocytes for modulation frequencies of 100 and 600 kHz. (Figure from [350], reproduced with permission, © 2020 AIP Publishing.)

In photoinduced processes, two processes contribute to the generated thermal wave: heat release during thermal relaxation of a photoexcited molecule and structural changes that occur in the system under study after photoexcitation [23, 357]. These processes can be studied using optoacoustic calorimetry. The optoacoustic signal can be described as $S_{\text{sam}} = KE_{\text{a}}\Phi(\Delta V_{\text{th}} + \Delta V_{\text{con}})$, where K is the instrument response constant, E_{a} is the absorbed energy, Φ is the quantum yield, and ΔV_{th} and ΔV_{con} are the thermal and conformational contributions to the change in the solution volume, respectively. The change in volume can be presented as $\Delta V_{\text{th}} = Q\beta/(C_p\rho)$, where Q is the heat transferred to the solvent, C_p is the specific isobaric heat, and ρ is the density. The contribution of the instrument response constant can be eliminated by using a reference compound, which rapidly converts the energy of the absorbed photon $E_{h\nu}$ into heat with a quantum yield Φ and does not undergo conformational changes. The amplitude of the optoacoustic signal for the reference compound is then described as $S_{\text{ref}} = KE_{\text{a}}E_{h\nu}Q\beta/(C_p\rho)$, and the signal, as a ratio of the sample and reference signals ϕ:

$$\phi E_{h\nu} = \frac{S}{R}\,E_{h\nu} = \Phi\left[Q + \frac{\Delta V_{\text{con}}}{\beta/(C_p\rho)}\right].$$

Transient optoacoustic calorimetry was used to study photoinduced nonradiative processes in solutions. Work on the photocyclization of triphenylamine [358] and methylated thienocarbazoles, which can initiate DNA photodestruction [359], is noteworthy. In studying the folding of proteins and peptides, protein rearrangements [360] in β-sheets, pH-induced unfolding of apomyoglobin, and the protein part of myoglobin [361] were studied. Proton transfer reactions have been studied for poly-L-glutamic acid [362]; complete acidic unfolding of myoglobin with photolabile 1-(2-nitrophenyl)ethyl sulfate at $\lambda = 633$ nm [363]; and nanosecond kinetics of β-sheet refolding at ambient temperature and pH without any denaturing agents [364]. Study [365] examined the role of specific interactions, such as bridge electrolyte and cation-π-interactions and in the stability and folding kinetics of α-chains of the model peptide RN80. Optoacoustic calorimetry was used to study the thermodynamics of ligand binding to proteins: photodissociation and conformational dynamics of the CO and Fe^{2+} complex from dehaloperoxidase isolated from the *Amphitrite ornate* worm [366] and photodissociation of the CO and cytochrome P450 complex.

To study the behavior of intermediates in irreversible reactions or reactions in which short-lived species are studied, the methods of dynamic thermal lattices [367] and transient thermal lens spectrometry [368] are used. These methods make it possible to quantify changes in enthalpy and molar volume during photochemical reactions [369, 370]. One of the practically important examples of the application of time-resolved measurements in the method of thermal dynamic lattices is the study of the dissociation of carboxymyoglobin [371, 372]. Measurements in the time range from 10^{-7} to 10^{-2} s made it possible to establish the main stages of the process: CO release ($10^{-7}-10^{-6}$ s), thermal diffusion ($10^{-6}-10^{-5}$ s), CO diffusion (10^{-5}–10^{-3} s), and bimolecular recombination ($10^{-3}-10^{-2}$ s). An increase in the number of protein fluctuations during the reaction is shown by the example of a photosensor protein isolated from the purple sulfobacterium *Ectothiorhodospira halophile* (14 kDa); in the time range of $10^{-6}-10^{-2}$ s, the following changes were observed: photoisomerization with the production of

an intermediate (red shift) (10^{-6} s), thermal diffusion ($10^{-6}-10^{-5}$ s), transformation of the intermediate into a new product (blue shift) ($10^{-4}-10^{-3}$ s), and diffusion of photoreaction products ($10^{-3}-10^{-2}$ s).

5.2 Reactions involving the excited triplet state of molecules

The generally accepted scheme of the behavior of a large organic molecule under the effect of radiation includes absorption with a transition from the ground singlet state S_0 to the excited state S_1. De-excitation can be implemented both by returning to the initial state S_0 and by transitioning to the metastable triplet state T_0, which also transforms into S_0 with time [373]. If the system contains foreign molecules, the triplet can enter into a chemical reaction with them, which can be considered another way of relaxation. The study of such reactions proceeding through a metastable triplet state is another area of application of photothermal spectroscopy.

The first work in this area was probably devoted to the interaction of diphenylketone with aniline [374]. The thermophysical parameters of this reaction were determined by the authors using optoacoustic calorimetry. A numerical theory of an optoacoustic experiment was developed. To substantiate the procedure for determining the enthalpy of a reaction involving particles with lifetime τ_0, the authors derived an explicit expression for the signal at the detector in the approximation of a point heat source and a point detector. The behavior of the latter is described by the approximation of a damped harmonic oscillator with oscillation frequency v_t and relaxation time τ_t:

$$U(t) = \frac{Q_{\text{th}} K_t}{4\pi r_0} \frac{v_t \tau_0}{1 + v_t^2 \tau_0^2} \left\{ \exp\left(-\frac{t}{\tau_0}\right) - \exp\left(-\frac{t}{\tau_t}\right) \times \left[\cos(v_t t) - \frac{1}{v_t}\left(\frac{1}{\tau_0} - \frac{1}{\tau_t}\right) \sin(v_t t) \right] \right\}, \quad (1)$$

where Q_{th} is the absorbed energy released as heat, K_t is the response constant of the instrument, and r_0 is the distance from the source to the detector. Strictly speaking, the approximation of a point heat source fails under the described conditions. Nevertheless, in measuring in time $t < 1/v_t$, the equations for the signal in the limiting cases of short-lived, $\tau_0 \ll 1/v_t$, and long-lived, $\tau_0 \gg 1/v_t$, particles should persist. Therefore, the relations

$$U_{\text{m}} = \frac{Q_{\text{th}} K_t}{4\pi r_0} = K' Q_{\text{th}}\,, \quad U_{\text{m}} = K' \phi_{\text{th}} E_{\text{a}} \quad (2)$$

used to determine the thermal yield $\phi_{\text{th}} = Q_{\text{th}}/E_{\text{a}}$ should be retained. A series of solutions of 9-fluorenone, anthracene, tetraphenylethylene, and rhodamine 6G in ethanol were used for calibration. Since all these substances, when absorbing stimulating radiation, emit fluorescent radiation with quantum yield $\Phi_{\text{fl},i}$ and frequency $v_{\text{fl},i}$, the value $\phi_{\text{th},i}$ can be calculated for them as

$$\phi_{\text{th},i} = 1 - \frac{\Phi_{\text{fl},i} v_{\text{fl},i}}{v}\,. \quad (3)$$

In the case of benzophenone, it was assumed that the resulting radicals are relatively stable and do not undergo any chemical changes during the experiment, while triplet benzophenone is formed in solution from benzophenone with a quantum yield equal to one and completely reacts with aniline. The reaction enthalpy ΔH_{r} is determined from Eqn (2) and $\Delta H_{\text{r}} = hv(1 - \phi_{\text{th}})$.

In considering the case of more than one competing reaction and the presence in the solution of n corresponding metastable particles, each of which is characterized by the lifetime τ_i of its own, a formula similar to Eqn (1) was derived in [375]. The parameters τ_i and $\phi_{\text{th},i}$ were selected using numerical methods, by minimizing the sum of squared deviations of the points on the experimental curve from the values calculated theoretically. The valerophenone photodissociation reaction was studied. The triplet state was excluded from consideration since it is formed very rapidly; the same refers to isomerization to diradical. Calibration was carried out using a solution of ferrocene in ethanol. The values of τ_i obtained by fitting enable assessing the kinetic parameters, and the value of $\phi_{\text{th},i}$, the thermodynamic parameters of the corresponding reaction stages:

$$k_1 = \frac{1}{\tau_1}\,, \quad \Delta H_1 = hv(1 - \phi_{\text{th},1})\,, \quad \Delta H_2 = hv(1 - \phi_{\text{th},1} - \phi_{\text{th},2})\,. \quad (4)$$

An alternative approach to the study of such reactions using PDS in a coaxial pulsed version was applied in [376] to determine the enthalpy and rate of the reaction of benzophenone with ethanol. This study is of interest, because it preliminarily considers all ongoing relaxation processes and provides an analytical expression for the heat Q_i produced or absorbed during the ith process. One of the main ideas on which the approach is based is the division of these processes into rapid and slow ones (Table 1) with respect to the time (of the order of 100 ns) needed for the density gradient to develop. For example, the lifetimes of molecules in the excited singlet and triplet states are quite small compared to the duration of the excitation laser pulse t_0. Thus, it can be assumed that, for the experimental times $t \gg T_0$, $Q_1 = \text{const}$ and $Q_2 = \text{const}$, i.e., stages 1 and 2 (see Table 1), have already been completed, and heat has been released by the time t.

The main assumptions used to describe the pulsed experiment are that the sample is irradiated with light in the fundamental transverse electromagnetic mode TEM_{00} for a very short time, which is much shorter than the characteristic heat transfer time and, hence, the characteristic diffusion time. Then the distribution of excited molecules in the sample, which have arisen as a result of the absorption of excitation radiation, should preserve the Gaussian profile of this beam [377]. The next step in solving the temperature distribution problem is based on the assumption that heat is released in

Table 1. Processes occurring in the reaction of benzophenone with ethanol and their parameters [376].

Stage	Process	Rate
1	Internal conversion and intersystem crossing of excited singlet state S_n'	Fast
2	Transition from excited state T_n to ground triplet state T_1	Fast
3	Relaxation of ground triplet state T_1 into ground singlet state S_0	Slow
4a	Transition of electron from T_1 to the energy level of the acceptor molecule with energy E_{acc}	Slow
4b	Further transformation of the primary product of the reaction between benzophenone and ethanol	Very slow

each process faster than it propagates beyond the irradiated area [376, 378]. Based on the basic PDS equations, the final expression for the deflection angle can be deduced:

$$\varphi(x,t) = -\frac{1}{n_0}\frac{\partial n}{\partial T}\frac{8E_0\mu l}{h\nu\pi\rho C_p(8D_t+\omega_e^2)^2}\sum_i Q_i(t)\,, \qquad (5)$$

where μ is the linear absorption coefficient, l is the optical path length, D is the thermal diffusivity coefficient, and ω_e is the radius of the excitation beam waist. In this case, the total heat $\sum_i Q_i(t)$ released by the time t is can be represented as

$$\sum_i Q_i(t) = A_\infty + A_d\exp(-k_d t) + A_a\exp(-k_a t)\,, \qquad (6)$$

where $A_\infty = Q_1+Q_2+Q_3+Q_{4a}+Q_{4b}$, $A_d = Q_{4b}k_a/(k_d-k_a) - Q_{4a}(\infty) - Q_3(\infty)$, $A_a = -Q_{4b}k_d/(k_d-k_a)$, $k_d = k_3 + k_{4a}[Q]$ is the total constant of the consumption of triplet benzophenone and $k_a = k_{4b}$ is the total constant of the consumption of radical products of the interaction of triplet benzophenone and ethanol (Q). The values of A_∞, A_d, A_a, k_d, k_a can be obtained by fitting the experimental signal with dependence (6). The approximation unexpectedly showed that the resulting expression contains only one exponent; therefore, it was taken that $Q_{4b}(t) \equiv 0$ and $k_a \equiv 0$. This model is used to describe many photochemical reactions. Most other work studying photothermal methods also assumes the existence of a long-lived triplet state, but this circumstance is not always taken into account explicitly.

5.3 Combination of photothermal spectroscopy with fluorimetry

Dual-beam TLS can be considered an alternative to fluorescence spectroscopy. Since TLS can be used in both thick samples and thin films, the method is advantageous with respect to fluorimetry [379]. This technique uses laser beams with a transverse mode close to TEM_{00} and samples with high uniformity of refractive index (opaque and highly dispersed systems are excluded) [36]. Initial studies in this area were carried out to estimate the quantum yields of fluorescence Φ and compare them with fluorimetric determination [380, 381]. TLS has been used for reactions that involve original fluorescent materials or products [382–385]. The equation for calculating the fluorescence quantum yield based on a thermal lens signal [386] has the form

$$\Phi = \left(1 - \frac{A_r\theta}{A\theta_r}\right)\frac{\lambda_f}{\lambda_a}\,, \qquad (7)$$

where λ_f is the fluorescence wavelength; λ_a is the absorption wavelength; θ and A are the thermal lens signal and sample absorbance, respectively; and θ_r and A_r are the thermal lens signal and absorbance of the reference light-absorbing substance, respectively. The equation for the phase shift of the probe beam yields

$$\theta = -\frac{P_e A_e l_0}{k\lambda_p}\phi\left(\frac{dS}{dT}\right), \qquad (8)$$

where P_e is the excitation laser power, A_e is the linear absorption coefficient at the excitation radiation wavelength, l_0 is the optical path length, and λ_p is the probe laser wavelength, while the proportion of energy converted into heat, ϕ, for fluorescent samples is found as $\phi = 1 - \eta(\lambda_a/\lambda_f)$. The quantity ϕ can be determined if a reference sample with the known quantum yield is used. PTS was applied to estimate the fluorescence quantum yield in reactions of various types, including singlet oxygen and quantum dots [385, 387–391].

The quantum yield is one of the most important optical properties of luminescent glasses, especially those that are used as active laser media. Attention is focused on glasses doped with rare earth metals (Nd, Yb, Eu, etc.) [294, 295, 392–394]. In many cases, the data on doped glass (E) are compared with those on the reference sample (E_{ref}): $E/E_{ref} = \phi/\phi_{ref} = \phi_{ref}^{-1}(1 - \Phi\lambda_{ex}/\lambda_{em})$, where λ_{ex} is the excitation wavelength and λ_{em} is the emission wavelength. The reference is a sample containing the same element in its composition. Dual-beam TLS has shown that the quantum efficiency of fluorescence decreases with increasing rare-earth element concentration [294] and temperature [295, 393]. A comparison of the results showed good agreement with calculations based on the Judd–Ofelt theory for Nd-doped glasses [395] and ceramics doped with Eu^{3+} and Tm^{3+} [396]. Single-beam TLS was used to estimate Φ for CdTe quantum dots with varying pH [397].

5.4 Fluorescence quenching

Photothermal and optoacoustic spectroscopy are used to study fluorescence quenching and energy transfer from fluorescent compounds to other molecules. The authors of [384] simplified the equation for the quantum yield (7) to $\Phi = (1 - \theta/\theta_r)\,\lambda_f/\lambda_a$. The thermal lens signals θ_0 and θ, measured, respectively, in the absence and the presence of a quencher, are related as follows: $\theta_0/\theta = (1 - \Phi_0 x)/(1 - \Phi x)$, where Φ_0 and Φ are the fluorescence quantum yields in the absence and the presence of a quencher and x is a parameter that takes into account the heat generated due to the Stokes shift. The known Φ_0 can be used to calculate Φ as a function of the quencher concentration c [386]. Furthermore, the quantum yield ratio can also be replaced in the Stern–Volmer equation by the thermal lens signal. Then, the expression takes the form $\theta_0/\theta = 1 - k_L\tau[c_0]$. This equation can be represented in terms of the concentrations of the donor, fluorophore, and the quencher, the acceptor (c_0 and c, respectively): $\theta_0/\theta = 1 - c_0/c$, where θ_0 and θ are the thermal lens signals for the donor and acceptor, respectively [398]. Based on these relations, the rates of energy transfer from the fluorophore to the quencher and the donor-acceptor distance R were estimated in terms of the acceptor concentration: $R = 7.35/(c_0)^{1/3}$ [398, 399].

The decrease in the fluorescence efficiency with the addition of a quencher should lead to a simultaneous increase in the thermal power released by the sample. Thus, it can be expected that the photothermal signal will change more significantly than the fluorescence intensity, since it is proportional to the amount of heat released [383, 400]. However, complete quenching may lead to incorrect values of the quantum yield. This effect was studied in several experiments [383, 386, 392] in various media, including ethanol, water, and micellar aqueous solutions. The results of photothermal measurements only agree with the data of fluorescence spectroscopy in a limited range of quencher concentrations. Study [383] reported an estimate of the quantum yield in aqueous and micellar solutions of rhodamine 6G with absorbance $A < 0.01$. Under these conditions, the relationship between the thermal lens signal and the fraction of absorbed energy in the coordinates 'fraction of

absorbed light $(1-10^{-A})$–photothermal signal θ' is linear [380]. Otherwise, the thermal energy produced by the quenching reaction is greater than the associated loss of radiation energy. Such deviations are a serious drawback if photothermal methods are used to study reactions that lead to fluorescence quenching.

5.5 Photothermal thermometry

Neural networks have been used to recognize the features of the fluorescence spectrum of a thermosensitive probe with the aim to create fluorescence thermometry with an accuracy of 200 mK, a bandwidth of 100 MHz, and high resistance to intensity fluctuations of a probe laser (532 nm) [401]. The concept has been implemented for rhodamine B-stained mixtures of $CuCl_2$ and glycerol. The temperature dependence of fluorescence is recorded in the temperature range from 234 to 311 K. The spatial dependence of the calibrated amplitude and phase of photothermally induced temperature oscillations along the excitation laser axis was determined at various modulation frequencies. The spatial and frequency dependence of the temperature signals is in good agreement with the 1D multilayer model of thermal diffusion [402]. In the implementation of the approach in the time domain, continuous laser radiation induces a gradual increase in temperature due to the accumulation of the constant component of the heat flux generated by laser pulses (1064 nm) and an immediate transient temperature change after each individual pulse is extracted from the received time sequences of fluorescence spectra induced by continuous laser radiation. Stroboscopic implementation of fluorescent thermometry using a pulsed probe laser with fluorescent radiation provides remote detection of temperature changes with a time resolution of 10 ns [401].

Presentation of photothermal thermometry in a broader sense as a branch of optical and, in general, radiation thermometry, is beyond the scope of this review. The results of the application of photothermal thermometry methods are laid out in detail in recent publications [403–405].

6. Studying chemical reactions

In Section 5, we presented a number of examples of how photothermal spectroscopy and optoacoustic spectroscopy are used for photochemical reactions. However, the scope of application of the considered methods is wider. First of all, since reactions can modify the absorption bands or thermophysical parameters of the sample, photothermal and optoacoustic spectroscopy, as well as other methods of optical or thermal spectroscopy, can be used to directly control these reactions. However, in addition, these methods can be used to determine the heat of formation of transition compounds and free radicals, since all chemical reactions are accompanied by the release or consumption of heat. As a result, the heat released in such processes causes thermal expansion of the solution under study and, consequently, a change in the refractive index, which is measured by photothermal methods.

A significant part of publications devoted to photothermal spectroscopy pays relatively little attention to the feasibility of using this technique to study chemical reactions. Studies devoted to this problem only consider in detail the specific features of the application of particular methods [58, 373, 406–408]. Thus, the issue of systematization of existing problems and approaches to their solution in this area remains relevant. We consider below some specific features related to the mechanism or conditions of the occurrence of specific chemical reactions, which were studied by photothermal and optoacoustic spectroscopy. This section is not an exhaustive description of all areas where the methods considered in the review are applied to study chemical reactions. Only some types of chemical reactions described by a particular thermooptical or thermophysical model, which differs somewhat from the general model, are considered. The use of PTS for studying biological processes is not considered. Each biological system is usually individual and requires a separate extended and detailed discussion, which is beyond the scope of this review [409–413]. Nevertheless, some studies describe features that must be taken into account in applying thermooptical methods to the exploration of specific biological objects [414, 415].

6.1 Monitoring chemical reactions by changes in the optical properties

Photothermal and optoacoustic methods are most often used as absorption spectroscopy methods to monitor chemical reactions. The dimerization of a moderately fluorescent compound with a dimerization constant higher than that of rhodamine 6G, zinc tetracarboxyphthalocyanine diamide (ZnTCPc), in an aqueous solution was studied. It has been confirmed that photothermal measurements are more sensitive than those made using spectrophotometry and fluorescence spectroscopy (provided that the wavelength is correctly chosen) [400]. If the monomer and dimer are absorbed at the same wavelength, spectrophotometry, as well as fluorescence measurements in the case of a small dimerization constant (rhodamine 6G), results in a deviation from the linearity of the dependence of the signal on concentration. The results obtained with TLS using pulsed laser excitation do not reveal such deviations. This may be related to the formation time of the thermal lens. In experiments with continuous laser excitation, the formation occurs over a considerable time, usually in a few milliseconds or seconds. In experiments with a pulsed laser, the sample is irradiated for a short time (5–10 ns), and the lens is formed over a period from several microseconds to several hundred microseconds. In this case, the characteristic time describing the heat transfer rate is in a wide range, from several hundred microseconds (chloroform, water, nitrobenzene) [416] to 1 ps–10 ns (for nanoobjects up to 100 nm in size) [417]. Therefore, TLS with a pulsed excitation laser is less sensitive to the presence of slow chemical and/or physical processes that hinder the formation of a thermal lens [386].

The study of intermolecular interactions makes it possible to predict the mechanisms of chemical reactions and describe the stability of colloidal systems. A model has been created to describe liquid binary mixtures (CH_3OH, CCl_4, CH_2Cl_2, dimethyl sulfoxide (DMSO)) taking into account changes in the physical parameters and the molecular properties of these solvents, such as interactions between molecules, hydrogen bonds, etc. [418].

To study photoisomerization processes using OAS, *isoptoacoustic points* are used [419, 420], i.e., the wavelengths, wavenumbers, or radiation frequencies at which the total energy radiated by the sample in the form of heat during optoacoustic heating does not change when a chemical reaction or a physical change in the sample occurs. The position of the isoptoacoustic point depends on the experimental conditions, while the difference between isosbestic

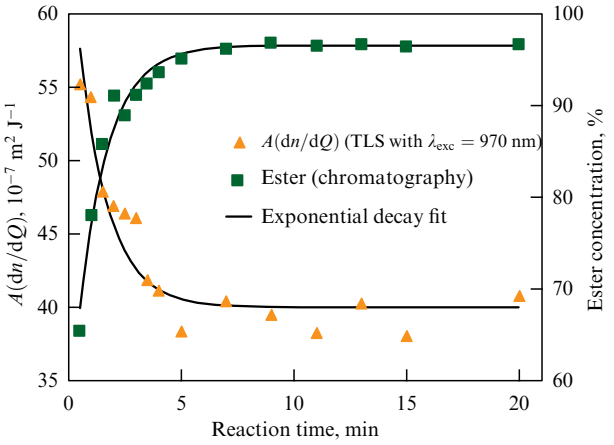

Figure 13. (Color online.) Product of absorption coefficient A and refractive index derivative of sample heat ($A\,\mathrm{d}n/\mathrm{d}Q$) at $\lambda_e = 970$ nm and ester concentration determined by chromatography as a function of reaction time. (Drawing from [421], reproduced with permission, © 2020 AIP Publishing.)

points in spectrophotometry and isoptoacoustic points is the result of a nonlinear relationship between the molar absorption coefficient and the optoacoustic signal, which can be used as a source of information.

6.2 Monitoring chemical reactions by changes in thermal diffusivity

If the thermophysical parameters of the objects under study are known, the mechanism of reactions in which the absorption spectra undergo weak changes can be studied. Photothermal and optoacoustic methods are used to this end somewhat less frequently than for optical monitoring, but the situation is beginning to change.

Dual-beam TLS in the near infrared region was used to control the interesterification reaction during the production of biodiesel to improve the quality of the produced fuel [421, 422]. The use of the method facilitates the optimization of biodiesel production, indicating the best time to stop the reaction (Fig. 13). The thermal diffusivity D as a function of the reaction time strongly depends on the viscosity [423], which makes it possible to use D and thermooptical parameters to determine the content of biodiesel in mixtures. Photochemical reactions can be studied by monitoring changes in D and absorbance A. TLS in the parallel-beam mode with continuous irradiation was used to assess the oxidative stability of various oils in the synthesis of biodiesel [422] and in monitoring the quality of vegetable oils [424].

Based on the measurements of D and the thermal conductivity coefficient k of barium glasses with various TiO_2 contents, the authors of [425] concluded that TiO_2 plays a key role in glass formation, which standard methods failed to reveal. A solid TiO_2-organic dye interface was examined to study processes occurring in solar cell elements [426].

PTR as a group of nondestructive methods is well suited for studying reactions in surface and near-surface regions due to the possibility of studying the surface structure, identifying various defects, damage, and inhomogeneous areas in materials, etc. PTR has been used in studying reactions by changes in the optical and thermal parameters of samples, to obtain images, and to evaluate various substances. For example, in studying the kinetics of the hardening of composite materials [427], two composites widely used in dentistry were employed (Fig. 14). If the initial and final values of thermal diffusivity are known, along with the times obtained by simulating experimental data, the calculation results can be interpreted as kinetic equations for the photohardening of polymers, in which the dependence of the monomer concentration $[\mathrm{M}](x,t)$ on time and depth is equal to the polymerization rate R_p:

$$R_p(x,t) = k_p[\mathrm{M}](x,t)\sqrt{\frac{\gamma\varepsilon[\mathrm{PI}]I_0\exp(-\eta x)}{k_t}}, \qquad (9)$$

where γ is the quantum yield of the polymerization reaction, ε is the molar extinction coefficient of the photoinitiator, [PI] is the concentration of the photoinitiator, I_0 is the excitation radiation intensity, η is the coefficient of attenuation of the excitation radiation by the sample, k_p is the chain growth rate, and k_t is the chain termination rate. If an assumption is made that the values under the root sign in Eqn (9) in the first approximation are unchanged, a first-order kinetic equation for the monomer concentration can be obtained:

$$[\mathrm{M}](t) = [\mathrm{M}]_0\exp\left(-\frac{t}{b}\right), \qquad (10)$$

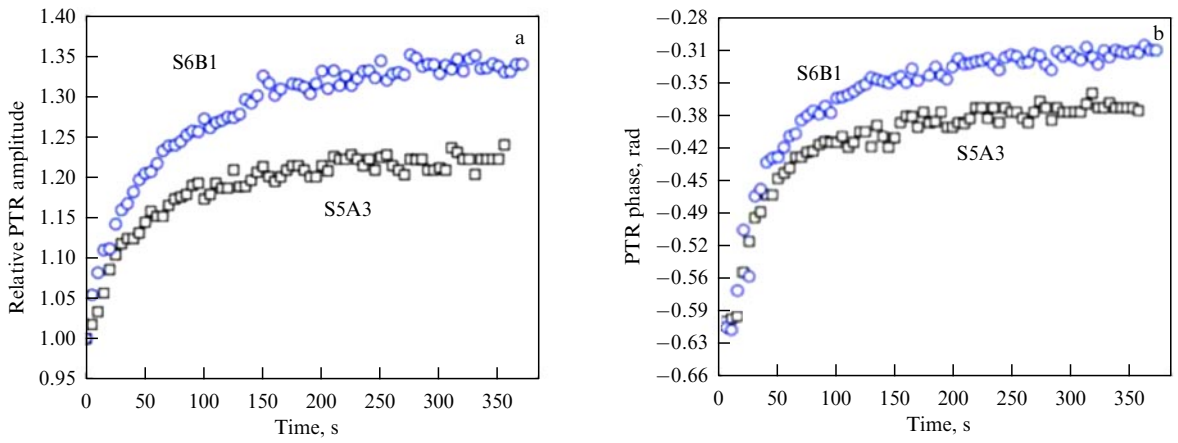

Figure 14. (Color online.) Behavior of the amplitude (a) and phase (b) of the PT-radiometry signal in time evolution of temperature diffusivity in dental resin photopolymerization. (Drawing from [427], reproduced with permission, © 2007 IOP Publishing.)

where $b = k_p^{-1}\left(\sqrt{\gamma\varepsilon[\mathrm{PI}]I_0\exp(-\eta x)/k_t}\right)^{-1}$. Thus, the first-order kinetics of changes in thermal diffusivity during polymerization is a direct consequence of the fact that changes in the monomer concentration also correspond to first-order kinetics. The relationship between the average degree of polymerization $P(x,t)$ and the diffusion depth is

$$P(x,t) = \frac{[\mathrm{M}]_0}{[\mathrm{M}](x,t)} = \exp\left[\left(\frac{\sqrt{D_\infty} - \sqrt{D_s(x)}}{\sqrt{D_\infty} - \sqrt{D_0}}\right)^{\eta/(2q)}\frac{t}{\tau}\right], \tag{11}$$

where D_∞ and D_0 are the thermal diffusivity of the resin at the end and before the start of hardening, respectively, and q is the rate of thermal diffusivity growth. Equation (11) provides a simple relationship between the depth-dependent thermal diffusivity D_s and the degree of hardening via $[\mathrm{M}](x,t)$. Thus, in the process of hardening, the thermal diffusivity increases, and its increase can be described by a first-order kinetic equation. Using the thermal diffusivity for each depth, it is possible to obtain the degree of polymerization as a function of depth and, thus, to assess the completeness of the hardening process [427–429].

The capabilities of time-resolved OAS enable studying photoinduced chemical processes and 'optically silent' intermediate products, i.e., those products that not exhibit changes in absorption or emission [406, 409]. Areas of research should be singled out that are related to the study of thermal and photothermal properties of NPs [430] or quantum yields of fluorescent organic molecules using reflection spectra [431]. Studies of quantum yields are based on the recording of the apparent reflection spectrum using an integrating sphere [432] or a data correction model [433]. For example, OAS was used to only examine a reaction of the pseudo-first order, parallel or sequential, including thermal equilibria [434]. The released heat is measured to determine energy levels of intermediate compounds provided that quantum yields are known. Vice versa, if an energy level of intermediate states is known from other spectroscopic methods, quantum yields can be determined for photoisomerization [435], charge transfer [436], phosphorescence [406], fluorescence, and energy transfer processes [437].

6.3 Reactions with the emergence or transfer of charge. Electrostriction

All photothermal methods intended for studying the thermodynamic characteristics of reactions are based on the separation of the enthalpy and nonenthalpy contributions to the signal. After laser radiation has been absorbed, heat is released as a result of the decay of short-lived excited species. On the other hand, the signal is also affected by other processes, e.g., a change in the molar volume ΔV_{rx} observed during chemical reactions. Of especial importance is taking into account the latter factor for reactions that proceed with a change in the number of moles or the distribution of electric charge [438].

The main approaches used to separate the contribution due to changes in volume from the enthalpy contribution are described using optoacoustic spectroscopy as an example [439]. All of them are based on the assumption that the total (molar) change in the volume in the chemical reaction ΔV_{rx} does not depend on temperature and remains constant when the initial solvent is replaced with another one with similar properties. However, if new charged species are produced as a result of the reaction or the charge distribution of the original charged species changes, then, due to the electrostriction effect, the assumption made may not be true. Using the Clausius–Mossotti relation for $\partial\varepsilon/\partial p$, the compression of the solvate shell of charged species in solution can be described as [440–442]

$$\Delta V_{el} = -\frac{\mu^2}{R^3}\frac{(\varepsilon+2)(\varepsilon-1)}{(2\varepsilon+1)^2}\kappa \tag{12}$$

for a dipole with a dipole moment μ and as

$$\Delta V_{el} = -\frac{Z^2e^2}{6R}\frac{(\varepsilon+2)(\varepsilon-1)}{\varepsilon^2}\kappa \tag{13}$$

for an ion with charge Z, where ε is the relative permittivity of the solvent, R is the radius of the cavity in the solvent structure in which the particle is located, and e is the elementary electric charge.

The change in volume for one molecule observed in practice in the course of a chemical reaction ΔV_r is due to both intramolecular changes in the dissolved substance (ΔV_{str}) and the rearrangement of the solvent near the molecules of this substance (ΔV_{sol}) [443]. The decrease in volume due to electrostriction is one of the main components of the contribution from ΔV_{sol}. In the general case, the issue of how strongly electrostriction determines the total volume change ΔV_r for a particular object is subject to discussion [440]. Nevertheless, a fairly large proportion of ΔV_{el}, up to $\Delta V_{el} \approx \Delta V_r$, can be expected [438, 441].

As can be seen from Eqns (12) and (13), if the electrostriction effect is significant, ΔV_r begins to depend on the parameters ε and κ, which generally change with temperature and replacement of solvent. The dielectric permittivity ε in replacing one alkane with another within the homologous series and with a change in temperature changes insignificantly, and this variation can be disregarded. However, the change in κ in the series of n-alkanes with increasing temperature is significant and must be taken into account. Under these conditions, the values obtained cannot be unambiguously interpreted as enthalpy and molar volume change [438, 441].

It was proposed in [438] to use isotopically substituted solvents. For example, in replacing an ordinary solvent with a deuterated one, the value of χ_s can undergo an increase (by 20–100%) sufficient to enable separation of the thermal and volume contributions. In this approach, reactions should be used that do not proceed through the stage of hydrogen transfer from the solvent. A simpler approach was applied in [441], where the formation of a zwitterion from large organic molecules with a donor–bridge–acceptor structure under the action of laser radiation was studied. An approach was used which is based on measurements in a series of normal alkanes. To exclude a change in ΔV_{rx} in replacing the solvent, the temperature of the experiment was selected for each alkane so that the value of $\kappa(\varepsilon+2)(\varepsilon-1)/(2\varepsilon+1)^2$ remained unchanged for the entire series of solvents (2.2×10^{-10} Pa^{-1}). Thus, the linear dependence

$$S_i = \phi_{th} + \frac{\Delta V_{rx}}{Q_{th}\chi_{s,i}}, \tag{14}$$

where $\chi_{s,i} = \beta/(C_p\rho)$ is thermal expansivity, which characterizes the solvent at a given temperature, should remain the same. The experimental value of ΔV_r (error of the order of 20%) is close to the values of ΔV_{el} estimated from Eqns (12) and (13), provided that the zwitterion is considered to be two

different oppositely charged ions with $|Z| = 1$. Based on the obtained value $\Delta V_r = \Delta V_{sol}$, the ion solvation entropy was calculated as $\Delta S_{sol} = \Delta V_{sol}\beta/\kappa$.

The use of thermooptical spectroscopy based on the measurement of the refractive index gradient can in some cases provide a partial solution for the signal separation problem, since the development of the acoustic gradient of the refractive index is accompanied by sound transmission. As a result, at the initial stage of the experiment, it is possible to monitor the formation and destruction of fairly short-lived particles without introducing corrections that take into account the signal caused by any volumetric changes. This approach is only applicable to the study of processes that involve very short-lived species, while the fact that in organic solvents a fully developed acoustic gradient of the refractive index makes a much larger contribution compared to the thermal one creates additional problems [438].

Reactions that result in charge redistribution are quite common in biological systems [375, 410, 444]; however, as mentioned above, the value of ΔV_r observed in such reactions cannot always be ascribed to electrostriction alone.

6.4 Unbranched chain reactions

A specific feature of unbranched chain reactions is the presence in the process scheme of several periodically repeating successive stages, during which all intermediate reaction particles absorbed at one of these stages are regenerated in subsequent ones. Unlike the reactions discussed above, chain reactions are often characterized by a significant exothermic effect, so the total heat released in the object may exceed the energy obtained due to the absorption of radiation. Owing to high selectivity and temporal resolution, PTS and OAS are those few approaches that provide direct observation of a chain reaction *in situ* [356, 445, 446].

The first study [447] which can be called a photothermal examination of a chain reaction was carried out using a mercury lamp and 50 thermocouples. Such a method can be classified as photothermal calorimetry. The subject of many studies [446, 448, 449] is the hydrogen reaction occurring in the gas phase with chlorine

$$H_2 + Cl_2 \xrightarrow{h\nu} 2HCl\,,$$

studied using OAS. This reaction is a convenient object of exploration, since the total number of moles in it does not change, which is of importance for gas-phase reactions [446]. The reaction mechanism is usually presented in the following form:

— initiation: $Cl_2 \xrightarrow{h\nu, k_1} 2Cl\cdot$;

— chain propagation: $Cl\cdot + H_2 \underset{k_{-2}}{\overset{k_2}{\rightleftarrows}} H\cdot + HCl\,,$

$H\cdot + Cl_2 \xrightarrow{k_3} Cl\cdot + HCl$;

— chain termination: $2Cl\cdot + M \underset{k_{-4}}{\overset{k_4}{\rightleftarrows}} Cl_2 + M\,,$

where M is an arbitrary inert species [446, 448, 449].

The quasi-stationary approximation was used in [448] to derive an explicit expression for the main frequency component p^{chain} of an optoacoustic signal, which was used to calculate the observed chain length Φ_{ph} using the relation

$$\frac{p^{chain}}{p^{diss}} = \frac{1}{2}\Phi_{ph}\frac{|\Delta H_{prop}|}{E_{Cl_2}}\,, \qquad (15)$$

where p^{diss} is the main frequency component of the signal obtained under conditions when the system only contains Cl_2 and M, as a result of which the chain reaction does not proceed, and the only process during which the initially absorbed energy is released is the recombination of the Cl· radical. It is assumed in using this calculation that the amount of heat $|\Delta H_{prop}|$ released during the chain propagation stages and the dissociation energy of molecular chlorine E_{Cl_2} are known. Similar expressions were used in [446] to determine the isotope effect of protium and deuterium for the rate constant k_2 in terms of the amplitudes on the detector ΔU:

$$\frac{p^{chain}_{(H)}}{p^{chain}_{(D)}} = \frac{k_{2,H}\,\Delta U_H}{k_{2,D}\,\Delta U_D}\,.$$

The authors of [446] note that a similar method should be considered not as an approach to determining kinetic characteristics of a chain reaction but rather to study the effect of laser intensity, purity of reagents, and other reaction parameters. The reaction itself and the detected signal are most strongly affected by the presence of impurities [446]. This observation was a basis of a rather nonstandard proposal to use this reaction to detect compounds at the end of a chromatographic column [450].

Nevertheless, the kinetic parameters of individual stages have not been determined in the experiments described above. In relation to this, of significant interest are studies [356, 445], in which the TLS method was used to study the reactions of halogenation of organic compounds RH in a liquid phase that occur according to a radical mechanism:

— initiation: $Hal_2 \xrightarrow{h\nu, k_1} 2Hal\cdot$;

— chain propagation: $RH + Hal\cdot \xrightarrow{k_2} R\cdot + HHal\,,$

$R\cdot + Hal_2 \xrightarrow{k_3} R{-}Hal + Hal\cdot$;

— chain termination:

monomolecular $Hal\cdot + X \rightarrow X{-}Hal\,,$

$R\cdot + X \rightarrow X{-}R\,,$

bimolecular $2Hal\cdot \rightarrow Hal_2\,,$

$2R\cdot \rightarrow R{-}R\,,$

$Hal\cdot + R\cdot \rightarrow R{-}Hal\,,$

where X is some extraneous species.

The monobromination reaction of toluene in the presence of light was studied in [445]. Expressions for the time dependence of the radical species concentration in the sample were used:

$$N_{d0}(t) = \begin{cases} \dfrac{P_e}{h\nu}\dfrac{2\kappa\Phi_1}{k_m}\left[1 - \exp\left(-k_m t\right)\right], & t \leqslant t_0\,, \\ \dfrac{P_e}{h\nu}\dfrac{2\kappa\Phi_1}{k_m}\left[1 - \exp\left(-k_m t_0\right)\right]\exp\left[-k_m(t - t_0)\right], & t > t_0 \end{cases} \qquad (16)$$

for a monomolecular termination with constant k_m and

$$N_{d0}(t) = \left(\frac{P_e}{h\nu}\frac{2\kappa\Phi_1}{k_b}\right)^{1/2}\tanh\left[2(\kappa\Phi_1 k_b t)^{1/2}\right],$$

$$N_d(t) = \begin{cases} N_{d0}(t)\,, & \leqslant t_0\,, \\ \dfrac{N_{d0}(t_0)}{1 + 2k_b(t - t_0)\,N_{d0}(t_0)}\,, & t > t_0 \end{cases} \qquad (17)$$

for a bimolecular termination with constant k_b, where t_0 is the length of a rectangular laser pulse and Φ_1 is the quantum yield of the initiation reaction. Then, the volumetric power of energy sources is defined as

$$H(t) = |\Delta H_{prop}| \frac{hv}{\tau_{prop}}, \quad (18)$$

where τ_{prop} is a quantity that has the meaning of the duration of a single stage of chain propagation. Equations (16)–(18) were used to analyze the formation of a thermooptical element; equations have been derived that correspond to the focal distances of the thermal lens for bimolecular and monomolecular chain termination. The measured values of focal distance

$$f = \frac{l\omega_{0c}^{pr}}{\omega_{0s}^{pr}} \left[\left(\frac{I_0^{pr}}{I_t^{pr}} \right)^{1/2} - 1 \right], \quad (19)$$

where l is the distance between the detector plane and the sample under study; I_0^{pr} and I_t^{pr} are the intensities of the probe beam that passes through the solution in the presence and in the absence of a thermal lens; and ω_{0s}^{pr} and ω_{0c}^{pr} are the radius of the probe beam that passes through the cell in the absence of the thermal lens and in the detector plane, respectively, were approximated using the derived equations. A satisfactory result was only obtained for the approximation based on the assumption of monomolecular termination. The value of ΔH_{prop} calculated using published data has been employed to calculate k_m and τ_{prop}. The monomolecular termination of the reaction probably corresponds in this case to neutralization of radicals on oxygen.

7. Photothermal and optoacoustic spectrometry in analytical and applied chemistry

This section presents the most relevant examples of how the methods considered are applied as highly sensitive power-based techniques of molecular absorption spectroscopy in spectroscopic chemical analysis and applications of microfluidic chips, as well as in some multidisciplinary studies.

OAS remains a relevant method in studying gas mixtures and atmospheric monitoring at industrial facilities and for other tasks [451–457]. Photothermal spectroscopy is used to measure ultralow absorptions for a variety of objects: gaseous and liquid samples, in bulks of solids, and on surfaces, while a large number of studies still involve measurements in the visible and near-UV regions [1, 18]. Photothermal spectroscopy is also applied as a nondestructive method for the analysis and control of various materials and as a detector in state-of-the-art separation methods [5, 15, 19, 458, 459]. Since, in most photothermal and optoacoustic methods, the signal is fairly weakly affected by light scattering and an uneven distribution of chromophores in the sample [460], this is used in the chemical analysis of colloidal solutions and in biomedical problems, although, in the latter case, microspectroscopic methods are at present preferred (see Section 3).

Historically, PTS and OAS were considered in analytical chemistry as a kind of extension of spectrophotometry and its methodological approaches [461–465]. In other words, it was generally believed that the most important task is to increase the sensitivity of the determination without specially emphasizing the purpose of the analysis, the availability of competitive methods, or the target groups of the compounds being determined (metal ions, anions, organic substances, etc.) [466, 467]. The emphasis was mainly on the determination of inorganic cations and anions in aqueous and organo-aqueous mixtures [1]. This area is still the most developed. However, the proportion of developments in methods for the photothermal and optoacoustic determination of inorganic compounds is steadily declining compared to that in 1980–2000 due to the emergence of more advanced technological solutions for inorganic analysis, first of all, atomic emission spectroscopy and elemental mass spectrometry [468, 469], as well as mass spectrometry of single nanoparticles [470], X-ray fluorescence, atomic absorption analysis, etc.

As a result, the use of PTS and OAS has shifted to areas related specifically to molecular analysis: (1) organic analysis; (2) the speciation determination of elements; (3) analysis without sample preparation, in particular *in situ* and *in vivo*; (4) material analysis in nanochemistry and supramolecular chemistry. Methods based on new approaches to sample preparation, which provide high sensitivity and selectivity of determination for specific target substances, are in less demand. Examples of material analysis in environmental objects include the determination of Cr(VI) in water using thermal lens microscopy [471]; determination of Fe(II)/Fe(III) [472]; extraction of Co(II) at the cloud point [473]; and determination of trace amounts of lead with preconcentration (microextraction) and a detection limit of 0.01 μg L^{-1}, the sensitivity of the determination not being inferior to that of mass spectrometry and atomic absorption spectroscopy with the sorption preconcentration [474].

The flow photothermal detection scheme for chromatographically separated dyes (indigo carmine, sunset yellow, Allura Red A, chromotrope 2R, etc.) is based on the temperature difference before and after the illumination point. To measure the change in temperature, a thermocouple with a diameter of 25 μm with two transitions was used. For methylene blue, the detection limit was 30 nM, which corresponds to 120 amol in the irradiated volume; the dye dimerization constant was estimated on the basis of experimental data [475].

As noted in Sections 3–6, the emphasis in applied studies of PTS/OAS is shifting towards more complex heterogeneous objects: micellar solutions, NP dispersions, and natural and human-made macromolecules [458, 476]. Of interest are microfluidic and microplate technologies, where a number of sequential processes (mixing, chemical reaction, separation, etc.) take place in a small volume (in a microflow or in a polymer matrix) [82, 477–481]. Highly sensitive detection systems are required to detect and probe mixture components in a microchannel. Due to the small optical path length in the microchannel, the transmission detectors used have an insufficiently high sensitivity, while the use of fluorescence spectroscopy is limited to fluorophores [482]. As a result, PTS is more widely applied in microfluidic chemical systems [483–487] (Fig. 15). The main difficulty of such research is related to technology and consists, in addition to manufacturing micrometer-sized manifolds (100 – 200 μm), of focusing beams in three directions.

OAS is in demand in clinical laboratory diagnostics [28, 32, 452, 488]. Pulsed IR optoacoustic spectroscopy has been used for noninvasive *in vivo* monitoring of glucose in the human epidermis (Fig. 16) [489]. A fluence below 1 mW mm^{-2} does not lead to skin destruction. The method is sensitive

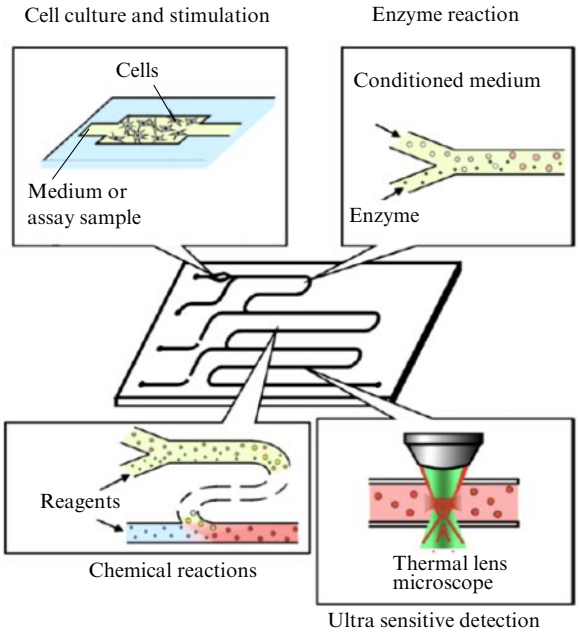

Figure 15. (Color online.) Microfluidic chip bioassay scheme using TLS. Cell culture, chemical reactions, and detection are integrated into a glass microfluidic chip [486].

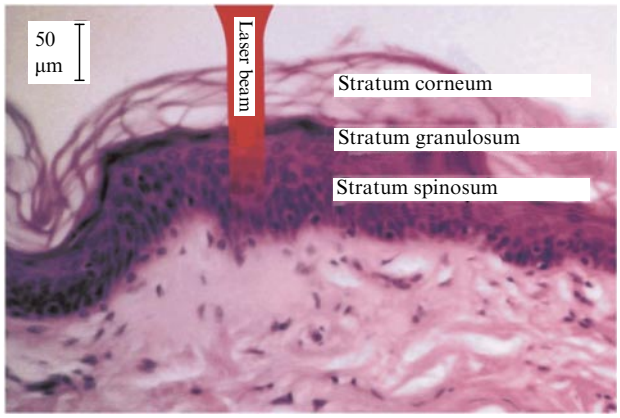

Figure 16. (Color online.) Human skin layers with a laser beam diagram visualizing the depth of laser beam penetration through the epidermis [489].

enough to ensure a continuous record of changes in glucose levels in a diabetic patient, and highly selective to distinguish glucose from other components of the interstitial fluid. The correlation between patients due to the different properties of the skin remains a problem. For example, changes in the thickness of the stratum corneum can affect the amplitude of the signal, due to which individual calibration may be required for each patient.

Based on thermal lens spectrometry, an approach to the noninvasive determination of the medium pH has been developed [490]. The concept of the method is to absorb visible light by a chromophore, which is introduced into the sample if it is absent there or the chromophore is initially present, e.g., in natural objects, plant cells. Thermal changes resulting from light absorption by the chromophore are measured using a fiber-optic Bragg grating sensor. As the pH changes, the light absorption and heat released by the chromophores change. The range of pH measurements is determined by the selection of chromophore, which is the main difficulty and nonuniversality of this method [490].

To obtain more complete information about the object, PTS/OAS is used in conjunction with other spectroscopic methods. For example, the combined use of laser-induced fluorescence spectrometry and TLS provides extended information about the analyzed sample. This makes it possible to study two aspects of an object: (1) quantitative detection of fluorophores and (2) detection of a photothermal signal generated by nonradiative relaxation of other sample components. This approach was used in studying molecular processes in crude oil microvolumes [491].

7.1 Simultaneous determination of concentration and thermophysical parameters

It is due to the fact that photothermal methods depend not only on the optical but also on the thermal properties of the objects under study that the thermal parameters of substances are used in a number of studies as signal sources. Some of these examples are given in Sections 5 and 6. Here, we complete the presentation with examples of applied research.

There are a number of studies in which food components are studied using TLS. In [424], where the photostability of soybean oil samples was examined, the coefficients of thermal diffusivity and thermal conductivity were determined. In addition, using time-resolved measurements, the difference between the photostability of pure oil and oils with the addition of natural and synthetic antioxidants has been shown. The coefficient of thermal diffusivity of cheeses was determined, linking its value with the quality of the cheese [492]. In [493], the thermal diffusivity was determined for various concentrations of crude oil, and the formation of aggregates was observed.

7.2 Forensic and art history expertise

Transient luminescence mapping [494] is widely used to identify changes made to documents, and if the modified part of the document does not have significant luminescent properties, optoacoustic mapping can be used. In the case of weakly absorbing samples, an optoacoustic wave is generated by the thermoelastic effect after photoexcitation [495]. The noninvasive optoacoustic imaging methodology is used to examine artistic works, especially to reveal hidden features such as original drawings or sketch lines [496]. Optoacoustic imaging has been used to determine the complex internal structure of oil miniatures on canvas [86]. Optoacoustic microscopic images obtained with a pulsed Nd: YAG laser (1064 nm, pulse duration ca. 1 ns) reliably reveal the presence of pencil lines on the reverse side of a canvas coated with several layers of paint thicker than 0.5 mm. By adjusting the bandwidth of optically induced ultrasonic waves, optoacoustic imaging can be used to study artifacts with various optical properties and geometric profiles, such as manuscripts, glass objects, or even stone sculptures.

In [496], the quality of reconstructed RGB images of simple test objects studied using a single-wavelength OAS, was assessed to confirm the capabilities of the method. The original images were decomposed into red, green, and blue (RGB) components, each of which was converted to grayscale intensity printed on a transparent film, and then measured using optoacoustic methods. To obtain a reconstructed RGB image, three optoacoustic images were combined. An experimental scheme for test objects has been created. It is expected

that more information-intensive results will be obtained by means of multispectral OAS that uses three sources with wavelengths corresponding to RGB channels.

7.3 Detection of single molecules or particles

In general, the number of studies on the thermooptical determination of NPs in solutions is still less than the number of applications in which basic parameters are determined and nanocomposite materials are studied. However, the sensitivity and selectivity inherent in photothermal methods are attractive for this purpose. PTS, especially its microvariants, provides sensitivity and contrast sufficient to detect single nanoobjects and large organic molecules, e.g., azo dyes with low fluorescence quantum yields [497].

Thermal diffusivity and thermal effusivity were studied for single-stranded and double-stranded DNA adsorbed on Au NPs of various shapes stabilized by citrate. Single-stranded DNA promotes an increase in thermal diffusivity, which makes it possible to develop biocompatible coolants or heat exchangers [498]. The thermal properties of resins for laser lithography in the manufacture of three-dimensional (3D) printed samples using TLS and an open optoacoustic cell [499], biodiesel fuel [500], have been studied.

Near-critical Xe or CO_2 are convenient media for amplifying a photothermal signal by more than two orders of magnitude [501]. In [502], an approach based on photothermal signal amplification for circular dichroism was implemented. The method combines an enantioselective circular-dichroism signal with the high sensitivity of photothermal microscopy, providing a high signal-to-noise ratio for the detection of chiral nanoobjects (2D-chiral NPs with C_4 symmetry). The advantage of the method is that the detection scheme is based on measuring the increase in the local temperature of the investigated nanostructure due to the absorption of photons with a known polarization. In addition, since the image is formed using the power-based photothermal method, the signal can be amplified within certain limits [503]. Tunable laser sources for the excitation beam can be used to convert photothermal circular dichroism into *photothermal circular-dichroism spectroscopy*.

It has been shown in [504] that single molecules can be detected in real time without the need to introduce labels due to amplification of the photothermal signal in NPs. The sensor consists of a single gold nanorod coated with biotin receptors, and the binding of individual proteins causes a change in the plasmon resonance of the nanorod and, thereby, a change in the photothermal effect around the NP during its interaction with the molecules of the test substances. The sensitivity of the instrument, which is 700 times higher than that of state-of-the-art plasmonic sensors, is limited by spectral diffusion at surface plasmon resonance.

The thermooptical flow determination of Au NPs using a microscopic version of thermal lens spectrometry was first reported by Japanese researchers led by T Kitamori [505] in 1998. Later, the same team published data on the successful determination of submolecular amounts of substances in the excitation beam volume [506], which are largely based on studies of single NPs using microfluidic chips (microchips). The detection of individual Au NPs in the microchip channel was shown, and the effect of particle immobilization on the channel surface under the action of laser radiation was demonstrated [507]. Papers [508, 509] indicate ways to increase the efficiency of the determination of NPs in a solution by increasing both the rapidity of analysis [508] (the frequency of thermooptical element excitation is 0.5–60 kHz) and the volume in which determination can take place without loss of sensitivity [509] (a 200-fold increase in detected volume). In study [510], the analytical characteristics of solutions of Au NPs obtained by thermal lens spectrometry are presented. The detection limit for the spectrometer configuration, which is optimal for measuring molecular solutions, is 100 NPs of Au (the size is ca. 250 nm) [510]. Another example of applying PTS to nanoscale biological objects is the detection of single NPs, cells, and organelles directly in blood [511] and lymphatic [512] vessels.

7.4 Infrared spectroscopy

Lately, in line with the general trends in analytical spectroscopy, the focus of new developments in photothermal spectroscopy has shifted to the IR range. Optoacoustic detection is most common in IR spectrometers, and there are fairly many developments of commercial Fourier-transform IR spectrometers. The measurements are based on 1D heat transfer models [6, 513]. IR radiation is directed from the interferometer to the OAS unit or attachment and focused on the sample in a closed cell filled with a working gas with a limited known volume (Fig. 17) [514]. The IR radiation modulated by the interferometer is absorbed by the test sample and converted into heat. Periodic temperature changes in the sample (thermal waves) depend on the interferometer modulation frequency, the absorption coefficients of the sample components, and its thermophysical parameters. Thermal waves generated by the sample, from a depth, which is limited by the thermal diffusion length (thermal wave attenuation length), enter the working gas [6, 513] and, as a result, generate acoustic waves there, which are picked up by a detector located near the main axis of the OAS unit.

Spectral information, which almost always is the main goal of measurements, is of decisive importance in interferometric OAS methods. Since most of the information about molecular structures, fragments, and functional groups is contained in the mid-IR region, most studies are carried out in this spectral range. Due to the linear dependence of the response on the light absorption coefficient, OAS is used to estimate the concentrations of substances in gaseous, liquid, and solid media in a wide dynamic range ($10^{-4}-10^{2}$ absorbance units) and with high accuracy (up to 0.1%) [27, 515]. Thus, OAS provides a wider measurement range and a higher sensitivity than those in transmission measurements.

IR-OAS spectroscopy uses two modes of interferometer operation: conventional, normal (continuous) scanning

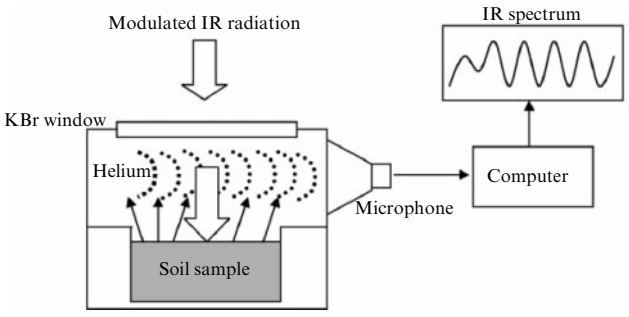

Figure 17. Setup for IR optoacoustic measurements [514].

implemented by most FT-IR spectrometers available on the market (fast or slow scanning modes, since low frequencies are usually required for thin-layer interferometer), and step scan. In a normal scan mode, which involves motion of the mirror, the mirror velocity is calibrated using a single wavelength and maintained constant during data acquisition, while in the step scan mode, the position of the moving mirror is controlled (with an accuracy of down to a few nanometers). The normal scan operation is convenient, but due to different frequencies corresponding to different wavelengths, it provides different signal generation depths in the final spectrum, which is especially pronounced in the IR range. The step scan mode provides a constant modulation frequency and, consequently, a constant acquisition depth of the OAS signal over the entire selected spectral range. This measurement option usually includes a built-in amplifier or digital signal processing techniques to detect and amplify the optoacoustic signal [516].

For solid samples, the key advantage of OAS is the possibility of obtaining spectra without sample preparation and dilution [517]. Another important advantage is the possibility of depth profiling of solid samples within a few hundred micrometers by changing the radiation source frequency or velocity [518, 519]. The IR-OAS results are less affected by the particle size of the sample than those of diffuse reflectance spectroscopy [520]. Compared to attenuated total reflection (ATR) methods, IR-OAS exhibits a higher sensitivity, while the signal is less affected by radiation scattering [521]. From a practical point of view, OAS is used to determine the absorption coefficients of materials and their components up to 1000 cm^{-1}. In complex samples, the most common application of OAS, in addition to biomedical applications, is the characterization of NPs and nanomaterials [66, 522–529]. In studying solid samples, various variants of OAS are used for polymeric materials [530].

IR-OAS is used in the quantitative analysis of the chemical composition of solid samples: paper [531], wood [532], biofilms [533], food products [534], and pesticides [304], and in microbiological studies [535]. The use of IR-OAS for the analysis, classification, and quality control of coffee blends [536] turned out to be a simple and fast alternative to existing methods (IR spectroscopy [537, 538], nuclear magnetic resonance [539, 540], Raman spectroscopy [541]). The role of IR-OAS spectroscopy in the analysis of soils and minerals is quite important [37, 514, 542–545]. The optoacoustic spectroscopy signal can be used for highly absorbing samples with minimal pre-treatment. The resulting spectrum differs from the transmission and reflection spectra, since nonradiative transitions in the sample appear in the OAS IR spectrum, and the intensity of the combined bands and overtones can change significantly [546].

The number of studies devoted to *IR thermal lens spectrometry* is relatively small [331, 547, 548]. Compared to most work in the visible range, in near-infrared measurements, the use of lasers tunable in the IR range or OPO is widespread, which makes it possible to record the spectra of a thermal lens signal. A thermal lens spectrometer for measuring absorption in the near-infrared range (860–1060 nm, tunable titanium-sapphire laser) has been developed. The thermal lens effect was probed in the visible range using a He–Ne-laser. The data obtained using multivariate calibration methods are used for nondestructive contactless determination of chemical and isotopic impurities in solvents. Water in D_2O and tetrahydrofuran can be detected at levels of 0.006 and 0.3 vol. %, respectively. The method has also been used for the simultaneous determination of water and dimethyl sulfoxide H6 (DMSO-H6) in DMSO-D6 and CH_3OH in CD_3OH, CD_2HOH and CDH_2OH at levels up to 10^{-3} wt. % [549].

IR-TLS has been used for the analysis of fuels [421, 550]. Overtone 4ν C–H at $\lambda = 916$ nm is typical of biodiesel, diesel fuel, and their mixtures. This made it possible to use TLS in the near-infrared range to control biodiesel quality [423]. Model compounds of isooctane and toluene were determined using near-infrared thermal lens spectrometry, well-resolved spectra of both compounds were obtained, and the positions of the absorption peaks are in good agreement with the data of other methods [96].

The disadvantages of IR-TLS are as follows. In measuring thermal lens spectra, only a scanning option is possible, as in spectrophotometry (the minimum time is 30 min for the entire range of 700–2300 nm with a resolution of 2 nm and the accumulation of 200 curves for a single wavelength), but not the interferometric version, as in IR-OAS. Thus, it is not possible to rapidly measure spectra in a wide range or with high resolution; if the maximum possible laser resolution of 0.1 nm is used, the time increases to 10 hours, and if weak and noisy signals are to be recorded, up to 2 days. While sufficiently high laser radiation powers are available in the visible range, in the IR range, especially in the microspectroscopic version, the use of high powers (> 1 W) and energies (100 mJ per pulse) to increase the sensitivity of measurements is hardly possible. This is due to the large number of thermal processes associated with the strong light absorption of the solvents themselves, possible thermochemical processes, etc. Thus, the options for a significant increase in detection sensitivity by the IR-TLS power component are limited.

PDS is one of the most convenient and widely used photothermal methods for obtaining surface images. The method has been very widespread for a long time in microscopic and nondestructive studies of semiconductors [551], metals [552–555], and optical materials [556]. PDS, in particular, is used for immunological studies with the isolation of a stained antigen–antibody complex on the surface of a solid substrate and subsequent photothermal detection of adsorption on the surface [557–559]. PDS was used to study optical absorption spectra of thin SnO films with the focus on bandgaps that exhibit a stable increase in intensity in the visible-light and IR range and a decrease in the UV range with an increase in the substrate temperature. It is believed that these trends are associated with the emergence of secondary phases caused by disproportionation [50]. A frequency-dependent turbulence model was used to determine the noise level as a function of the modulation frequency of 5–5000 Hz for a probe beam at several distances from the sample [560].

An ATR-IR-PDS method was proposed, which is based on the use of an excitation laser in the mid-IR range and a probe laser in the visible range [85, 561, 562]. The principle of the method is displayed in Fig. 18. The method combines the advantages of ATR-IR spectroscopy (the ability to analyze near-surface absorption and aqueous solutions and biological tissues without sample preparation) and PDS (inexpensive probe lasers and the ability to separately measure concentration and thermal characteristics of the sample). Compared to ATR-IR spectroscopy, ATR-IR-PDS makes it possible to explore deeper penetration depths (determined by the thermal diffusivity of the sample), which enhances the

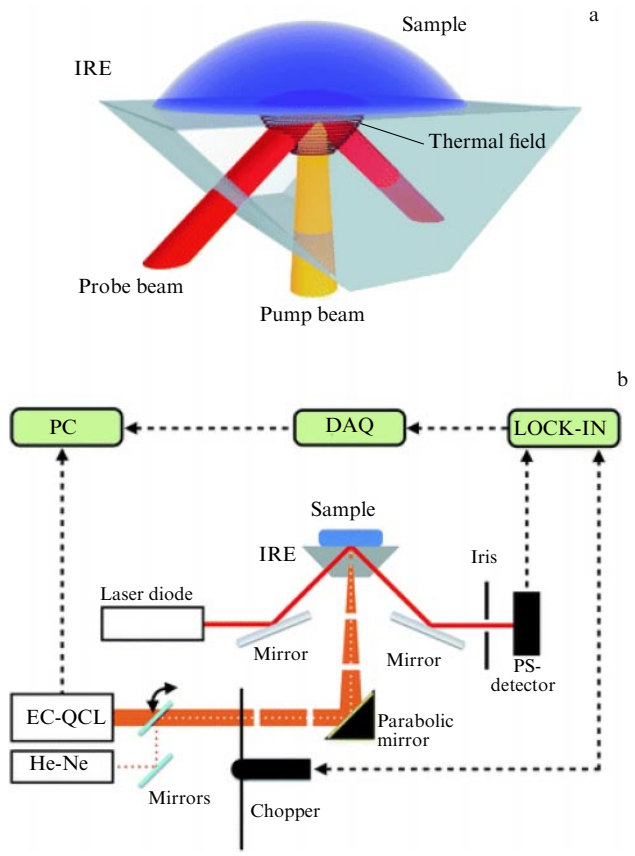

Figure 18. (Color online.) (a) Operation principle of the ATR-IR-PDS spectrometer. IRE (Internal reflection element) is the region of total internal reflection. (b) Tunable pulsed beam of an external-cavity quantum cascade laser (EC-QCL) modulated by a chopper serves as the excitation laser and is used to irradiate the sample, and creates a thermal field due to the absorption of IR radiation. Thermal field penetrates into the IRE, where the probe beam of the laser diode is fully reflected. Presence of the thermal field changes the refractive index as a result of which the probe beam deflects from the original direction. The deflection is measured via the change in intensity using a position-sensitive photodiode detector (PS detector). Pinhole is used to block interfering light. Photodiode signal is amplified by a lock-in amplifier. PC is a personal computer [561].

measurement sensitivity. The capabilities of the method have been demonstrated in the analysis of human skin for glucose without sample preparation. A correlation has been shown between the glucose content in the epidermis and the blood of patients with type 1 diabetes [561]. Similar to most existing problems of IR spectroscopy, the authors of [561] recommended using chemometric models, in particular, principal component analysis and partial least-squares (PLS) regression.

8. Biomedical applications of photothermal and optoacoustic spectroscopy

Conventional absorption spectroscopy in biomedicine includes transmission spectroscopy (spectrophotometry), reflection spectroscopy, and laser spectroscopy, which are most often used to measure the light absorption of hemoglobin-saturated blood or tissues [563, 564]. For a long time, these methods have been the main techniques employed in the study of biological system components (proteins, especially heme proteins) and associated diseases and pathologies. However, with the emergence of alternative methods (primarily fluorescence spectroscopy) capable of performing *in vivo* analysis, especially in flow, the role and importance of absorption spectroscopy has decreased [565].

The introduction of photothermal and optoacoustic methods made is possible to significantly expand the range of biomedical problems in spectroscopy, primarily absorption spectroscopy, in terms of both measurement sensitivity and spectral resolution [5, 107, 171, 566]. The advantages of PTS/OAS are that, unlike fluorescence microscopy and spectroscopy, these techniques can be used without fluorophores or contrast media, agents or substances that can break down, metabolize, or affect the sample properties [96, 113, 567]. The advantages of photothermal and optoacoustic spectroscopy for biomedical applications can be summarized as follows:

(1) real-time monitoring using multisignal and multispectral data [568];

(2) the ability to distinguish the light absorption of molecules and nanosized objects from a natural (biological or physiological) background [96, 171, 172, 569, 570];

(3) the ability to determine light absorption and the thermophysical properties of substances and to carry out depth profiling also against the background, including background light absorption of natural origin [569, 571];

(4) high measurement sensitivity, which makes it possible to handle small amounts of toxic substances while not requiring expensive reagents.

Microspectroscopic PTS and OAS applications are considered in Section 3, and the mechanisms of reactions of biologically active substances are discussed in Sections 5 and 6. Sections 8.1–8.4 present applications related to the determination of thermophysical and optical parameters and implementation of photothermal and optoacoustic diagnostics and theranostics.

8.1 Thermophysical parameters of biological systems

Interest in the thermophysical properties of biological systems, living organisms, and tissues is constantly growing. For example, thermophysical properties can be used as an effective tool for analyzing the conformational dynamics of proteins [572]. The distinction between energy and heat flows in proteins is the key to understanding how the optimum temperature is maintained in biological systems. Determining the mechanisms that control efficient and fast dissipation and energy transfer makes it possible to understand the complex biological processes that regulate the vital functions of organisms [573]. Modeling human and animal tissues for medical purposes, in particular, conducting radiofrequency ablation of the heart, interstitial operations using microwave instruments, etc., requires solving heat transfer equations, which include the thermal diffusivity and specific heat of the medium. In many cases, the values of these coefficients are also calculated, while experimental data can be a much more accurate tool for building models.

Another developing area of medicine that requires the determination of thermophysical parameters is therapy using nanomaterials, on the basis of which complex approaches are being developed, primarily theranostics. A typical example is the use of single-walled carbon nanotubes as a material for the selective destruction of cancer cells. Therapy and theranostics often require models of heat transfer and dissipation into cells with nanomaterials introduced [574].

Table 2. Some parameters and conditions for the use of thermal lens spectrometry for quantitative determination of biologically active compounds.

Target compound	Parameters of excitation radiation		References
	λ, nm	Power, mW	
Hemoglobin species in solution	488.0; 514.5	1 – 120	[575]
Bilirubin in solution	476	120	[576]
Bilirubin in the presence of biliverdin in endothelial cells	457.9	130	[577]
Bilirubin in plasma	457.9	130	[578]
Bilirubin in the presence of biliverdin	407	115	[458]

Studies of various types of materials, including those discussed in Section 4, show that PTS and OAS make it possible to determine the required experimental thermophysical parameters of target biomedical materials in a wide range of substances, concentrations, and sample volumes. Some examples of the use of photothermal spectroscopy for determining thermophysical parameters and detecting various biomolecules are given in Table 2. PTS and OAS solve simultaneously several problems: determining the component, describing its thermophysical parameters and observing conformational dynamics in various processes. The main parameter to be determined is the thermal diffusivity, and the main task is the quantitative description of the sample [458, 575–578]. For example, study [579] examined denaturation of hemoglobin, albumin, and human blood plasma. The temperature behavior of the temperature diffusivity coefficient depends on the specific area, unambiguously indicating the onset of denaturation. The data correlate with those obtained by other methods (e.g., differential scanning calorimetry) that describe conformational changes in samples. Optoacoustic spectroscopy was used as a cell diagnostics method [580]. Studies of the thermophysical parameters of biomolecules along with a lack of comprehensive data confirm the necessity to create a platform for the simultaneous quantitative and thermophysical description of such systems.

8.2 Optical parameters and quantitative measurements

More numerous are examples when PTS and OAS are used to determine the optical and spectral parameters of biological systems and for highly sensitive biomedical analysis (cells, biological fluids, tissues). These objects, as a rule, are studied using photothermal microscopy and optoacoustic microspectroscopy, while components and microcomponents (down to single molecules) are studied using both fast photothermal spectroscopy in the time domain and thermal lens spectrometry. Optoacoustic spectroscopy is used to describe microbiological objects (cells and tissues). For example, a model was developed [105] for determining cell components and various NPs in biological fluids.

Photothermal spectroscopy, especially TLS, is used to obtain protein absorption spectra as a sensitive method for quantifying the concentration parameters of proteins in solutions and, as discussed above, for monitoring photochemical reactions [96, 170, 581]. TLS was used to determine various species of hemoglobin, and, for all the studied species, the thermooptical response linearly depends on the laser radiation power in the range of 1–50 mW [575]. The accuracy of measurements of thermal lens absorption spectra of some heme proteins is suitable for studying both solutions and the composition of cell components [170]. The effect of medium change on the thermal lens signal has been described, which clearly indicates the expediency of using certain substances as a modifier (e.g., polyethylene glycol) [582]. The limits of detection of hemoglobin species are at the level of nanomolar concentrations [94].

TLS was used combined with other methods to separate and determine biological object components. For example, the combined use of TLS and high-performance liquid chromatography makes it possible to determine several nanomoles of bilirubin formed during the cleavage of heme proteins [577, 578], bilirubin, and biliverdin that are simultaneously present [458]. PTS and OAS were used to detect endogenous and exogenous antioxidants in biological fluids and endothelial vascular cells, to determine biomarkers of cardiovascular and oncological diseases, and antibodies and viruses, and to characterize multilayer biomedical aerogels consisting of a drug and a natural polymer using photothermal microscopy and its combination with liquid chromatography [16, 458, 577, 583].

One of the methods of photothermal radiometry — *optothermal transient emission radiometry* (OTTER) — was created specifically for noninvasive and contactless registration of absorption spectra of any complex surfaces, including human skin and complex technological samples [14, 584]. The most common tasks of OTTER are to quantify water and its distribution in the skin and to obtain information on the concentration of a solvent or drug directly in the skin. Mathematical models have been developed to reliably establish the distribution of water in the stratum corneum and the depth profiles of water or another solvent (e.g., ethylene glycol) in the stratum corneum [14, 585–587]. OTTER satisfies the main requirements for *in vivo* diagnostics: (1) fast response (registration of a spectrum takes about 15 min), (2) a nondestructive character, (3) a noninvasive nature, (4) an insignificant increase in the temperature of the skin area under study ($< 1\,^{\circ}$C), (5) a contactless nature, and (6) insensitivity to sample displacements and irregularities.

Pulsed PTR is used together with diffuse reflectance spectroscopy as complementary methods for studying surfaces, including biological objects: PTR measures the dynamics of processes on the sample surface after interaction with a mid-IR range light pulse, and, in relation to this, PTR is also used to study the optical properties of human skin, including in combination with other methods [588–591]. PTR is sensitive to the depth distribution of chromophores, while diffuse reflectance spectroscopy provides information over a wide range of wavelengths in the visible range and thus distinguishes between several chromophores. The instruments for both methods are independent of each other, but the received signals are processed together [588].

Thus, photothermal and optoacoustic spectroscopy make it possible to analyze and characterize biological objects at both the microlevel and the macrolevel and provide new opportunities for both studying basic biological processes

and solving practical problems of clinical laboratory diagnostics and therapy.

8.3 Photothermal and optoacoustic flow cytometry

Flow cytometry, a method that is operative at the sub-cellular and molecular levels, is based on measuring the response of living cells to a short-term laser pulse. The most common detection methods employed in flow cytometry are light scattering and laser-induced fluorescence of antibodies related to fluorescent dyes [592]. However, flow cytometry has some limitations; most importantly, this is an *in vitro* method and its adaptation to *in vivo* cell monitoring in some blood vessels is a challenging problem. One of the problems is light scattering by the skin, vessel walls, and artifacts, autofluorescence of the skin and vessel walls, and light absorption by blood and surrounding tissues. The fluorescence methods used in animal models have shown the ability to detect labeled hematopoietic stem cells or circulating tumor cells. However, the cytotoxicity of fluorescent tags and the difficulty of assessing only surface microvessels with a diameter of 50–100 μm at low flow rates and a depth of less than 200 μm are significant problems.

To overcome these limitations, *in vivo* flow cytometry using optoacoustic and photothermal methods has been employed [593, 594]. PTS detects in a noninvasive way unlabeled biomolecules at a level comparable to that of the detection that uses fluorescent labels [506, 595]. An increase in the photothermal temperature by $0.1-0.5\,^{\circ}\mathrm{C}$ at a low fluence of laser radiation (5–20 mJ cm^{-2}) is below the laser safety standards (30–100 mJ cm^{-2}) in the optical range [7]. The method is used for nondestructive control of living cells and control of selective photothermolysis in DNA studies. Methods based on the integration of *in vivo* optoacoustic flow cytometry and photothermal theranostics for early diagnosis and therapy of malignant neoplasms and infectious and cardiovascular diseases have been presented. These methods make it possible to detect and destroy cancer cells circulating in blood, bacteria, and blood clots at the early stages of the disease [96, 99,171, 511, 512, 594, 596–604].

8.4 Photothermal therapy, theranostics, and drug delivery

The problems of modern photothermal spectroscopy and photothermal imaging *in vivo* are closely related to laser therapy, theranostics, and drug delivery schemes. The concept of photothermal therapy and theranostics was actually first proposed as a variant of the implementation of the photothermal effect without contrast agents [605] and with NPs as photothermal contrast agents [606–611]. Later, photothermal imaging was transformed into laser diagnostics and therapy, which use agents that strongly absorb electromagnetic radiation, for diagnostics and detection of target objects or cells *in vivo*, and then for destroying malignant cells by means of radiationless heating using photothermal phenomena.

Photothermal therapy using nanoparticles is a highly selective and cost-effective method of treating cancer alone or in combination with other therapies such as radiation therapy or chemotherapy [612–619]. The future application of this method mainly depends on the development and synthesis of new multifunctional NPs that could overcome existing shortcomings such as limited penetration depth and lack of therapy control.

Photothermal theranostics is usually carried out using contrast agents, noble metal NPs, semiconductor and carbon nanomaterials, and organic (supramolecular) complexes and vesicles [22, 620–622]. In carrying out photothermal therapy, a temperature of lesions at a level of $42-45\,^{\circ}\mathrm{C}$ or even higher is usually achieved. This temperature destroys cancer cells, but also increases damage to normal tissues near the affected area due to thermal conduction, and thus causes a larger number of side effects and deteriorates therapeutic accuracy. Study [623] used $NdVO_4$ NPs with a size of 2.4 nm *in vivo*, which are capable of local heating of tissues upon excitation with $\lambda = 808$ nm, while simultaneously providing deep penetration for IR fluorescence imaging [623]. The study [624] used carbon composites of rare-earth NPs based on $NaLuF_4$:Yb and Er@$NaLuF_4$ with temperature feedback conversion combined with a photothermal material for real-time monitoring of changes in the microobject temperature. The local temperature of the photothermal material under illumination is high enough to destroy cancer cells, but too low to damage healthy tissue. Based on this phenomenon, photothermal ablation of a labeled tumor with a high spatial resolution is additionally implemented with minimal damage to normal tissues *in vivo*.

Review [612] presents approaches to the development of nanotechnological platforms for the targeted delivery of photosensitive agents that provide a local increase in temperature *in vivo* upon irradiation, leading to thermal ablation. An advantage of such nanopreparations is their multifunctionality, since they can provide targeted delivery, feature photosensitivity, and are combinations of chemotherapeutic and anticancer substances. Information is presented on preclinical studies of multimodal photothermal therapy for colorectal cancer, with an emphasis on potential clinical applications in a wide range of electromagnetic radiation with a wavelength of 700 to 2000 nm.

Theranostic methods, which are under development, are based on the use of nanostructured particles in combination with state-of-the-art methods of preclinical and clinical studies (magnetic resonance imaging, fluorescence tomography, optoacoustic flow cytometry and tomography, and optical coherence tomography) to create drug delivery schemes that combine navigation, imaging, *in vivo* monitoring of biochemical processes, and remotely activated release of bioactive substances *in vivo*, depending on the patient's condition. The possibility of using laser skin perforation to provide transdermal delivery of nanostructured theranostic objects has been demonstrated [530, 625].

In one of the most recent papers, optoacoustic wave generation was used in a thermoelastic material exposed to a short laser pulse to create temporary mechanical deformations of the cell membrane and facilitate the delivery of plasmid DNA into cells. This mechanism made it possible to perform optoacoustic transfection of a plasmid DNA labeled with a green fluorescent protein (gWizGFP, 3.74 MDa) into a monkey COS-7 fibroblast cells with an efficiency of 5% ($20\,^{\circ}\mathrm{C}$) in 10 min. It is noted that optoacoustic transfection is a scalable and quite simple procedure and allows localization in nuclei, while the dosage is easily controlled by the excitation radiation parameters [626].

9. Problems and prospects

Based on the above, it may be concluded that the methods of photothermal and optoacoustic spectroscopy are currently being developed in many directions (Fig. 19), all of which are based on five main features of the method, which we outlined

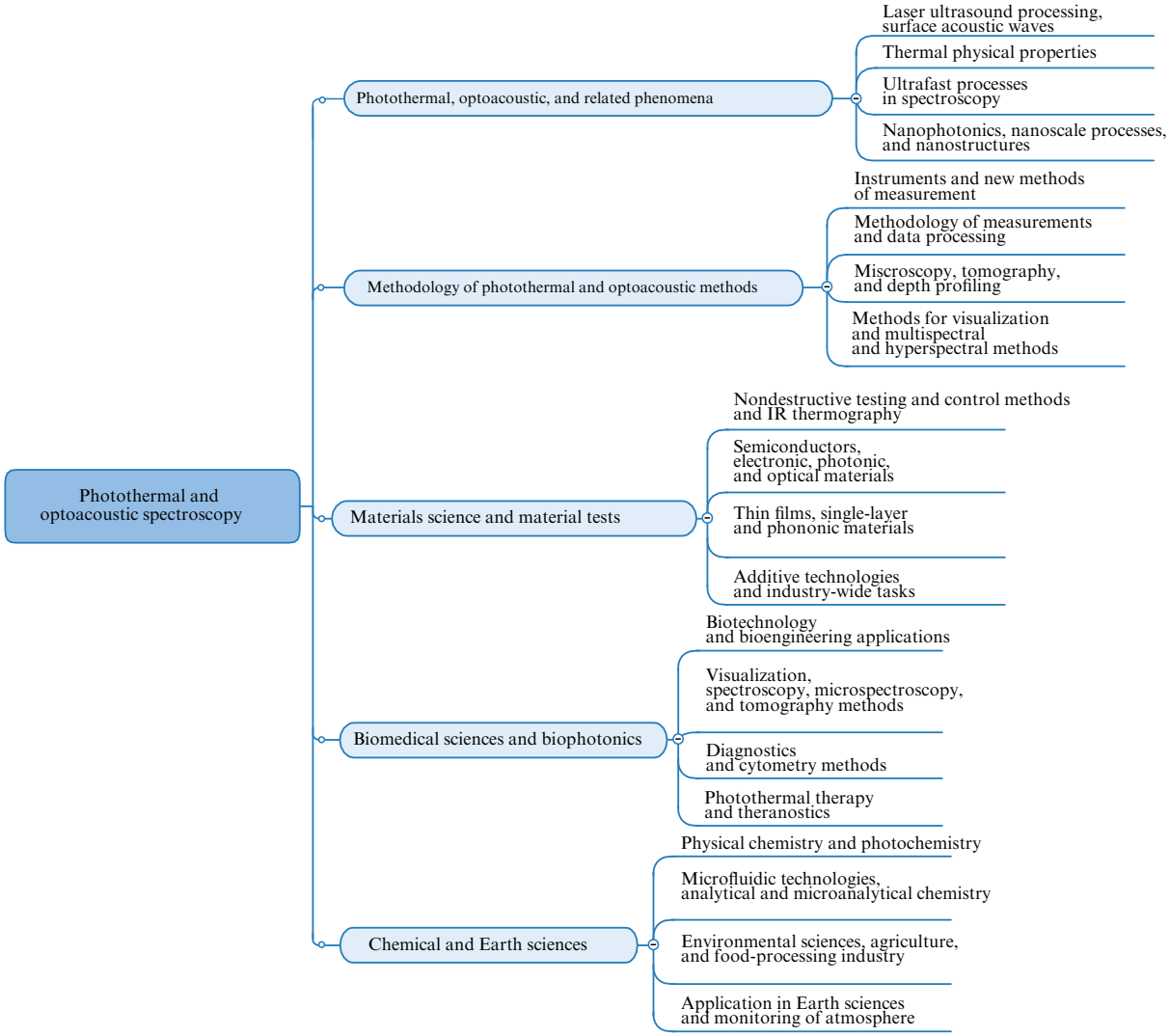

Figure 19. Main areas of the development of photothermal and optoacoustic spectroscopy.

in the introduction, namely: (1) a high sensitivity of measurements; (2) the possibility of simultaneous nondestructive determination of the optical and thermophysical parameters of the object under study; (3) a wide spectral range; (4) high spatial resolution, and (5) a wide range of objects, including those with a complex geometry and/or composition and undergoing dynamical changes.

The classification and structuring of the entire vast array of studies in the field considered in this review are fairly complex tasks. As a result, we divided all publications into five groups (see Fig. 19) related to problems or objects: basic research on photothermal, optoacoustic, and related phenomena and activities in the field of practical methodology of PTS and OAS, as well as their application in the biomedical sciences, materials science, chemistry, and geosciences. Not all tasks are equally developed, but there are significant advances in all twenty directions (see Fig. 19).

Biomedical topics have undoubtedly become dominant in recent years. Their main areas — methods of diagnostics and cytometry, visualization, microspectroscopy and tomography, and photothermal therapy and theranostics — are discussed in several sections of the review from the perspective of both basic and applied problems, in particular, topical medical problems. No less important are the applications of materials science, which are solved using photothermal and optoacoustic spectroscopy: first of all, this is the development of nondestructive testing and control methods (including IR thermography) and studies of target materials, such as semiconductors and electronic, photonic, and optical materials, as well as thin films.

In the basic research on photothermal and optoacoustic phenomena, in addition to the development of the general theory of photothermal and optoacoustic effects, to which a significant proportion of studies is devoted, attention is increasingly focused on the description of surface phenomena, dynamics, and the equilibrium state of thermal phenomena for nanoscale processes and nanostructures and ultrafast processes. Theoretical and basic research is almost always accompanied by applied and instrumental development of measurement and data processing methodology. In this relation, it is of importance to develop microscopy, visualization, imaging and microspectroscopy, tomography, and depth profiling and multispectral, full-spectrum, and, in the future, hyperspectral methods.

Finally, in the field of chemical and Earth sciences, in addition to the already established areas of development — atmospheric monitoring, analytical and physical chemistry — microfluidic technologies are being introduced, and a

renaissance of research in the field of photochemistry is observed. Important areas are the development of methods for the joint study of thermophysical and fluorescent properties and the use of PTS and OAS in industry, the study of environmental samples, and solving problems of agriculture and land use.

In accordance with this classification, problems in developing the methods considered in the review are discussed in Sections 9.1–9.4. Some of them, apparently, are currently being solved as this field is developed, some are due to the complexity of introducing new methods (e.g., for chemical sciences and geosciences) in the already existing practice, and some are associated with unsolved problems of theory and experiment.

9.1 Theory and methodology

Despite the large number of papers devoted to studying complex objects by means of photothermal spectroscopy, a generalized theory is still lacking that could describe photothermal phenomena, including experimentally observed patterns, in complex heterogeneous media. Moreover, the photothermal methods are developed to some extent separately, and this circumstance hinders the joint use of data from different methods and often represents both a theoretical and a methodological issue. Further improvement in the methodology of the photothermal studies of complex objects will require solving the following problems.

(1) In many photothermal methods, the theory refers either to homogeneous media or to a single nanoscale object [1]. Thus, it is necessary either to develop a theory of photothermal signal generation in complex objects [24, 115, 213–215, 409–413] or to refine and generalize existing theories. This task is especially important for slow methods based on an ensemble of particles, such as TLS and PDS, which encounter a wide range of problems precisely in the comprehensive description of equilibria in complex objects.

(2) Planning the experiment also requires taking into account factors related both to the features of the objects and to the possible operating modes of the instruments, which should provide both time-resolved and steady-state measurements. For TLS, minimal changes are required, while significant efforts are needed to have other photothermal methods adapted.

9.2 Instrumentation

As was mentioned above, a clear trend has been witnessed recently towards the development of commercial instruments. Simultaneously, commercial instruments are increasingly widely used to implement both optoacoustic methods, primarily as instruments for tomography and multispectral tomography, and photothermal methods, as well as microscopic, optical, and probe-based methods. In addition, in the last 3–5 years, a number of papers have been published in which photothermal and optoacoustic instruments are considered precisely as prototypes of commercial ones [627–632], i.e., not only are their principles of operation published, but so are options for software and hardware implementation. Nevertheless, there is currently a problem related primarily to photothermal methods, which is the lack of standardized instruments; it is typical of all types of problems for which photothermal spectroscopy is used. In our opinion, the following problems should be solved in this area.

(1) One of the key issues is the unification of photothermal instruments. Although several companies, industrial applications, and prototypes are available on the market, many authors create home-made photothermal instruments on a one-time basis for specific research purposes. This yields apparatuses that are hardly compatible, even if based on the same principle, which in turn leads to the absence of standard samples for measurements and detailed data on the error curves of instruments and techniques of photothermal research.

(2) It is probably necessary to create specialized facilities for certain tasks, since measurements and analysis of complex objects require choosing the measurement time, concentration, and excitation power. In particular, many methods that are used specifically for solid samples (PDS and PTR) require special cells for liquid media.

(3) Significant progress in the development of photothermal methods in many industries and research already requires special initiative consortium projects. They are fairly actively implemented in the European Union and the USA for the most important technologies that have yet obtained support from major companies, with the purpose of creating a market for photothermal instruments and generating demand.

The area under consideration has already witnessed an important precedent — a boom in optoacoustic tomography and MSOT [29–33, 84, 132–139, 151, 154]. In fact, after more than a decade of development, the efforts of researchers and developers, who have correctly invested in innovative projects, and relatively small commercial companies have resulted in steady progress in both creating commercial equipment and solving practical problems of preclinical and clinical laboratory diagnostics, which are introduced into practical medicine. Despite the complexity of such methodological, instrumental, and data processing problems [633], they are solvable, and the creation of commercial instruments is certainly necessary for photothermal spectroscopy as well.

Regarding the development of instruments and methodology, it is worth mentioning another important feature of photothermal measurements: their *multisignal* nature. In our opinion, an interesting task is to create a hardware/software basis and methodology for the simultaneous measurement of not only the main (photothermal) but also luminescent and photometric signals, as well as light scattering and, eventually, measurement of particle size (at least obtaining an estimate) (Fig. 20) to extract the maximum amount of information from the sample under study. First and foremost, this refers to combined photothermal and/or optoacoustic and luminescent measurements [634]. Examples of simultaneous detection already exist [482, 635, 636]; however, for photothermal spectroscopy, the optimum characteristics of such an instrument (geometric and energy), which provide high sensitivity of both photothermal and fluorescence detection, have not yet been established. The performance parameters of the determination and parameters (of both substances, e.g., quantum yield, and the object as a whole, e.g., optical and thermal parameters of the medium) that affect the accuracy and precision of measurements are not considered.

Spatial resolution. In biomedical research, in particular optoacoustic microspectroscopy, the entire scale of spatial resolutions actually has already been demonstrated: it ranges from mesoscopy to nanoscopy and from the molecular to the nanostructural level. In the case of photothermal spectroscopy, the methodology of nanoscopy and detection of single molecules is being developed, moreover, simultaneously in several directions, including optical confocal, correlation,

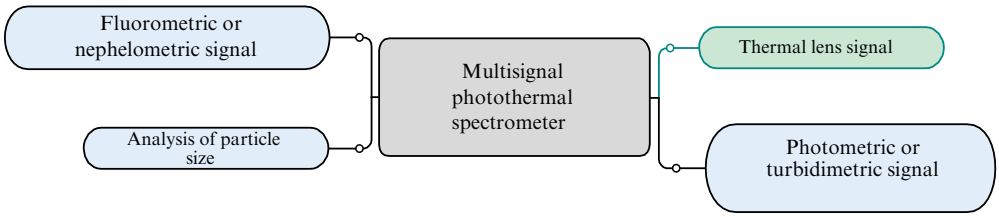

Figure 20. Main channels and the signals that can in principle be used to obtain information on photothermal studies (using as an example a thermal-lens spectrometer).

and probe spectroscopy. The latter technique is the most in demand, since it is operative in the IR range with an obviously higher diffraction limit than that in the visible range. Being a microspectroscopy method, photothermal probe spectroscopy provides high resolution imaging and mapping [245, 246, 637]. So far, reliable results have not been obtained for all objects, but this, in our opinion, is a methodological rather than an instrumental or technical problem, and a further increase in the spatial resolution of photothermal microscopy can be expected.

Multispectral analysis. As we discussed above, single-wavelength measurements are and will remain in demand for years to come in both photothermal and optoacoustic spectroscopy due to their relevance to many tasks (thermophysical measurements of materials, detection, determination and mapping of specific target substances in biomedicine, etc.). However, due to the versatile application and general extension of the capabilities of the methods under consideration, an increase in the number of operating wavelengths is becoming urgent in most photothermal and optoacoustic instruments. In addition to the most characteristic example of MSOT [134, 135, 141, 159, 160, 638–640], multispectral measurements are involved in solving almost all problems [94, 172, 180, 512, 641]. This trend, as was noted, is very similar to the situation with the development of multispectral methods in fluorescence microspectroscopy and Raman microspectroscopy, where single-wavelength measurements are no longer predominant, and instruments can perform two-wavelength (RGB) or multiwavelength measurements. As a result, this led to a breakthrough in the capabilities of fluorescence and Raman spectroscopies, which logically culminated in the development of hyperspectral methods [155, 176, 177]. There can hardly be any doubt that optoacoustic and photothermal methods will follow the same path.

Another option for the development of multispectral measurements is the use of continuous spectrum sources, tunable lasers, IR sources, or white light, as is the case in spectrophotometry and IR spectroscopy. The key problems here, which are quite obvious so far, are associated with scanning versions of photothermal measurements, which hinder rapid measurements of spectra in a wide range or with high resolution, especially when detection in a flow or of intermediate products is needed. In addition, there are a number of methodological and applied features, due to which photothermal spectroscopy with continuous spectra is little used, although technical difficulties have largely been overcome.

Compact instruments. The use of non-laser sources, in addition to multispectral measurements, has another important feature. Despite the use of compact lasers, the optical schemes of photothermal instruments with laser sources are still far from the concept of compact, portable, or mobile devices. However, the capabilities of photothermal methods in a compact version are attractive [180, 627, 628, 642]. From this point of view, in our opinion, 'slow' photothermal methods, such as TLS, PDS, or PTR, have the greatest potential. Their implementation in the form of compact setups will make it possible to use all the capabilities of molecular spectroscopy in chemical analysis (field analysis) and rapid tests in nondestructive testing combined with high-sensitivity photometric detection. Consequently, simple and convenient protocols of measurement can be developed for both solid phases and solutions. Such a strategy has been successful in thermal lens spectrometry [643].

9.3 Biomedical problems

In Sections 3–8, we discussed in detail the capabilities and achievements of and prospects for the development of photothermal and optoacoustic spectroscopy intended for biomedical problems. Actually, it is now one of the most developed and at the same time rapidly developing areas. Nevertheless, an analysis of the literature and comparison of studies related to various types of objects require noting several problems in this area as well.

The focus of optoacoustic spectroscopy and tomography on complex real living systems is apparent, but in some cases these methods are also in demand for solving problems of biomaterials science. In particular, studies in biotechnology and bioengineering, in which it is necessary to determine the optical and thermal characteristics of objects, and in the developing 'organ-on-a-chip' field of research are yet fairly infrequent. In addition, at the molecular structural level, data on the thermophysical parameters of biomolecules (primarily proteins and lipids), where the significance of photothermal and optoacoustic spectroscopy is beyond doubt, are still insufficient.

Both existing studies of biological systems and those not yet implemented confirm the need to create *ex vivo*/*ex situ* platforms for the simultaneous determination of the quantitative composition and thermophysical parameters. Indeed, in assessing the toxicity, biocompatibility, and biotoxicity of drugs and nanoparticles, there is often a discrepancy between *in vivo* studies and preclinical *in vitro* trials. This is due to the fact that, at the stages of *in vitro* research, e.g., high doses and short times of irradiation/exposure to external factors are used due to the difficulties of maintaining living systems. This problem is relevant for optical and radiological diagnostics, laser therapy, theranostics, and the concept of targeted drug delivery.

On the other hand, in testing and studying nanomaterials themselves in applied problems (catalysis, preconcentration), it is necessary to prepare nanoparticles with certain properties and study these properties *in situ*. Such analysis or testing should include carrying out quite varied tasks: determining

the chemical composition of the obtained particles (conceived as a substance or compound) and studying materials based on them. This requires clarifying the characteristic size, studying the physical and chemical properties, and assessing the impact of various chemical and physical factors. Exactly the same ideology and methodology are in demand in the case of analysis or testing of nanomaterials, when the substance under study is separated, concentrated, and immobilized (or fixed in the case of NPs, cells, etc.) to study the properties under the conditions most advantageous for the researcher.

Lately, there has been a convergence of problems of both types. In particular, it has been shown that complexes of proteins with lipids exhibit the properties of nanoparticles and nanotubes; the possibilities of medical application of carbon nanoparticles in the form of complexes with proteins are considered; many issues of photodynamic therapy and problems of apoptosis are associated with the dispersed properties of natural systems; and polymer-modified media are a key feature of protein crystallization, in virology, etc.

Thus, both for biological objects and for technological nanomaterials, complex methods of analysis and diagnostics should be developed, and sufficiently versatile (structured) media suitable for the analysis and testing of complex objects should be used [644]. Such a methodology (platform) for the analysis and testing of biological and nanomaterials should ensure the convenience, reliability, and reproducibility of operations with various materials at the level of trace amounts and concentrations of analytes *in vitro*/*in situ*, and on the other hand, include a fairly wide range of methods of analysis and research. Such a platform should also support research, on the one hand, in sufficiently thin layers to obtain primary information, and, on the other hand, in materials with a 3D structure that simulates a real system. In addition, both the immobilization of NPs and their rather soft fixation are necessary to reproduce as accurately as possible conditions for the existence of the objects under study in real systems. Similar systems can be created using water-soluble polymers, thin polymer layers, and hydrogels that model various components of real biological and technological systems [645–647]. The relevance of suchlike research is evidenced by a large number of research papers and surveys in the area under consideration [648, 649]. Apparently, these platforms are fairly independent of the measurement method, but both in concept and in measurement capabilities they are certainly complementary to most photothermal and optoacoustic methods.

9.4 Materials science and chemical sciences

Similar to the case of biomedical problems, it is fairly apparent that the determination of the properties of materials is one of the main avenues in the development of photothermal and optoacoustic spectroscopy. In the near future, it is natural to expect an increase in the number of studies related both to the development of methods and to their application to various objects. Interestingly, in the last five to seven years, studies related to the assessment of the thermophysical parameters of materials in non-destructive testing have already been using the methods of photothermal, optoacoustic, and complex diagnostics as fairly standard and routine measurements.

However, not all problems in this area have been solved so far. As was mentioned in Section 9.2, there is a need for standardization and unification of measurements, as well as the development of methodological approaches and universal platforms for testing complex objects. In addition, the trueness and accuracy of photothermal measurements has not yet been ensured for all problems, which often hinders the wider dissemination of the methods under consideration.

Thus, one can expect an increase in the number of studies devoted to the application of photothermal and optoacoustic spectroscopy for new materials [650, 651]. Now, carbon nanomaterials can be cited as a typical example [287, 526, 652–654], but the application of photothermal and optoacoustic spectroscopy can be expanded and extended to other problems associated with the use of additive technologies, single-layer materials, photonic crystals, and phononic materials.

Analytical chemistry. The number of objects and tasks of chemical analysis is constantly growing, and the number of methods for sample preparation and analysis is increasing as well. As a result, the selection of sample preparation and analysis method depends on a very large number of factors. The researcher should take into account the requirements for the correctness and precision of the analysis, the cost of instruments and the analysis itself, the qualifications of personnel, the scale and rapidity of analysis, etc., as well as the availability of regulatory documents and the current capabilities of commercially available instruments with certain operating characteristics offered by manufacturers.

In view of the above requirements, the role of photothermal and optoacoustic spectroscopy in analytical chemistry is ambiguous: due to the absence of analytical instruments and, as a result, the absence of fully developed and certified procedures and reference materials, these methods are less competitive than spectrofluorimetry, liquid chromatography, and electrochemical methods. Moreover, the exploitation in the past of, in fact, the only parameter — sensitivity, considered the most important analytical characteristic of PTS/OAS for all test substances, including metal ions, where it is difficult to compete with the atomic spectroscopy methods — was quite erroneous. Such a bias in the development of other chemical-analysis methods resulted in the absence of a niche for photothermal and optoacoustic spectroscopy, despite interesting methodological developments in the analysis of complex mixtures and detection in chromatography [458, 655–657]. In fact, analytical photothermal and optoacoustic methods of significance for practice only began to appear after the concepts of microfluidic chips and microspectroscopic analysis of small amounts of biologically active compounds had been created.

Now, in our opinion, another not entirely positive trend is forming: a breakthrough in the field of biomedical topics, it might seem, urgently requires a direct combination of physical principles and theories with biomedical problems. However, practice shows that such a statement of the problem, which actually excludes the methodology of chemical measurements as a connecting link, is not fully justified. In addition to skipping such a link, as we discussed above (*in vitro*, *ex vivo*/*ex situ*, *in vivo*/*in situ*), neglecting the chemistry of the interaction is fraught with the loss of both the trueness and accuracy of measurements, since it is precisely the stages of sample preparation or derivatization that primarily contribute to the bias and random errors of the entire measurement cycle. Finally, it is incorrect to disregard the developed methodology of chemical analytical methods of molecular absorption spectroscopy. Selective derivatization, background masking, chemical signal amplification, orthogonal reactions — all this can ensure significant gains

in areas that are not formally related to analytical chemistry but are associated with the determination of optical, concentrational, and size parameters using photothermal and optoacoustic measurements.

We discussed above possible ways to solve problems associated with instruments and methodology. It should be emphasized that activities are also needed for metrological support for photothermal and optoacoustic measurements based on modern requirements: the concept of measurement traceability and uncertainty (ISO/IEC 17025-2019 and the ISO 5725 series) and experiment design. For the most commonly used method–task links, it is probably necessary to calculate the uncertainty budget, since, for a mature method, and even more so when a method is introduced into testing practice, the number of factors in the uncertainty budget increases, the proportion of type A factors increases, and the overall accuracy class is enhanced. An assessment of the measurement uncertainty will make it possible to show the areas of applied sciences in which photothermal spectroscopy is really in demand, taking into account the fact that commercially produced instruments are already available.

From the perspective of practical, 'purely' chemical problems of photothermal and optoacoustic spectroscopy, it can be predicted that those techniques will be in demand that offer two or more channels for the simultaneous collection of information about the sample without sample preparation, e.g., spectral information or simultaneous detection of light absorption and luminescence or light scattering. Currently, this refers primarily to biological samples, but in the nearest future the emergence of methods designed for the analysis of complex natural samples or microspectroscopy should be expected. Today, the methodology of applied measurements is not sufficiently developed.

It can be asserted in conclusion that, owing to the complex and multisignal nature of photothermal and optoacoustic spectroscopy methods, they are a very valuable and flexible tool. Even interfering factors (foreign chemical components, the influence of thermophysical parameters and particle size of the dispersed phase, the competitive nature of fluorescence, thermal effects of reactions, etc.) can be turned into advantages of new methods of chemical analysis and applied chemistry. We presented above fairly many examples of such multisignal solutions and their successful implementation. Moreover, most of these works are focused on research not only in chemistry but also in other fields of application of photothermal and optoacoustic spectroscopy.

This study was financially supported by the Russian Foundation for Basic Research as part of scientific project no. 19-13-50278 ('Expansion' 2019).

10. Glossary

Probe laser is, in *photothermal spectroscopy*, a laser whose radiation passes through the thermal perturbation region (*thermooptical element*), and the change in this radiation is used to make conclusions regarding light absorption or thermal parameters of the sample.

Excitation source is, in *photothermal spectroscopy*, a source of electromagnetic radiation (usually a laser), which is absorbed by a sample and causes *photothermal effects*.

Molecular thermal spectroscopy is a set of spectroscopy methods that combine the capabilities of optical spectroscopy or IR spectroscopy (providing information about electromagnetic spectra and the quantitative chemical composition of a test sample) and *thermal spectroscopy*.

Optoacoustic (photoacoustic) spectroscopy is a subgroup of methods of ***photothermoacoustic spectroscopy***, which measure density waves (*acoustic waves*) caused by an electromagnetic pulse and thermal expansion of the sample during the absorption of electromagnetic radiation by its components (atoms, crystal lattice sites, molecules, supramolecular structures, nanoparticles, etc.) leading to local heating of the sample and subsequent nonradiative relaxation. The change in pressure is recorded using a microphone or a piezoelectric transducer.

Thermal spectroscopy is a set of spectroscopic methods that provide diagnostics and analysis of materials based on the change in the optical spectra of probe radiation due to changes in the thermophysical parameters of a test sample with temperature change. If the source of heating is the *photothermal effect*, the corresponding subgroup of thermal spectroscopy is referred to as *photothermal spectroscopy*.

Photothermal deflection (thermal deflection, mirage effect) is a *photothermal effect* that manifests itself in the deflection of the direction of propagation of the *probe laser* beam from the direction parallel to the surface of a solid body irradiated by the light of an *excitation source* under the action of a *photothermal element* similar to a prism (*thermal prism*). Thermal deflection is usually measured using a positional (four-quadrant) optical detector.

Photothermal deflection spectroscopy (PDS, thermal deflection spectroscopy, or mirage spectroscopy) is a *thermooptical* method of photothermal spectroscopy. The principle of the method based on the *photothermal deflection* phenomenon consists of irradiating a solid sample with a flat surface with light from an *excitation source* with a certain frequency, directed along the normal to the surface under study. Under the effect of irradiation, the sample is heated; the extent of heating depends on the local thermophysical properties of the material in the irradiation region. In a liquid or gaseous medium (most often air), which is in direct contact with the test sample, due to its heating by the sample itself, a *photothermal element* is formed. It acts like a prism (*thermal prism*) on the radiation of a *probe laser*, which propagates along the surface of the sample.

Thermal lens spectrometry is a *thermooptical* method of *photothermal spectroscopy*, in which a thermal perturbation causes the formation of a refractive index profile in an isotropic medium that leads to the formation of a *thermooptical element*, the behavior of which is similar to that of a diverging lens (*photothermal lens*). As a result of heating, a spatial gradient of the refractive index is established. The broadening of the laser beam on the resulting thermooptical element is proportional to the absorption of the sample. The use of TLS in light absorption measurements is based on the fact that the optical power of a photothermal lens is directly proportional to the absorbance of the object and, according to the Bouguer–Lambert–Beer law, to the concentration and absorption coefficient of the test compound. For quantitative registration, dual-beam schemes are used in which a change in the divergence of (low-power) radiation from a *probe laser*

that has passed through a photothermal lens is measured. TLS is most often used to determine the quantitative composition of solutions and light absorption coefficients.

Thermooptical element is a spatial temperature perturbation caused by the *photothermal effect*, which leads to a change in the temperature-dependent thermophysical properties of a sample and, as a result, to the formation of a refractive index profile. In the first approximation, this profile can be considered an analogue of an optical element (lens, prism, mirror, diffraction grating, etc.).

Photothermal spectroscopy is a group of molecular absorption spectroscopy methods based on the measurement of light absorption by the regular thermal disturbance caused by it, the *photothermal effect*. Photothermal spectroscopy methods, which relate to *thermal spectroscopy*, depend on power (the intensity of the *excitation source* radiation) and are based on *photothermal effects*. As a result of heating and the photothermal effect, a spatial gradient of the refractive index is established. The broadening or deflection of the *probe laser* beam on the element that emerges depends on the thermophysical parameters of the test sample and the concentrations of its light-absorbing components.

> ***Photothermal radiometry*** is a subgroup of *photothermal spectroscopy* methods based on the direct detection of thermal radiation caused by photothermal effects.
>
> ***Thermooptical spectroscopy*** is a subgroup of *photothermal spectroscopy* methods based on recording changes in the optical properties of a sample upon excitation of a thermal perturbation.

Photothermal microspectroscopy is a variant of *photothermal spectroscopy*, in which the optical scheme of the instrument is that of an optical microscope, while the main task is to obtain spectral and quantitative information about the sample.

Photothermal microscopy is a variant of *photothermal spectroscopy*, in which the optical scheme of the instrument is that of an optical microscope, while the main tasks are obtaining spatial information about the absorption of the sample and visualization of the spatial absorption profile.

Photothermal element is a spatial temperature perturbation caused by the *photothermal effect*, which leads to a change in the temperature-dependent thermophysical properties of the sample (primarily, the thermal conductivity and density) and, as a result, to the formation of a refractive index profile; this profile can be considered in the first approximation an analogue of an optical element (lens, prism, mirror, diffraction grating, etc.). In *photothermal deflection spectroscopy*, a photothermal element is referred to as a ***thermal prism***.

Photothermal effect (photothermal phenomenon) is the name of any changes in temperature (*thermal perturbation*) and the temperature-dependent physical parameters of an object (density, refractive index, sound speed, volume, shape, etc.) due to absorption of electromagnetic radiation by the object. As a rule, electromagnetic radiation lies in the *optical* or *IR range*. Photothermal effects are understood both as the final (equilibrium or steady-state) distribution of temperature and related phenomena (e.g., *photothermal deflection spectroscopy*) and the dynamics of temperature propagation (thermal waves).

References

1. Bialkowski S E, Astrath N G C, Proskurnin M A *Photothermal Spectroscopy Methods* (Weinheim: Wiley, 2019)
2. Skvortsov L A *Osnovy Fototermicheskoi Radiometrii i Lazernoi Termografii* (Basics of Photothermal Radiometry and Laser Thermography) (Moscow: TEKhNOSFERA, 2017)
3. Sell J A (Ed.) *Photothermal Investigations of Solids and Fluid* (Boston: Academic Press, 2012)
4. Franko M, Tran C D *Thermal Lens Spectroscopy* (Encyclopedia of Analytical Chemistry, Eds R A Meyers, R A Meyers) (Weinheim: John Wiley and Sons, 2010) https://doi.org/10.1002/9780470027318.a9079
5. Proskurnin M A "Photothermal spectroscopy", in *Laser Spectroscopy for Sensing*: *Fundamentals, Techniques and Applications* (Electronic and Optical Materials, Vol. 43, Ed. M Baudelet) (Cambridge: Woodhead, 2014) Ch. 11
6. Michaelian K H *Photoacoustic IR Spectroscopy*: *Instrumentation, Applications and Data Analysis* (Weinheim: Wiley-VCH, 2010)
7. Wang L V (Ed.) *Photoacoustic Imaging and Spectroscopy* (Boca Raton, FL: CRC Press, 2009)
8. Wang L V, Wu H *Biomedical Optics*: *Principles and Imaging* (Weinheim: Wiley, 2012)
9. Georges J *Talanta* **48** 501 (1999)
10. Franko M *Talanta* **54** 1 (2001)
11. Navas M J, Jiménez A M *Crit. Rev. Anal. Chem.* **33** (2) 77 (2003)
12. Kitamori T *Fresenius J. Anal. Chem.* **371** 89 (2001)
13. Blanchard G J *Appl. Spectrosc.* **55** 110A (2001)
14. Xiao P *Cosmetics* **3** (1) 10 (2016)
15. Proskurnin M A, Bendrysheva S N, Smirnova A P *J. Anal. Chem.* **71** 431 (2016); *Zh. Anal. Khim.* **71** 451 (2016)
16. Liu M, Franko M *Int. J. Thermophys.* **37** 67 (2016)
17. Franko M et al. *Anal. Sci.* **32** (1) 23 (2016)
18. Proskurnin M A et al. *J. Anal. Chem.* **70** 249 (2015); *Zh. Anal. Khim.* **70** 227 (2015)
19. Cassano C L et al. *Electrophoresis* **35** 2279 (2014)
20. Skvortsov L A *Quantum Electron.* **43** 1 (2013); *Kvantovaya Elektron.* **43** 1 (2013)
21. Proskurnin M A, Kononets M Yu *Russ. Chem. Rev.* **73** 1143 (2004); *Usp. Khim.* **73** 1235 (2004)
22. Jain P K et al. *Acc. Chem. Res.* **41** 1578 (2008)
23. Peters K S, Watson T, Marr K *Annu. Rev. Biophys. Biophys. Chem.* **20** 343 (1991)
24. Selmke M, Cichos F, arXiv:1510.08669
25. Tuchin V V, Tárnok A, Zharov V P *Cytometry A* **79** 737 (2011)
26. Dadarlat D *Laser Phys.* **19** 1330 (2009)
27. Haisch C *Meas. Sci. Technol.* **23** 012001 (2011)
28. Attia A B E et al. *Photoacoustics* **16** 100144 (2019)
29. Jeon S et al. *Photoacoustics* **15** 100141 (2019)
30. Liu W, Zhang H F *Photoacoustics* **4** (3) 112 (2016)
31. Schellenberg M W, Hunt H K *Photoacoustics* **11** 14 (2018)
32. Steinberg I et al. *Photoacoustics* **14** 77 (2019)
33. Zhang H F, Razansky D *Photoacoustics* **4** (3) 81 (2016)
34. Escola F Z et al. *Proced. Mater. Sci.* **8** 665 (2015)
35. Dazzi A, in *Thermal Nanosystems and Nanomaterials* (Topics in Applied Physics, Vol. 118, Ed. S Volz) (Berlin: Springer, 2009) p. 469
36. Lima S M et al. *J. Non-Cryst. Solids* **273** 215 (2000)
37. Volkov D S et al. *Photoacoustics* **17** 100151 (2020)
38. Adhikari S et al. *ACS Nano* **14** 16414 (2020)
39. Malinski M et al. *Int. J. Thermophys.* **26** 255 (2005)
40. Waloszek A et al. *Photosynthetica* **40** 279 (2002)
41. Mandelis A, Guo X *Phys. Rev. E* **84** 041917 (2011)
42. Teng Y C, Royce B S H *Appl. Opt.* **21** 77 (1982)
43. Rosencwaig A, Gersho A *J. Appl. Phys.* **47** 64 (1976)
44. Proskurnin M A et al. *Int. J. Thermophys.* **39** 81 (2018)
45. Heber A, Selmke M, Cichos F *ACS Photon.* **4** 681 (2017)
46. Korte D, Franko M *Int. J. Thermophys.* **35** 2352 (2014)
47. Korte D et al. *Int. J. Thermophys.* **35** 2107 (2014)
48. Vargas H, Miranda L C M *Rev. Sci. Instrum.* **74** 794 (2003)
49. Zhang X, Li B *Rev. Sci. Instrum.* **89** 024901 (2018)

50. Toyama T et al. *Thin Solid Films* **555** 148 (2014)
51. Macías J D et al. *AIP Conf. Proc.* **2126** 020002 (2019)
52. Ramírez-Rincón J A et al. *Appl. Phys. A* **124** 252 (2018)
53. Fleurence N et al. *Phys. Status Solidi A* **212** 535 (2015)
54. Guo X et al. *Biomed. Opt. Express* **5** 2333 (2014)
55. Liu Y J, Mandelis A, Guo X *Rev. Sci. Instrum.* **86** 115003 (2015)
56. Chrobak L, Maliński M, Pawlak M *Infrared Phys. Technol.* **67** 604 (2014)
57. Rojas-Rodríguez I et al. *Int. J. Thermophys.* **33** 2382 (2012)
58. Gensch T, Viappiani C *Photochem. Photobiol. Sci.* **2** 699 (2003)
59. Abad B, Borca-Tasciuc D-A, Martin-Gonzalez M S *Renew. Sust. Energ. Rev.* **76** 1348 (2017)
60. Loeb S, Li C, Kim J-H *Environ. Sci. Technol.* **52** 205 (2018)
61. Mandelis A *J. Phys. A* **24** 2485 (1991)
62. Inoue K et al. *Biophys. J.* **92** 2028 (2007)
63. Terazima M *Chem. Phys. Lett.* **304** 343 (1999)
64. Nakajima N, Hirota N, Terazima M *J. Photochem. Photobiol. A* **120** (1) 1 (1999)
65. Verstraeten B et al. *Photoacoustics* **3** (2) 64 (2015)
66. Kouyaté M et al. *Int. J. Thermophys.* **36** 3211 (2015)
67. Leys J et al. *Mater. Renew. Sustain. Energy* **5** 4 (2016)
68. Katayama K, Shibamoto K, Sawada T *Chem. Phys. Lett.* **345** 265 (2001)
69. Harata A et al. *Anal. Chim. Acta* **299** 349 (1995)
70. Leduc C et al. *ACS Nano* **5** 2587 (2011)
71. Absil E et al. *Opt. Express* **18** 780 (2010)
72. Berciaud S et al. *Phys. Rev. B* **73** 045424 (2006)
73. Usoltseva L O, Korobov M V, Proskurnin M A *J. Appl. Phys.* **128** 190901 (2020)
74. Lenart V M et al. *J. Appl. Phys.* **123** 085107 (2018)
75. Kozich V P et al. *Appl. Spectrosc.* **48** 1419 (1994)
76. Proskurnin M A, Volkov M E *Appl. Spectrosc.* **62** 439 (2008)
77. Marcano A O et al. *Appl. Spectrosc.* **57** 1278 (2003)
78. Rohling J H et al. *J. Phys. D* **34** 407 (2001)
79. Barbero C, Kótz R, Haas O *Synth. Met.* **101** 170 (1999)
80. Franko M, Bicanic D *Isr. J. Chem.* **38** 175 (1998)
81. Bialkowski S E et al. *Appl. Spectrosc.* **46** 1335 (1992)
82. Bayareh M *Chem. Eng. Process. Process Intensif.* **153** 107984 (2020)
83. Barrett K E et al. *Ganong's Review of Medical Physiology* 26th ed. (New York: McGraw-Hill Education, 2019)
84. Lawrence D J et al. *Sci. Rep.* **9** 558 (2019)
85. Bauer A et al. *J. Biophoton.* **11** e201600261 (2018)
86. Tserevelakis G J et al. *Sci. Rep.* **7** 747 (2017)
87. Li Voti R et al. *Nanoscale Adv.* **3** 4692 (2021)
88. Jeng G-S et al. *Nat. Commun.* **12** 716 (2021)
89. Nedosekin D A, Proskurnin M A, Kononets M Yu *Appl. Opt.* **44** 6296 (2005)
90. Miyazaki J, Kobayahsi T *Photonics* **4** (2) 32 (2017)
91. Nedosekin D A et al. *Drug Metabolism Rev.* **47** 346 (2015)
92. Vermeulen P, Cognet L, Lounis B *J. Microsc.* **254** 115 (2014)
93. Selmke M, Braun M, Cichos F *ACS Nano* **6** 2741 (2012)
94. Proskurnin M A et al. *Cytometry A* **79** 834 (2011)
95. Bai Y et al. *J. Phys. Chem. B* **121** 10249 (2017)
96. Nedosekin D A et al. *Biophys. J.* **102** 672 (2012)
97. Moreau J, Loriette V *Jpn. J. Appl. Phys.* **45** 7141 (2006)
98. Moreau J, Loriette V *Opt. Lett.* **29** 1488 (2004)
99. Nedosekin D A et al. *Small* **10** 135 (2014)
100. Sreekumar K, Mandelis A *Int. J. Thermophys.* **34** 1481 (2013)
101. Mandelis A *Int. J. Thermophys.* **33** 1776 (2012)
102. Guo X et al. *Biomed. Opt. Express* **3** 3012 (2012)
103. Malacarne L C et al. *Appl. Spectrosc.* **65** (1) 99 (2011)
104. Tokeshi M et al. *Anal. Chem.* **74** 1565 (2002)
105. Nedosekin D A et al. *J. Biophoton.* **6** 523 (2013)
106. Nedosekin D A et al. *J. Biophoton.* **6** 425 (2013)
107. Galanzha E I, Zharov V P *Methods* **57** 280 (2012)
108. Nedosekin D A et al. *Cytometry A* **79** 825 (2011)
109. Khodakovskaya M V et al. *Proc. Natl. Acad. Sci. USA* **108** 1028 (2011)
110. Harada M et al. *Anal. Sci.* **15** 647 (1999)
111. Shokoufi N et al. *Anal. Bioanal. Chem.* **411** 6119 (2019)
112. Shimizu H, Mawatari K, Kitamori T *Anal. Chem.* **82** 7479 (2010)
113. Brusnichkin A V et al. *J. Biophoton.* **3** 791 (2010)
114. Wang L V *Nat. Photon.* **3** 503 (2009)
115. Selmke M, Braun M, Cichos F *Opt. Express* **20** 8055 (2012)
116. Kotaidis V, Plech A *Appl. Phys. Lett.* **87** 213102 (2005)
117. Zharov V P, Galitovsky V, Viegas M *Appl. Phys. Lett.* **83** 4897 (2003)
118. Lin C P, Kelly M W *Appl. Phys. Lett.* **72** 2800 (1998)
119. Roegener J, Brinkmann R, Lin C P *J. Biomed. Opt.* **9** 367 (2004)
120. Olson N E et al. *Anal. Chem.* **92** 9932 (2020)
121. Klementieva O et al. *Adv. Sci.* **7** 1903004 (2020)
122. Kansiz M et al. *Anal. Chem.* **93** 11081 (2021)
123. Beltran V et al. *Angew. Chem. Int. Ed.* **60** 22753 (2021)
124. Spadea A et al. *Anal. Chem.* **93** 3938 (2021)
125. Bertussi B, Natoli J-Y, Commandré M *Appl. Opt.* **45** 1410 (2006)
126. Natoli J-Y et al. *Opt. Express* **11** 824 (2003)
127. Rashidi-Huyeh M, Palpant B *J. Appl. Phys.* **96** 4475 (2004)
128. Galkin M V et al. *Moscow Univ. Chem. Bull.* **65** (2) 91 (2010); *Vestn. Mosk. Univ. Ser. 2 Khim.* **51** (2) 115 (2010)
129. Milanic M, Majaron B *Proc. SPIE* **8207** 82070G (2012)
130. Vidovič L, Milanić M, Majaron B *Int. J. Thermophys.* **36** 849 (2015)
131. O'Brien C M et al. *Sci. Rep.* **10** 12549 (2020)
132. Schoustra S M et al. *Proc. SPIE* **10878** 1087813 (2019)
133. Razansky D et al. *Nat. Photon.* **3** 412 (2009)
134. Razansky D, Buehler A, Ntziachristos V *Nat. Protoc.* **6** 1121 (2011)
135. Ntziachristos V, Razansky D *Chem. Rev.* **110** 2783 (2010)
136. Attia A B E et al. *Photoacoustics* **7** 20 (2017)
137. Bychkov A S et al. *Photoacoustics* **5** 10 (2017)
138. Deán-Ben X L, Razansky D *Photoacoustics* **4** (4) 133 (2016)
139. Oraevsky A A et al. *Photoacoustics* **12** 30 (2018)
140. Gusev V E *Photoacoustics* **20** 100205 (2020)
141. Taruttis A, Ntziachristos V *Nat. Photon.* **9** 219 (2015)
142. Rebling J et al. *Adv. Sci.* **8** 2170078 (2021)
143. Bulsink R et al. *Sensors* **21** 283 (2021)
144. Omar M, Aguirre J, Ntziachristos V *Nat. Biomed. Eng.* **3** 354 (2019)
145. Wang L et al. *Phys. Rev. Lett.* **113** 174301 (2014)
146. Shi J et al. *Nat. Photon.* **13** 609 (2019)
147. Liu S et al. *J. Am. Chem. Soc.* **141** 5359 (2019)
148. Xue X, Lindstrom A, Li Y *Bioconjugate Chem.* **30** 1585 (2019)
149. Gargiulo S, Albanese S, Mancini M *Contrast Media Mol. Imaging* **2019** 5080267 (2019)
150. Suzuki M et al. *Opt. Eng.* **59** 034106 (2020)
151. Wang L V, Hu S *Science* **335** 1458 (2012)
152. Turchin I V *Phys. Usp.* **59** 487 (2016); *Usp. Fiz. Nauk* **186** 550 (2016)
153. Xia J, Yao J, Wang L H V *Prog. Electromagn. Res.* **147** 1 (2014)
154. Choi W, Oh D, Kim C *J. Appl. Phys.* **127** 230903 (2020)
155. Krafft C et al. *J. Biophoton.* **11** e201700236 (2018)
156. Schoustra S M et al. *Photoacoustics* **21** 100238 (2021)
157. Li L, Wang L V *BME Frontiers* **2021** 9823268 (2021)
158. Suheshkumar Singh M, Paul S, Thomas A, in *LED-Based Photoacoustic Imaging*: *A Theoretical Tutorial* (Progress in Optical Science and Photonics, Vol. 7, Ed. M Kuniyil Ajith Singh) (Singapore: Springer, 2020) p. 3
159. Knieling F et al. *New Engl. J. Med.* **376** 1292 (2017)
160. Neuschmelting V et al. *Photoacoustics* **4** (1) 1 (2016)
161. Svanberg S, in *Laser Spectroscopy for Medical Applications. Diagnostics, Therapy and Surgery* (Ed. H Jelínková) (Cambridge: Woodhead Publ., 2013)
162. Yang J M et al. *PLoS ONE* **10** (4) e0120269 (2015)
163. Yang J-M et al. *Nat. Med.* **18** 1297 (2012)
164. Shu C et al. *Proc. SPIE* **11190** 111901V (2019)
165. Miranda C, Barkley J, Smith B S *J. Biomed. Opt.* **23** 046008 (2018)
166. Pavone F S, Shoham S (Eds) *Handbook of Neurophotonics* (Boca Raton, FL: CRC Press, 2020)
167. Brunker J, Beard P *Sci. Rep.* **6** 20902 (2016)
168. Na S, Wang L V *Biomed. Opt. Express* **12** 4056 (2021)
169. Hofmann U A T et al. *Opt. Lett.* **45** 2522 (2020)
170. Tishchenko K et al. *Arab. J. Chem.* **10** 781 (2017)
171. Zharov V P *Nat. Photon.* **5** 110 (2011)
172. Nedosekin D A et al. *Cytometry A* **77** 1049 (2010)
173. Attia A B E et al. *Biomed. Opt. Express* **6** 591 (2015)
174. Kim M et al. *Photoacoustics* **19** 100192 (2020)
175. Märk J et al. *Commun. Phys.* **1** 3 (2018)
176. Lu G, Fei B *J. Biomed. Opt.* **19** 010901 (2014)
177. Dong X et al. *Appl. Spectrosc. Rev.* **54** 285 (2019)
178. Marcano A et al. *Appl. Spectrosc.* **68** 680 (2014)

179. Marcano A, Ojeda J, Melikechi N *Appl. Spectrosc.* **60** 560 (2006)
180. Cabrera H et al. *Talanta* **183** 158 (2018)
181. Tamaki E et al. *Lab Chip* **5** 129 (2005)
182. Lindfors K et al. *Phys. Rev. Lett.* **93** 037401 (2004)
183. Bialkowski S E *Photochem. Photobiol. Sci.* **2** 779 (2003)
184. Bialkowski S E, Chartier A B *Anal. Sci.* **17** (Suppl.) i99 (2001)
185. Bialkowski S E *Isr. J. Chem.* **38** (3) 159 (1998)
186. Chartier A, Bialkowski S E *Opt. Eng.* **36** 303 (1997)
187. Liang S et al. *Photoacoustics* **11** 56 (2018)
188. Khokhlova T D, Pelivanov I M, Karabutov A A *Acoust. Phys.* **55** 674 (2009); *Akust. Zh.* **55** 672 (2009)
189. Karabutov A A, Savateeva E V, Oraevsky A A *Laser Phys.* **13** 711 (2003)
190. Deán-Ben X L et al. *Chem. Soc. Rev.* **46** 2158 (2017)
191. Razansky D, Klohs J, Ni R *Eur. J. Nucl. Med. Mol. Imaging* **48** 4152 (2021)
192. Karlas A et al. *Photoacoustics* **23** 100283 (2021)
193. Deán-Ben X L, Razansky D *Light Sci. Appl.* **3** e137 (2014)
194. Gottschalk S et al. *Nat. Biomed. Eng.* **3** 392 (2019)
195. Link S, El-Sayed M A *Int. Rev. Phys. Chem.* **19** 409 (2000)
196. Cognet L et al. *Anal. Chem.* **80** 2288 (2008)
197. Boyer D et al. *Science* **297** 1160 (2002)
198. Cognet L et al. *Proc. Natl. Acad. Sci. USA* **100** 11350 (2003)
199. Tamaki E et al. *J. Chromatogr. A* **987** 197 (2003)
200. Shimizu H et al. *Anal. Chem.* **89** 6043 (2017)
201. Shirai K et al. *Analyst* **143** 943 (2018)
202. Tsuyama Y, Mawatari K *Anal. Chem.* **91** 9741 (2019)
203. Berciaud S et al. *Phys. Rev. Lett.* **93** 257402 (2004)
204. Papernov S et al. *J. Appl. Phys.* **109** 113106 (2011)
205. Blab G A et al. *Biophys. J.* **90** L13 (2006)
206. Berciaud S et al. *Nano Lett.* **7** 1203 (2007)
207. Berciaud S, Cognet L, Lounis B *Nano Lett.* **5** 2160 (2005)
208. Mërtiri A et al. *Appl. Phys. Lett.* **101** 044101 (2012)
209. Li Z et al. *J. Phys. Chem. B* **121** 8838 (2017)
210. Pavlovetc I M et al. *J. Appl. Phys.* **127** 165101 (2020)
211. Pavlovetc I M et al. *Proc. SPIE* **11246** 1124613 (2020)
212. Radünz R et al. *J. Phys. Chem. A* **113** 1674 (2009)
213. Selmke M et al. *Appl. Phys. Lett.* **105** 013511 (2014)
214. Selmke M, Braun M, Cichos F *J. Opt. Soc. Am. A* **29** 2237 (2012)
215. Selmke M et al. *RSC Adv.* **3** 394 (2013)
216. Hammiche A et al. *Appl. Spectrosc.* **53** 810 (1999)
217. Pollock H M, Hammiche A *J. Phys. D* **34** R23 (2001)
218. Bozec L et al. *Meas. Sci. Technol.* **13** 1217 (2002)
219. Dazzi A, Glotin F, Carminati R *J. Appl. Phys.* **107** 124519 (2010)
220. Ramer G, Aksyuk V A, Centrone A *Anal. Chem.* **89** 13524 (2017)
221. Katzenmeyer A M, Aksyuk V A, Centrone A *Anal. Chem.* **85** 1972 (2013)
222. Kjoller K et al. *Nanotechnology* **21** 185705 (2010)
223. Bozec L et al. *J. Appl. Phys.* **90** 5159 (2001)
224. Hammiche A et al. *Spectroscopy* **19** (2) 20 (2004)
225. Hammiche A et al. *Biophys. J.* **88** 3699 (2005)
226. Hammiche A et al. *J. Biochem. Biophys. Meth.* **70** 675 (2007)
227. German M J et al. *Biophys. J.* **90** 3783 (2006)
228. Jakob D S et al. *Anal. Chem.* **91** 8883 (2019)
229. Wang L et al. *Sci. Adv.* **3** e1700255 (2017)
230. Dazzi A et al. *Appl. Spectrosc.* **66** 1365 (2012)
231. Yamanaka K, Nakano S *Appl. Phys. A* **66** S313 (1998)
232. Gasser G (Ed.) *Inorganic Chemical Biology*: *Principles, Techniques and Applications* (Chichester: John Wiley and Sons, 2014)
233. Strelcov E et al. *Sci. Adv.* **3** e1602165 (2017)
234. Deniset-Besseau A et al. *Appl. Spectrosc.* **75** 1538 (2021)
235. Ghosh S et al. *Nat. Mater.* **14** 505 (2015)
236. Chae J et al. *Nano Lett.* **15** 8114 (2015)
237. Morsch S, Bastidas P D, Rowland S M *J. Mater. Chem. A* **5** 24508 (2017)
238. Barnes J R et al. *Nature* **372** 79 (1994)
239. Kim S et al. *ECS Trans.* **50** 459 (2013)
240. Krause A R et al. *J. Appl. Phys.* **103** 094906 (2008)
241. Van Neste C W et al. *Appl. Phys. Lett.* **92** 134102 (2008)
242. Skvortsov L A, Maksimov E M *Quantum Electron.* **40** 565 (2010); *Kvantovaya Elektron.* **40** 565 (2010)
243. Bagheri M et al. *Sensors Actuators B* **191** 765 (2014)
244. Yun M et al. *Appl. Phys. Lett.* **100** 204103 (2012)
245. Li C et al. *Anal. Chem.* **89** 4863 (2017)
246. Zhang D et al. *Sci. Adv.* **2** e1600521 (2016)
247. Zong H et al. *ACS Photon.* **8** 3323 (2021)
248. Mityurich G S et al. *J. Appl. Spectrosc.* **87** 724 (2020)
249. Leong K Y et al. *Renew. Sust. Energ. Rev.* **53** 1092 (2016)
250. Noroozi M, Zakaria A, in *Nanofluid Heat and Mass Transfer in Engineering Problems* (Ed. M S Kandelousi) (London: IntechOpen, 2017) https://doi.org/10.5772/65789
251. Jiménez Pérez J L et al. *J. Nano Res.* **9** 55 (2010)
252. Alvarado E M et al. *Int. J. Thermophys.* **34** 948 (2013)
253. Shen J, Mandelis A, Aloysius B D *Int. J. Thermophys.* **17** 1241 (1996)
254. Balderas-López J A, Mandelis A, Garcia J A *Rev. Sci. Instrum.* **71** 2933 (2000)
255. López-Muñoz G A et al. *Nanoscale Res. Lett.* **7** 667 (2012)
256. Noroozi M et al. *Sci. World J.* **2018** 9458952 (2018)
257. Nisha M R, Philip J *Phys. Scr.* **88** 015602 (2013)
258. Balderas-López J A *Rev. Sci. Instrum.* **78** 064901 (2007)
259. Balderas-López J A, Mandelis A *Int. J. Thermophys.* **23** 605 (2002)
260. Sokolovskaya Yu G, Podymova N B, Karabutov A A *Acoust. Phys.* **66** 268 (2020); *Akust. Zh.* **66** 284 (2020)
261. López-Muñoz G A et al. *Nanoscale Res. Lett.* **7** 423 (2012)
262. Agresti F et al. *Thermochim. Acta* **619** 48 (2015)
263. El-Brolossy T A, Saber O *Exp. Therm. Fluid Sci.* **44** 498 (2013)
264. Dubyk K et al. *SN Appl. Sci.* **1** 1440 (2019)
265. Carbajal-Valdéz R et al. *Thermochim. Acta* **671** 83 (2019)
266. Dantas A L L et al. *Braz. J. Phys.* **28** 428 (1998)
267. Saadallah F et al. *Sensors Actuators A* **138** 335 (2007)
268. Lu B et al. *J. Opt. Soc. Am. B* **37** 433 (2020)
269. Käding O W et al. *Appl. Phys. A* **61** 253 (1995)
270. Manjusha M V, Philip J *AIP Conf. Proc.* **1349** 469 (2011)
271. Zhao D et al. *J. Electron. Packag.* **138** 040802 (2016)
272. Wang J, Fiebig M *Int. J. Thermophys.* **16** 1353 (1995)
273. Kim J H et al. *Measurement* **15** 159 (1995)
274. Schmidt A J et al. *J. Appl. Phys.* **103** 083529 (2008)
275. Stoklasová P et al. *Exp. Mech.* **61** 663 (2021)
276. Venerus D C et al. *J. Appl. Phys.* **100** 094310 (2006)
277. Kusiak A, Pradere Ch, Battaglia J L *Meas. Sci. Technol.* **21** 015403 (2010)
278. Prakash A et al. *Physica E* **107** 203 (2019)
279. Rajesh Kumar B et al. *J. Therm. Anal. Calorim.* **119** 453 (2015)
280. Shahriari E, Mat Yunus W M, Zamiri R *J. Eur. Opt. Soc. Rapid Publ.* **8** 13026 (2013)
281. John J et al. *J. Phys. D* **48** 335301 (2015)
282. Zamiri R et al. *J. Eur. Opt. Soc. Rapid Publ.* **7** 12022 (2012)
283. Rusconi R, Rodari E, Piazza R *Appl. Phys. Lett.* **89** 261916 (2006)
284. Luna-Sánchez J L et al. *Thermochim. Acta* **678** 178314 (2019)
285. Joseph S A et al. *Opt. Commun.* **283** 313 (2010)
286. Hari M et al. *Int. J. Therm. Sci.* **64** 188 (2013)
287. Mikheev I V et al. *J. Phys. Chem. C* **120** 28270 (2016)
288. Chirtoc M et al., in *Spectroscopy of Polymer Nanocomposites* (Eds S Thomas, D Rouxel, D Ponnamma) (Norwich, NY: William Andrew Publ., 2016) p. 312
289. Miyako E et al. *Lab Chip* **9** 788 (2009)
290. Astrath N G C et al. *Phys. Rev. B* **71** 214202 (2005)
291. Nunes A R et al. *Appl. Phys. Lett.* **84** 5183 (2004)
292. Remes Z et al. *Phys. Status Solidi A* **207** 1722 (2010)
293. Figueiredo M S et al. *Opt. Mater.* **35** 2400 (2013)
294. Andrade A A et al. *J. Non-Cryst. Solids* **352** 3624 (2006)
295. Astrath N G C et al. *J. Non-Cryst. Solids* **354** 574 (2008)
296. Martins V M et al. *Opt. Mater.* **37** 211 (2014)
297. Starobor A V, Mironov E A, Palashov O V *Opt. Mater.* **98** 109469 (2019)
298. Starobor A V et al. *Opt. Mater.* **99** 109542 (2020)
299. Wang Z et al. *Opt. Laser Technol.* **42** 873 (2010)
300. Niu R et al. *Optik* **122** 1931 (2011)
301. Anjos V, Andrade A A, Bell M J V *Appl. Surf. Sci.* **255** 698 (2008)
302. Lima S M et al. *J. Non-Cryst. Solids* **352** 3603 (2006)
303. Dias D T et al. *Diam. Relat. Mater.* **48** 1 (2014)
304. Armenta S et al. *Anal. Chim. Acta* **567** 255 (2006)
305. Charpentier P, Lepoutre F, Bertrand L *J. Appl. Phys.* **53** 608 (1982)
306. El-Qahtani Z et al. *Mater. Sci. Semicond. Process.* **20** 68 (2014)
307. Schmitt M et al. *Eng. Geol.* **220** 183 (2017)
308. Badawi A *J. Mater. Sci. Mater. Electron.* **27** 7899 (2016)

309. Salazar A, Sánchez-Lavega A *Rev. Sci. Instrum.* **65** 2896 (1994)
310. Ilahi S et al. *Curr. Appl. Phys.* **13** 610 (2013)
311. Loges A et al. *J. Power Sources* **325** 104 (2016)
312. Fontenot R S, Mathur V K, Barkyoumb J H *J. Quant. Spectrosc. Radiat. Transf.* **204** 1 (2018)
313. Battaglia J-L et al. *Measurement* **158** 107691 (2020)
314. Kusiak A et al. *Thermochim. Acta* **556** 1 (2013)
315. Mingolo N, Martínez O E *J. Appl. Phys.* **111** 123526 (2012)
316. Georges J *Spectrochim. Acta A* **59** 519 (2003)
317. Hou L et al. *New J. Phys.* **17** 013050 (2015)
318. Zaytsev M E et al. *J. Phys. Chem. C* **124** 5861 (2020)
319. Kavokine N et al. *Nat. Commun.* **11** 50 (2020)
320. Proskurnin M A et al. *Anal. Bioanal. Chem.* **375** 1204 (2003)
321. Luk'yanov A Yu, Novikov M A *Tech. Phys.* **45** 1470 (2000); *Zh. Tekh. Fiz.* **70** (11) 99 (2000)
322. Cruz R A et al. *Opt. Lett.* **34** 1882 (2009)
323. Marcano O A, Melikechi N *Appl. Spectrosc.* **61** 659 (2007)
324. Cruz R A et al. *Talanta* **85** 850 (2011)
325. Cruz R A et al. *Synth. Met.* **163** 38 (2013)
326. Stubenvoll M et al. *Rev. Sci. Instrum.* **87** 023904 (2016)
327. Marcano A O et al. *J. Opt. Soc. Am. B* **28** 281 (2011)
328. Ryasnyanskiy A I et al. *Phys. Solid State* **51** 55 (2009); *Fiz. Tverd. Tela* **51** 52 (2009)
329. Usoltseva L O et al. *Photoacoustics* **12** 55 (2018)
330. Sogandares F M, Fry E S *Appl. Opt.* **36** 8699 (1997)
331. Dwivedi Y, Rai S B *Vibr. Spectrosc.* **49** 278 (2009)
332. Liu M, Franko M *Int. J. Thermophys.* **35** 2178 (2014)
333. Dudko V S et al. *Russ. J. Gen. Chem.* **82** 2146 (2012); *Ross. Khim. Zh.* **55** 111 (2011)
334. Vidovič L, Milanič M, Majaron B *Proc. SPIE* **8941** 894112 (2014)
335. Commandré M, Natoli J-Y, Gallais L *Eur. Phys. J. Spec. Top.* **153** 59 (2008)
336. Ono H et al. *Opt. Mater.* **15** (1) 33 (2000)
337. Beaudoin M et al. *J. Cryst. Growth* **425** 245 (2015)
338. Lobo N et al. *J. Cryst. Growth* **310** 4747 (2008)
339. Beaudoin M et al. *J. Cryst. Growth* **311** 1662 (2009)
340. Loubiri D et al. *Synth. Met.* **206** 1 (2015)
341. Ryasnyansky A et al. *Appl. Opt.* **44** 2839 (2005)
342. Klapshina L G et al. *New J. Chem.* **30** 615 (2006)
343. Liaros N, Fourkas J T *Laser Photon. Rev.* **11** 1700106 (2017)
344. Rodriguez L, Chiesa M *Appl. Opt.* **50** 3240 (2011)
345. Bass M, Van Stryland E W, Stewart A F *Appl. Phys. Lett.* **34** 142 (1979)
346. Isozaki T et al. *J. Phys. Chem. A* **120** 6137 (2016)
347. Olaizola A M *J. Opt. Soc. Am. B* **36** 2907 (2019)
348. Marcano A, Loper C, Melikechi N *J. Opt. Soc. Am. B* **19** 119 (2002)
349. Falconieri M *J. Opt. A* **1** 662 (1999)
350. Lu S et al. *Appl. Phys. Lett.* **96** 113701 (2010)
351. Astrath N G C et al. *J. Phys. Conf. Ser.* **214** 012014 (2010)
352. Astrath N G C et al. *Appl. Phys. Lett.* **95** 191902 (2009)
353. Pedreira P R B et al. *J. Appl. Phys.* **100** 044906 (2006)
354. Pedreira P R B et al. *Chem. Phys. Lett.* **396** 221 (2004)
355. Herculano L S et al. *J. Phys. Chem. B* **117** 1932 (2013)
356. Cambron R T, Harris J M *Anal. Chem.* **67** 365 (1995)
357. Barker B, Larsen R *J. Biochem. Mol. Biol. Biophys.* **5** 407 (2001)
358. Chattopadhyay N et al. *Phys. Chem. Chem. Phys.* **3** 70 (2001)
359. Seixas de Melo J et al. *Photochem. Photobiol.* **77** 121 (2003)
360. Chen E H-L et al. *Sci. Rep.* **7** 8691 (2017)
361. Mikšovská J, Larsen R W *J. Protein Chem.* **22** 387 (2003)
362. Abbruzzetti S et al. *Biophys. J.* **79** 2714 (2000)
363. Abbruzzetti S et al. *Photochem. Photobiol. Sci.* **5** 621 (2006)
364. Chen R P-Y et al. *Proc. Natl. Acad. Sci. USA* **101** 7305 (2004)
365. Jesus C S H et al. *J. Phys. Chem. B* **122** 3790 (2018)
366. Mikšovská J et al. *Biochemistry* **47** 11510 (2008)
367. Terazima M *Bull. Chem. Soc. Jpn.* **77** (1) 23 (2004)
368. Terazima M *Isr. J. Chem.* **38** (3) 143 (1998)
369. Terazima M *Chem. Lett.* **48** 802 (2019)
370. Ikoma M, Nakasone Y, Terazima M *J. Photochem. Photobiol. B* **221** 112252 (2021)
371. Sakakura M, Morishima I, Terazima M *J. Phys. Chem. B* **105** 10424 (2001)
372. Sakakura M et al. *J. Am. Chem. Soc.* **123** 4286 (2001)
373. Diebold G J, in *Photoacoustic, Photothermal and Photochemical Processes in Gases* (Topics in Current Physics, Vol. 46, Ed. P Hess) (Berlin: Springer, 1989) p. 125
374. Rothberg L J et al. *J. Am. Chem. Soc.* **105** 3464 (1983)
375. Rudzki J E, Goodman J L, Peters K S *J. Am. Chem. Soc.* **107** 7849 (1985)
376. Poston P E, Harris J M *J. Am. Chem. Soc.* **112** 644 (1990)
377. Sontag H, Tam A C, Hess P *J. Chem. Phys.* **86** 3950 (1987)
378. Yeh S-R, Falvey D E *J. Photochem. Photobiol. A* **87** (1) 13 (1995)
379. González M G et al. *Sensors Actuators B* **150** 770 (2010)
380. Fischer M, Georges J *Chem. Phys. Lett.* **260** 115 (1996)
381. Georges J, Ghazarian S *Anal. Chim. Acta* **276** 401 (1993)
382. Isak S J et al. *J. Photochem. Photobiol. A* **134** 77 (2000)
383. Fischer M, Georges J *Spectrochim. Acta A* **53** 1419 (1997)
384. Santhi A et al. *Spectrochim. Acta A* **60** 1077 (2004)
385. Santhi A et al. *Appl. Phys. B* **79** 629 (2004)
386. Fischer M, Georges J *Spectrochim. Acta A* **54** 101 (1998)
387. Estupiñán-López C, Tolentino Dominguez C, de Araujo R E *Opt. Express* **21** 18592 (2013)
388. Cruz R A, Pilla V, Catunda T *J. Appl. Phys.* **107** 083504 (2010)
389. Tanaka F et al. *Phys. Chem. Chem. Phys.* **6** 1219 (2004)
390. Yamaji M et al. *Phys. Chem. Chem. Phys.* **3** 5470 (2001)
391. Würth C et al. *Anal. Bioanal. Chem.* **407** 59 (2015)
392. Sampaio J A et al. *J. Non-Cryst. Solids* **351** 1594 (2005)
393. Peliçon E et al. *J. Non-Cryst. Solids* **304** 244 (2002)
394. Lima S M et al. *Opt. Mater.* **63** 19 (2017)
395. Martins V M et al. *J. Lumin.* **162** 104 (2015)
396. Poma P Y et al. *J. Lumin.* **161** 306 (2015)
397. Estupiñán-López C et al. *J. Lumin.* **174** 17 (2016)
398. Shemeena Basheer N et al. *J. Lumin.* **137** 225 (2013)
399. Kurian A et al. *Spectrochim. Acta. A* **61** 2799 (2005)
400. Georges J *Spectrochim. Acta A* **51** 985 (1995)
401. Liu L et al. *J. Appl. Phys.* **118** 184906 (2015)
402. Glorieux C, Fivez J, Thoen J *J. Appl. Phys.* **73** 684 (1993)
403. Liu Y, Mandelis A *Exp. Meth. Phys. Sci.* **42** 297 (2009)
404. Zhou J et al. *Nat. Meth.* **17** 967 (2020)
405. Zeng J et al. *Int. J. Heat Mass Transf.* **170** 120989 (2021)
406. Braslavsky S E, Heibel G E *Chem. Rev.* **92** 1381 (1992)
407. Iwata K, Terazima M, Masuhara H *Biochim. Biophys. Acta Gen. Subj.* **1862** 335 (2018)
408. Terazima M, in *Advances in Photochemistry* Vol. 24 (Eds D C Neckers, D H Volman, G Von Bunau) (New York: Wiley, 1998) p. 255
409. Gensch T, Viappiani C, Braslavsky S E "Laser induced optoacoustic spectroscopy", in *Encyclopedia of Spectroscopy and Spectrometry* 3rd ed. (Eds-in-Chief J C Lindon, G E Tranter, D W Koppenaal) (Oxford: Academic Press, 2017) p. 539
410. Losi A, Braslavsky S E *Phys. Chem. Chem. Phys.* **5** 2739 (2003)
411. Losi A et al. *Biophys. J.* **77** 3277 (1999)
412. Losi A et al. *Photochem. Photobiol.* **69** 75S (1999)
413. Losi A et al. *Biophys. J.* **76** 2183 (1999)
414. Klauss A et al. *Photosynth. Res.* **102** 499 (2009)
415. Mikšovská J, Gennis R B, Larsen R W *FEBS Lett.* **579** 3014 (2005)
416. Chen H M, Schelly Z A *Chem. Phys. Lett.* **145** 102 (1988)
417. Marín E *Lat. Am. J. Phys. Educ.* **4** (1) 56 (2010)
418. Bhattacharyya I, Kumar P, Goswami D *J. Phys. Chem. B* **115** 262 (2011)
419. Braslavsky S E *Pure Appl. Chem.* **79** 293 (2007)
420. Bilmes G M, Tocho J O, Braslavsky S E *J. Phys. Chem.* **93** 6696 (1989)
421. Deus W B et al. *Fuel* **253** 1090 (2019)
422. Constantino R et al. *Fuel* **202** 78 (2017)
423. Ventura M et al. *Fuel* **212** 309 (2018)
424. Savi E L et al. *Spectrochim. Acta A* **145** 125 (2015)
425. Jacinto C et al. *J. Non-Cryst. Solids* **352** 3577 (2006)
426. Serpa C et al. *J. Am. Chem. Soc.* **130** 8876 (2008)
427. Zambrano-Arjona M A, Medina-Esquivel R, Alvarado-Gil J J *J. Phys. D* **40** 6098 (2007)
428. Martínez-Torres P et al. *Int. J. Thermophys.* **33** 1892 (2012)
429. Martínez-Torres P, Mandelis A, Alvarado-Gil J J *J. Appl. Phys.* **106** 114906 (2009)
430. Blaszkiewicz P et al. *J. Phys. Chem. C* **123** 27181 (2019)
431. Tomasini E P, San Román E, Braslavsky S E *Langmuir* **25** 5861 (2009)

432. Mirenda M, Lagorio M G, San Román E *Langmuir* **20** 3690 (2004)
433. Lagorio M G et al. *J. Chem. Soc. Faraday Trans.* **94** 419 (1998)
434. Gensch T et al. *Isr. J. Chem.* **38** 231 (1998)
435. Churio M S, Angermund K P, Braslavsky S E *J. Phys. Chem.* **98** 1776 (1994)
436. Schaberle F A et al. *Inorg. Chem.* **56** 2677 (2017)
437. Rizzi A C et al. *J. Phys. Chem. A* **112** 4215 (2008)
438. Zimmt M B, Vath P A *Photochem. Photobiol.* **65** (1) 10 (1997)
439. Callis J B, Parson W W, Gouterman M *Biochim. Biophys. Acta Bioenerg.* **267** 348 (1972)
440. le Noble W J, Kelm H *Angew. Chem. Int. Ed. Engl.* **19** 841 (1980)
441. Wegewijs B, Paddon-Row M N, Braslavsky S E *J. Phys. Chem. A* **102** 8812 (1998)
442. Wegewijs B, Verhoeven J W, Braslavsky S E *J. Phys. Chem.* **100** 8890 (1996)
443. Wu X-Z, Hobo T *Anal. Chim. Acta* **316** 111 (1995)
444. Krivanek R, Dau H, Haumann M *Biophys. J.* **94** 1890 (2008)
445. Darée K *Opt. Commun.* **4** 238 (1971)
446. Wyers S G, Diebold G J, in *Photoacoustic and Photothermal Phenomena* (Springer Series in Optical Sciences, Vol. 58, Eds P Hess, J Pelzl) (Berlin: Springer, 1988) p. 66
447. Magee J L, Daniels F *J. Am. Chem. Soc.* **62** 2825 (1940)
448. Diebold G J, Hayden J S *Chem. Phys.* **49** 429 (1980)
449. O'Connor M T, Diebold G J *Nature* **301** 321 (1983)
450. Choi J G, Diebold G J *Anal. Chem.* **57** 2989 (1985)
451. Zhang X, Cheng Z, Li X *Infrared Phys. Technol.* **78** 31 (2016)
452. Navas M J, Jiménez A M, Asuero A G *Clin. Chim. Acta* **413** 1171 (2012)
453. Rochowski P, Niedzialkowski P, Pogorzelski S J *Int. J. Pharm.* **580** 119233 (2020)
454. Ma Y et al. *Appl. Phys. Lett.* **110** 031107 (2017)
455. Spagnolo V, Patimisco P, Tittel F K, in *Mid-infrared Optoelectronics. Materials, Devices, and Applications* (Woodhead Publishing Series in Electronic and Optical Materials, Eds E Tournié, L Cerutti) (Cambridge: Woodhead Publ., 2020) p. 597
456. Pinto D et al. *Photoacoustics* **22** 100244 (2021)
457. Ma Y et al. *Photoacoustics* **20** 100206 (2020)
458. Martelanc M et al. *Talanta* **154** 92 (2016)
459. Proskurnin M A et al. *Analyst* **121** 419 (1996)
460. Georges J *Spectrochim. Acta A* **69** 1063 (2008)
461. Proskurnin M A et al. *Talanta* **57** 831 (2002)
462. Chernysh V V et al. *J. Anal. Chem.* **55** 338 (2000)
463. Filimonova T A et al. *Photoacoustics* **1** (3–4) 54 (2013)
464. Alimarin I P et al. *Zh. Anal. Khim.* **42** (1) 5 (1987)
465. Pakhomova S V et al. *J. Anal. Chem.* **56** 910 (2001); *Zh. Anal. Khim.* **56** 1042 (2001)
466. Kazemi E et al. *Talanta* **147** 561 (2016)
467. Ventura M et al. *Spectrochim. Acta. A* **188** 32 (2018)
468. Nawar S et al. *Appl. Spectrosc. Rev.* **55** 525 (2020)
469. Bings N H, Orlandini von Niessen J O, Schaper J N *Spectrochim. Acta B* **100** 14 (2014)
470. Mozhayeva D, Engelhard C *J. Anal. At. Spectrom.* **35** 1740 (2020)
471. Cedeño E et al. *Talanta* **170** 260 (2017)
472. Budasheva H et al. "Determination of Fe (III) and Fe (II) in natural waters using passive DGT samplers and non-destructive BDS analysis", Ph.D. Thesis (Novi Gorici: Univ. v Novi Gorici, 2019)
473. Han Q et al. *Anal. Lett.* **48** 2096 (2015)
474. Shokoufi N, Hamdamali A *Anal. Chim. Acta* **681** (1) 56 (2010)
475. Chouhan B, Dasgupta P K *Anal. Chem.* **91** 2923 (2019)
476. Mikheev I V et al. *Int. J. Thermophys.* **36** 956 (2015)
477. Whitesides G M *Nature* **442** 368 (2006)
478. Castro E R, Manz A *J. Chromatogr. A* **1382** 66 (2015)
479. Moreira N S et al. *Anal. Chim. Acta* **1119** 1 (2020)
480. Shi H et al. *Chem. Eng. J.* **361** 635 (2019)
481. Smirnova A et al. *J. Sep. Sci.* **31** 904 (2008)
482. Yamauchi M et al. *J. Chromatogr. A* **1106** 89 (2006)
483. Sato K et al. *Adv. Drug Del. Rev.* **55** 379 (2003)
484. Tanaka Y et al. *J. Chromatogr. A* **894** 45 (2000)
485. Yamaoka S et al. *Sensors Actuators B* **228** 581 (2016)
486. Goto M et al. *Anal. Chem.* **77** 2125 (2005)
487. Tanaka Y et al. *Biosens. Bioelectron.* **23** 449 (2007)
488. Rui W, Tao C, Liu X *Ultrason. Sonochem.* **66** 105095 (2020)
489. Pleitez M A et al. *Anal. Chem.* **85** 1013 (2013)
490. Hartings M R et al. *Sensors Actuators B* **301** 127076 (2019)
491. Watanabe Y N, Lima Â M V, Lopes Tavares da Mata Hermida-Quintella C M A *Fuel* **160** 568 (2015)
492. Jiménez Pérez J L et al. *Eur. Phys. J. Spec. Top.* **153** 511 (2008)
493. Lima A M V et al. *30a Reunião Anual da Sociedade Brasileira de Química* **1** 1 (2007)
494. Suzuki M et al. *Opt. Eng.* **55** 014101 (2016)
495. Tam A C *Rev. Mod. Phys.* **58** 381 (1986)
496. Miris L et al. *Sens. Imaging* **20** (1) 13 (2019)
497. Gaiduk A et al. *Science* **330** 353 (2010)
498. John J et al. *RSC Adv.* **6** 62390 (2016)
499. Jiménez-Pérez J L et al. *Appl. Phys. A* **122** 556 (2016)
500. Savi E L et al. *Fuel* **217** 404 (2018)
501. Hou L et al. *Nano Lett.* **17** 1575 (2017)
502. Spaeth P et al. *Nano Lett.* **19** 8934 (2019)
503. Gaiduk A et al. *Chem. Sci.* **1** 343 (2010)
504. Zijlstra P, Paulo P M R, Orrit M *Nat. Nanotechnol.* **7** 379 (2012)
505. Mawatari K, Kitamori T, Sawada T *Anal. Chem.* **70** 5037 (1998)
506. Tokeshi M et al. *Anal. Chem.* **73** 2112 (2001)
507. Mawatari K et al. *Anal. Sci.* **22** 781 (2006)
508. Adler D C et al. *Opt. Express* **16** 4376 (2008)
509. Kulzer F et al. *ChemPhysChem* **9** 1761 (2008)
510. Brusnichkin A V et al. *Appl. Spectrosc.* **61** 1191 (2007)
511. Zharov V P et al. *J. Biomed. Opt.* **12** 051503 (2007)
512. Galanzha E I et al. *Cytometry A* **73** 884 (2008)
513. McClelland J F, Jones R W, Bajic S J "Photoacoustic spectroscopy", in *Handbook of Vibrational Spectroscopy* (Eds J M Chalmers, P R Griffiths) (New York: John Wiley and Sons, 2006)
514. Du C et al. *Vib. Spectrosc.* **49** (1) 32 (2009)
515. Pelivanov I M et al. *Quantum Electron.* **36** 1089 (2006); *Kvantovaya Elektron.* **36** 1089 (2006)
516. Kizil R, Irudayaraj J "Fourier Transform Infrared Photoacoustic Spectroscopy (FTIR-PAS)", in *Encyclopedia of Biophysics* (Ed. G C K Roberts) (Berlin: Springer, 2013) p. 840, https://doi.org/10.1007/978-3-642-16712-6_124
517. Bozóki Z, Pogány A, Szabó G *Appl. Spectrosc. Rev.* **46** (1) 1 (2011)
518. Urban M W, Koenig J L *Appl. Spectrosc.* **40** 994 (1986)
519. Du C et al. *J. Soils Sed.* **10** 855 (2010)
520. Du C, Zhou J *Appl. Spectrosc. Rev.* **46** 405 (2011)
521. Di Bartolo B, Forte O (Eds) *Frontiers of Optical Spectroscopy: Investigating Extreme Physical Conditions with Advanced Optical Techniques* (NATO Science Series. Ser. II, Vol. 168) (Dordrecht: Kluwer, 2005)
522. Leahu G L et al. *AIP Conf. Proc.* **1603** 62 (2014)
523. Li Voti R et al. *J. Phys. IV France* **125** 483 (2005)
524. Contreras-Gallegos E et al. *Food Biophys.* **10** 19 (2015)
525. Sermeus J et al. *J. Appl. Phys.* **116** 023503 (2014)
526. Kaźmierczak-Balata A et al. *Int. J. Thermophys.* **35** 2328 (2014)
527. Bodzenta J, Kaźmierczak-Balata A, Mazur J *Central Eur. J. Phys.* **8** 207 (2010)
528. Mansano E S B et al. *Photochem. Photobiol.* **94** (1) 88 (2018)
529. Tunin L M et al. *Pharm. Biol.* **54** 139 (2016)
530. Mokrousov M D et al. *Biomed. Opt. Express* **10** 4775 (2019)
531. Wahls M W C, Kenttä E, Leyte J C *Appl. Spectrosc.* **54** 214 (2000)
532. Bjarnestad S, Dahlman O *Anal. Chem.* **74** 5851 (2002)
533. Schmid T et al. *Anal. Bioanal. Chem.* **375** 1124 (2003)
534. Sivakesava S, Irudayaraj J *J. Sci. Food Agric.* **80** 1805 (2000)
535. Irudayaraj J, Yang H, Sakhamuri S *J. Mol. Struct.* **606** 181 (2002)
536. Dias R C E et al. *Food Chem.* **255** 132 (2018)
537. Esteban-Díez I et al. *Talanta* **71** 221 (2007)
538. Moreira I, Scarminio I S *Talanta* **107** 416 (2013)
539. Defernez M et al. *Food Chem.* **216** 106 (2017)
540. Schievano E et al. *J. Agric. Food Chem.* **62** 12309 (2014)
541. Wermelinger T et al. *J. Agric. Food Chem.* **59** 9074 (2011)
542. Ma F et al. *Chemometr. Intellig. Lab. Syst.* **171** 9 (2017)
543. Ma F et al. *CATENA* **152** 190 (2017)
544. Volkov D S et al. *Agronomy* **11** 1879 (2021)
545. Volkov D S et al. *Agronomy* **11** 1822 (2021)
546. Krivoshein P K et al. *Photoacoustics* **18** 100162 (2020)
547. Amador-Hernández J, Fernández-Romero J M, Luque de Castro M D *Talanta* **49** 813 (1999)
548. Grishko V I, Tran C D, Duley W W *Appl. Opt.* **41** 5814 (2002)
549. Tran C D, Grishko V I, Baptista M S *Appl. Spectrosc.* **48** 833 (1994)

550. Vieira F S, Pasquini C *Fuel* **117** 1004 (2014)
551. Ikari T, Roger J P, Fournier D *Rev. Sci. Instrum.* **74** 553 (2003)
552. Bertolotti M et al. *Int. J. Thermophys.* **19** 603 (1998)
553. Bertolotti M et al. *J. Appl. Phys.* **83** 966 (1998)
554. Bertolotti M et al. *Appl. Phys. B* **67** 641 (1998)
555. Janssen S et al. *Fresenius J. Anal. Chem.* **360** 788 (1998)
556. Kreiter M J S, Mittler-Neher S *Thin Solid Films* **342** 244 (1999)
557. Harada M et al. *Anal. Chem.* **65** 2181 (1993)
558. Kimura H et al. *Anal. Chem.* **68** 3063 (1996)
559. Tu C Y et al. *Anal. Chem.* **65** 3631 (1993)
560. Elliott C R, Chen A T *Opt. Eng.* **51** 023603 (2012)
561. Pleitez M A et al. *Analyst* **140** 483 (2015)
562. Hertzberg O et al. *Analyst* **142** 495 (2017)
563. McMurdy J et al. *J. Biophoton.* **2** 277 (2009)
564. Upstone S L "Ultraviolet/visible light absorption spectrophotometry in clinical chemistry", in *Encyclopedia of Analytical Chemistry: Applications, Theory and Instrumentation* (Hoboken, NJ: Wiley, 2013) https://doi.org/10.1002/9780470027318.a0547.pub2
565. Nagel R L (Ed.) *Hemoglobin Disorders: Molecular Methods and Protocols* (Methods in Molecular Medicine, Vol. 82) (Totowa, NJ: Humana Press, 2003)
566. Tokeshi M et al. *Anal. Chem.* **77** 626 (2005)
567. Oraevsky A A *Photoacoustics* **3** (1) 1 (2015)
568. Galanzha E I, Kim J-W, V P *J. Biophoton.* **2** 725 (2009)
569. Vidovič L, Milanič M, Majaron B *J. Biomed. Opt.* **20** 017001 (2015)
570. Majaron B et al. *Lasers Surg. Med. Suppl.* **20** 3 (2008)
571. Milanič M, Serša I, Majaron B *Phys. Med. Biol.* **54** 2829 (2009)
572. Kyoo Park B et al. *Appl. Phys. Lett.* **99** 163702 (2011)
573. Lervik A et al. *Phys. Chem. Chem. Phys.* **12** 1610 (2010)
574. Duong H M et al. *Int. J. Heat Mass Transf.* **52** 5591 (2009)
575. Brusnichkin A V et al. *Moscow Univ. Chem. Bull.* **64** 45 (2009); *Vestn. Mosk. Univ. Ser. 2 Khim.* (1) 55 (2009)
576. Passamonti S et al. *FEBS J.* **272** 5522 (2005)
577. Ziberna L et al. *Sci. Rep.* **6** 29240 (2016)
578. Martelanc M et al. *Anal. Chim. Acta* **809** 174 (2014)
579. Dias D T et al. *J. Phys. IV France* **125** 657 (2005)
580. Menyaev Yu A et al. *Biomed. Opt. Express* **7** 3643 (2016)
581. Margon A et al. *J. Phys. IV France* **125** 717 (2005)
582. Galimova V R et al. *Anal. Lett.* **51** 1743 (2018)
583. Liu M, Malovrh S, Franko M *Anal. Methods* **8** 5053 (2016)
584. Imhof R E, McKendrick A D, Xiao P *Rev. Sci. Instrum.* **66** 5203 (1995)
585. Xiao P et al. *Anal. Sci.* **17** S349 (2001)
586. Xiao P, Cowen J A, Imhof R E *Rev. Sci. Instrum.* **74** 767 (2003)
587. Cui Y, Xiao P, Imhof R E *Int. J. Thermophys.* **26** 213 (2005)
588. Verdel N et al. *Proc. SPIE* **10413** 104130O (2017)
589. Verdel N et al. *Proc. SPIE* **10037** 100370H (2017)
590. Verdel N et al. *Biomed. Opt. Express* **11** 1679 (2020)
591. Verdel N et al. *Biomed. Opt. Express* **10** 944 (2019)
592. Shapiro H M *Practical Flow Cytometry* (New York: Wiley-Liss, 2003)
593. Zharov V P, Galanzha E I, Tuchin V V *Opt. Lett.* **30** 628 (2005)
594. Zharov V P, Galanzha E I, Tuchin V V *J. Cell. Biochem.* **97** 916 (2006)
595. Harada M et al. *Anal. Chim. Acta* **299** 343 (1995)
596. Biris A S et al. *J. Biomed. Opt.* **14** 021007 (2009)
597. Kim J-W et al. *Nat. Nanotechnol.* **4** 688 (2009)
598. Galanzha E I et al. *Cancer Res.* **69** 7926 (2009)
599. Nedosekin D A et al. *Opt. Express* **18** 8605 (2010)
600. Tanev S et al. *J. Biophoton.* **2** 505 (2009)
601. Guo X et al. *J. Biophoton.* **6** 911 (2013)
602. Jakobsohn K et al. *Int. J. Nanomed.* **7** 4707 (2012)
603. Loginova E V et al. *Photonic Sens.* **6** 42 (2015)
604. Cai C et al. *Anal. Cell. Pathol.* **2016** 2642361 (2016)
605. Philipp C M, Rohde E, Berlien H-P *Seminars Surg. Oncol.* **11** 290 (1995)
606. Huang W, El-Sayed M A *Eur. Phys. J. Spec. Top.* **153** 325 (2008)
607. Dickerson E B et al. *Cancer Lett.* **269** 57 (2008)
608. Jain P K, El-Sayed I H, El-Sayed M A *Nano Today* **2** (1) 18 (2007)
609. Huang X H et al. *Photochem. Photobiol.* **82** 412 (2006)
610. Huang X et al. *J. Am. Chem. Soc.* **128** 2115 (2006)
611. El-Sayed I H, Huang X, El-Sayed M A *Cancer Lett.* **239** 129 (2006)
612. Khot M I et al. *Clin. Colorectal Cancer* **18** e200 (2019)
613. Zhou X et al. *RSC Adv.* **8** 18647 (2018)
614. Liu T et al. *ACS Nano* **12** 3917 (2018)
615. Li L et al. *Theranostics* **8** 860 (2018)
616. Li J et al. *Theranostics* **8** 1042 (2018)
617. Leng C B et al. *Small* **14** 1703077 (2018)
618. Pan U N et al. *ACS Appl. Mater. Interfaces* **9** 19495 (2017)
619. Abbas M et al. *Adv. Mater.* **29** 1605021 (2017)
620. Lv R et al. *Sci. Rep.* **7** 13562 (2017)
621. Song X et al. *Small* **10** 4362 (2014)
622. Chu M et al. *Biomaterials* **33** 7071 (2012)
623. del Rosal B et al. *Adv. Opt. Mater.* **4** 782 (2016)
624. Zhu X et al. *Nat. Commun.* **7** 10437 (2016)
625. German S V et al. *Sci. Rep.* **8** 17763 (2018)
626. Silva A D, Serpa C, Arnaut L G *Sci. Rep.* **9** 2553 (2019)
627. Dada O O, Bialkowski S E *Appl. Spectrosc.* **65** 201 (2011)
628. Luk'yanov A Yu et al. *Rev. Sci. Instrum.* **74** 656 (2003)
629. Guo X et al. *Appl. Opt.* **48** (7) C11 (2009)
630. Yarai A, Nakanishi T *Rev. Sci. Instrum.* **78** 054903 (2007)
631. Mandelis A, Riopel Y *J. Vac. Sci. Technol. A* **18** 705 (2000)
632. Proskurnin M A et al. *Appl. Spectrosc.* **59** 1470 (2005)
633. Gröhl J et al. *Photoacoustics* **22** 100241 (2021)
634. Turchin I et al., in *2020 Intern. Conf. Laser Optics* (*ICLO*) (2020) https://doi.org/10.1109/ICLO48556.2020.9285541
635. Xiong B et al. *Talanta* **88** 168 (2012)
636. Turchin I V et al. *Proc. SPIE* **11220** 112200V (2020)
637. Kurouski D et al. *Chem. Soc. Rev.* **49** 3315 (2020)
638. Karlas A et al. *Ann. Translat. Med.* **9** (1) 36 (2021)
639. MacCuaig W M et al. *Radiology Imaging Cancer* **2** e200066 (2020)
640. Chlis N-K et al. *Photoacoustics* **20** 100203 (2020)
641. Gandolfi M, Banfief F, Glorieux C *Photoacoustics* **20** 100199 (2020)
642. Pelivanov I et al. *Sci. Rep.* **8** 14425 (2018)
643. Proskurnin M A, Chernysh V V *J. Anal. Chem.* **55** 943 (2000); *Zh. Anal. Khim.* **55** 1049 (2000)
644. Lengert E et al. *ACS Appl. Mater. Interfaces* **9** 21949 (2017)
645. Zhai D et al. *ACS Nano* **7** 3540 (2013)
646. Sahiner N *Prog. Polym. Sci.* **38** 1329 (2013)
647. Yang Y et al. *ACS Appl. Mater. Interfaces* **10** 7688 (2018)
648. Mansfield E et al. *Nanotoxicology* **8** 394 (2014)
649. Li L et al. *Chem. Eur. J.* **23** 18180 (2017)
650. Vorobyev R I et al. *Acoust. Phys.* **66** 132 (2020); *Akust. Zh.* **66** 148 (2020)
651. Sokolovskaya Yu G, Podymova N B, Karabutov A A *Acoust. Phys.* **66** 81 (2020); *Akust. Zh.* **66** 86 (2020)
652. Neelgund G M, Oki A *Ind. Eng. Chem. Res.* **57** 7826 (2018)
653. Leahu G et al. *Int. J. Thermophys.* **36** 1349 (2015)
654. Kuriakose M et al. *J. Appl. Phys.* **113** 044502 (2013)
655. Shimizu H, Mawatari K, Kitamori T *J. Sep. Sci.* **34** 2920 (2011)
656. Kitagawa F, Akimoto Y, Otsuka K *J. Chromatogr. A* **1216** 2943 (2009)
657. Bicanic D et al. *Instrum. Sci. Technol.* **34** 129 (2006)